Control and observation of switched systems. Application to power converters

Gerardo de Jesus Becerra

▶ **To cite this version:**

Gerardo de Jesus Becerra. Control and observation of switched systems. Application to power converters. Electronics. Université de Lyon; Pontificia universidad javeriana (Bogotá). Facultad de teología, 2019. English. NNT : 2019LYSEI123 . tel-02900567

HAL Id: tel-02900567
https://theses.hal.science/tel-02900567v1

Submitted on 16 Jul 2020

HAL is a multi-disciplinary open access archive for the deposit and dissemination of scientific research documents, whether they are published or not. The documents may come from teaching and research institutions in France or abroad, or from public or private research centers.

L'archive ouverte pluridisciplinaire **HAL**, est destinée au dépôt et à la diffusion de documents scientifiques de niveau recherche, publiés ou non, émanant des établissements d'enseignement et de recherche français ou étrangers, des laboratoires publics ou privés.

N°d'ordre NNT : 2019LYSEI123

THESE de DOCTORAT DE L'UNIVERSITE DE LYON
opérée au sein de
INSA LYON
En cotutelle internationale avec
PONTIFICIA UNIVERSIDAD JAVERIANA

Ecole Doctorale N° 160
Electronique, Electrotechnique, Automatique

Spécialité / discipline de doctorat :
Automatique

Soutenue publiquement le 02/12/2019, par :
Gerardo de Jesus BECERRA

Control and Observation of Switched Systems. Application to Power Converters

---

Devant le jury composé de :

DJEMAI, Mohamed	Professeur des Universités	University of Valenciennes	Rapporteur
QUIJANO, Nicanor	Profesor Asociado	Universidad de los Andes	Rapporteur
GODOY, Emmanuel	Professeur des Universités	CentraleSupélec	Examinateur
COLORADO, Julian	Profesor Asociado	Pontificia Universidad Javeriana	Examinateur
LIN-SHI, Xuefang	Professeur des Universités	INSA Lyon	Directrice de thèse
PHAM, Minh Tu	Maître de Conférence HDR	INSA Lyon	Co-directeur de thèse
PATIÑO, Diego	Profesor Asociado	Pontificia Universidad Javeriana	Co-directeur de thèse, Invité
RUIZ, Fredy	Professore Associato	Politecnico di Milano	Invité

Cette thèse est accessible à l'adresse : http://theses.insa-lyon.fr/publication/2019LYSEI123/these.pdf
© [G. J. Becerra], [2019], INSA de Lyon, tous droits réservés

Cette thèse est accessible à l'adresse : http://theses.insa-lyon.fr/publication/2019LYSEI123/these.pdf
© [G. J. Becerra], [2019], INSA de Lyon, tous droits réservés

Département FEDORA – INSA Lyon - Ecoles Doctorales – Quinquennal 2016-2020

SIGLE	ECOLE DOCTORALE	NOM ET COORDONNEES DU RESPONSABLE
CHIMIE	**CHIMIE DE LYON** http://www.edchimie-lyon.fr Sec. : Renée EL MELHEM Bât. Blaise PASCAL, 3e étage secretariat@edchimie-lyon.fr INSA : R. GOURDON	M. Stéphane DANIELE Institut de recherches sur la catalyse et l'environnement de Lyon IRCELYON-UMR 5256 Équipe CDFA 2 Avenue Albert EINSTEIN 69 626 Villeurbanne CEDEX directeur@edchimie-lyon.fr
E.E.A.	**ÉLECTRONIQUE, ÉLECTROTECHNIQUE, AUTOMATIQUE** http://edeea.ec-lyon.fr Sec. : M.C. HAVGOUDOUKIAN ecole-doctorale.eea@ec-lyon.fr	M. Gérard SCORLETTI École Centrale de Lyon 36 Avenue Guy DE COLLONGUE 69 134 Écully Tél : 04.72.18.60.97 Fax 04.78.43.37.17 gerard.scorletti@ec-lyon.fr
E2M2	**ÉVOLUTION, ÉCOSYSTÈME, MICROBIOLOGIE, MODÉLISATION** http://e2m2.universite-lyon.fr Sec. : Sylvie ROBERJOT Bât. Atrium, UCB Lyon 1 Tél : 04.72.44.83.62 INSA : H. CHARLES secretariat.e2m2@univ-lyon1.fr	M. Philippe NORMAND UMR 5557 Lab. d'Ecologie Microbienne Université Claude Bernard Lyon 1 Bâtiment Mendel 43, boulevard du 11 Novembre 1918 69 622 Villeurbanne CEDEX philippe.normand@univ-lyon1.fr
EDISS	**INTERDISCIPLINAIRE SCIENCES-SANTÉ** http://www.ediss-lyon.fr Sec. : Sylvie ROBERJOT Bât. Atrium, UCB Lyon 1 Tél : 04.72.44.83.62 INSA : M. LAGARDE secretariat.ediss@univ-lyon1.fr	Mme Emmanuelle CANET-SOULAS INSERM U1060, CarMeN lab, Univ. Lyon 1 Bâtiment IMBL 11 Avenue Jean CAPELLE INSA de Lyon 69 621 Villeurbanne Tél : 04.72.68.49.09 Fax : 04.72.68.49.16 emmanuelle.canet@univ-lyon1.fr
INFOMATHS	**INFORMATIQUE ET MATHÉMATIQUES** http://edinfomaths.universite-lyon.fr Sec. : Renée EL MELHEM Bât. Blaise PASCAL, 3e étage Tél : 04.72.43.80.46 infomaths@univ-lyon1.fr	M. Luca ZAMBONI Bât. Braconnier 43 Boulevard du 11 novembre 1918 69 622 Villeurbanne CEDEX Tél : 04.26.23.45.52 zamboni@maths.univ-lyon1.fr
Matériaux	**MATÉRIAUX DE LYON** http://ed34.universite-lyon.fr Sec. : Stéphanie CAUVIN Tél : 04.72.43.71.70 Bât. Direction ed.materiaux@insa-lyon.fr	M. Jean-Yves BUFFIÈRE INSA de Lyon MATEIS - Bât. Saint-Exupéry 7 Avenue Jean CAPELLE 69 621 Villeurbanne CEDEX Tél : 04.72.43.71.70 Fax : 04.72.43.85.28 jean-yves.buffiere@insa-lyon.fr
MEGA	**MÉCANIQUE, ÉNERGÉTIQUE, GÉNIE CIVIL, ACOUSTIQUE** http://edmega.universite-lyon.fr Sec. : Stéphanie CAUVIN Tél : 04.72.43.71.70 Bât. Direction mega@insa-lyon.fr	M. Jocelyn BONJOUR INSA de Lyon Laboratoire CETHIL Bâtiment Sadi-Carnot 9, rue de la Physique 69 621 Villeurbanne CEDEX jocelyn.bonjour@insa-lyon.fr
ScSo	**ScSo*** http://ed483.univ-lyon2.fr Sec. : Véronique GUICHARD INSA : J.Y. TOUSSAINT Tél : 04.78.69.72.76 veronique.cervantes@univ-lyon2.fr	M. Christian MONTES Université Lyon 2 86 Rue Pasteur 69 365 Lyon CEDEX 07 christian.montes@univ-lyon2.fr

*ScSo : Histoire, Géographie, Aménagement, Urbanisme, Archéologie, Science politique, Sociologie, Anthropologie

Cette thèse est accessible à l'adresse : http://theses.insa-lyon.fr/publication/2019LYSEI123/these.pdf
© [G. J. Becerra], [2019], INSA de Lyon, tous droits réservés

Cette thèse est accessible à l'adresse : http://theses.insa-lyon.fr/publication/2019LYSEI123/these.pdf
© [G. J. Becerra], [2019], INSA de Lyon, tous droits réservés

Abstract

Current trends in global energy production indicate that renewables will continue to increase their market share due to continuous efficiency improvements and cost reductions. Power converters constitute the interfaces that enable energy transfers in microgrids between sources, storage and loads, playing a fundamental role in their operation. These devices are required to meet particular efficiency, robustness and stability requirements to guarantee a proper operation. The present work is focused on two particular problems present in the operation of power converters: control and observation. These problems are hard to solve because of the nonlinearities and complex behaviors present in power converters. The mathematical model used to represent power converters is the switched system. Based on this model we take elements from subjects like Lyapunov stability, the method of moments, algebraic geometry and direct filtering, and propose novel approaches to control and observation of switched systems. We introduce moment relaxations of switched systems. These representations allow to obtain models where the switching input is mapped to a moment space. This map removes the nonlinearity associated to the switching input and yields a model which is more suitable for performing numerical computations. This is the fundamental idea in the proposed parameter-varying control method. After computing a control signal for the relaxed model, the control signal for the switched system can be recovered. This approach has shown good performance with respect to reference tracking and stability. A data-driven approach for the observation of switched systems is proposed. This method involves the design of a direct filter that computes worst-case bounds on the estimation error. This method is applied to the case of power converters operating in continuous and discontinuous modes. A practical implementation is described, and its performance is compared with other estimation approaches.

Cette thèse est accessible à l'adresse : http://theses.insa-lyon.fr/publication/2019LYSEI123/these.pdf
© [G. J. Becerra], [2019], INSA de Lyon, tous droits réservés

Cette thèse est accessible à l'adresse : http://theses.insa-lyon.fr/publication/2019LYSEI123/these.pdf
© [G. J. Becerra], [2019], INSA de Lyon, tous droits réservés

Résumé

En matière de production énergétique, les tendances actuelles indiquent que la part de marché mondiale des énergies renouvelables continuera d'augmenter du fait de l'amélioration continue de l'efficacité des équipements et de la réduction de leurs coûts. Les convertisseurs de puissance jouent un rôle fondamental dans le fonctionnement des réseaux électriques car ils permettent les transferts d'énergie entre les sources, les éléments de stockage et les charges. Ces dispositifs doivent répondre à des exigences particulières d'efficacité, de robustesse et de stabilité pour garantir un fonctionnement correct. Le travail présenté dans ce mémoire est centré sur deux problèmes particuliers liés au comportement des convertisseurs de puissance : la commande et l'observation. Ces problèmes sont difficiles à résoudre en raison des non-linéarités et des phénomènes physiques complexes présents dans ces composants. Le modèle mathématique utilisé pour représenter les convertisseurs de puissance est le modèle dit à commutation. Sur la base de ce modèle, nous exploitons des outils abordés dans des problématiques telles que la stabilité de Lyapunov, la méthode des moments, la géométrie algébrique et le filtrage direct. Nous proposons des approches novatrices pour commander et observer ces systèmes commutés. Nous introduisons notamment la notion de moments de relaxation pour les systèmes commutés. Ces représentations permettent d'obtenir des modèles permettant d'établir une cartographie de l'entrée de commutations dans l'espace des moments. Cette carte supprime la non-linéarité associée à l'entrée de commutation et fournit un modèle plus approprié pour effectuer les calculs numériques de la commande. C'est l'idée fondamentale de la méthode de commande à variation de paramètres proposée. Après avoir calculé un signal de commande pour le modèle relaxé, le signal d'entrée pour le système commuté peut alors être déduit. Cette approche a montré de bonnes performances en termes de suivi de référence et de stabilité. Une approche reposant sur les données pour l'observation des systèmes commutés est proposée. Cette méthode implique la synthèse d'un filtre direct qui calcule les limites du cas le plus défavorable sur l'erreur d'estimation. Cette méthode est appliquée au cas des convertisseurs de puissance fonctionnant en mode continu et discontinu. Une mise en oeuvre pratique est effectuée et ses performances sont comparées à d'autres méthodes d'estimation.

Cette thèse est accessible à l'adresse : http://theses.insa-lyon.fr/publication/2019LYSEI123/these.pdf
© [G. J. Becerra], [2019], INSA de Lyon, tous droits réservés

Cette thèse est accessible à l'adresse : http://theses.insa-lyon.fr/publication/2019LYSEI123/these.pdf
© [G. J. Becerra], [2019], INSA de Lyon, tous droits réservés

Acknowledgements

This research work would not have been possible without the support of my advisors, Diego Patiño at Pontificia Universidad Javeriana and Minh Tu Pham and Xuefang Lin-Shi at INSA Lyon. I would like to thank Diego for taking me as his student so long ago during my masters studies. His professionalism and work ethic have inspired me to continue advancing in my research career. He introduced me to interesting ideas in the context of switched systems that motivated part of this work. I would also like to thank Minh Tu for his dedication and support. Our lengthy discussions were fundamental for the developments achieved in this work. I found in him not only a mentor, but a friend. I will always be grateful for his support during my doctoral studies. I also thank Xuefang for her invaluable guidance and patience. Her experience in power electronics was very important to achieve the results obtained in this thesis.

I thank the members of my jury, specially Mohamed Djemai and Nicanor Quijano for honoring me by reviewing my thesis. Their comments and suggestions were important to improve the quality of this work. I also thank Emmanuel Godoy and Julian Colorado for accepting to be part of the jury.

I would like to give special thanks to Fredy Ruiz for his collaboration in the subject of estimation for nonlinear systems with unknown model. His ideas were fundamental for the results presented in this thesis regarding the observation of power converters.

I would like to thank the team at Laboratoire Ampère for receiving me and providing the tools and resources needed for carrying out the experimental work in this thesis.

Finally, I would like to thank my friends and family for their love and support. I thank my parents and sisters for helping me during difficult times. I thank my mother-in-law for welcoming me as a son. For my wife, I have nothing but love and gratitude for her patience and support during these long years.

Cette thèse est accessible à l'adresse : http://theses.insa-lyon.fr/publication/2019LYSEI123/these.pdf
© [G. J. Becerra], [2019], INSA de Lyon, tous droits réservés

Cette thèse est accessible à l'adresse : http://theses.insa-lyon.fr/publication/2019LYSEI123/these.pdf
© [G. J. Becerra], [2019], INSA de Lyon, tous droits réservés

Contents

Cette thèse est accessible à l'adresse : http://theses.insa-lyon.fr/publication/2019LYSEI123/these.pdf
© [G. J. Becerra], [2019], INSA de Lyon, tous droits réservés

Cette thèse est accessible à l'adresse : http://theses.insa-lyon.fr/publication/2019LYSEI123/these.pdf
© [G. J. Becerra], [2019], INSA de Lyon, tous droits réservés

Cette thèse est accessible à l'adresse : http://theses.insa-lyon.fr/publication/2019LYSEI123/these.pdf
© [G. J. Becerra], [2019], INSA de Lyon, tous droits réservés

Cette thèse est accessible à l'adresse : http://theses.insa-lyon.fr/publication/2019LYSEI123/these.pdf
© [G. J. Becerra], [2019], INSA de Lyon, tous droits réservés

List of Figures

Cette thèse est accessible à l'adresse : http://theses.insa-lyon.fr/publication/2019LYSEI123/these.pdf
© [G. J. Becerra], [2019], INSA de Lyon, tous droits réservés

Cette thèse est accessible à l'adresse : http://theses.insa-lyon.fr/publication/2019LYSEI123/these.pdf
© [G. J. Becerra], [2019], INSA de Lyon, tous droits réservés

Cette thèse est accessible à l'adresse : http://theses.insa-lyon.fr/publication/2019LYSEI123/these.pdf
© [G. J. Becerra], [2019], INSA de Lyon, tous droits réservés

Cette thèse est accessible à l'adresse : http://theses.insa-lyon.fr/publication/2019LYSEI123/these.pdf
© [G. J. Becerra], [2019], INSA de Lyon, tous droits réservés

List of Tables

Cette thèse est accessible à l'adresse : http://theses.insa-lyon.fr/publication/2019LYSEI123/these.pdf
© [G. J. Becerra], [2019], INSA de Lyon, tous droits réservés

Cette thèse est accessible à l'adresse : http://theses.insa-lyon.fr/publication/2019LYSEI123/these.pdf
© [G. J. Becerra], [2019], INSA de Lyon, tous droits réservés

A mis padres, por su amor y apoyo incondicional. A Sara, mi amada, mi compañera, mi preciosa. A Jacobo y Valentín, por traer a mi vida alegría que nunca imaginé poder experimentar.

Cette thèse est accessible à l'adresse : http://theses.insa-lyon.fr/publication/2019LYSEI123/these.pdf
© [G. J. Becerra], [2019], INSA de Lyon, tous droits réservés

Cette thèse est accessible à l'adresse : http://theses.insa-lyon.fr/publication/2019LYSEI123/these.pdf
© [G. J. Becerra], [2019], INSA de Lyon, tous droits réservés

Chapter 1

General Introduction

1.1 Outline

This thesis focuses on the development of novel approaches to the control and observation of switched systems, which can be applied to the particular case of power converters. Our main motivation stems from the importance of power converters in real-world applications, and from the interest in applying and testing recent theoretical advances in control and observation of nonlinear and switched systems.

Power converters are devices that manage the power transfer between different elements in a power system. They can modify the levels and waveforms of the voltages and currents to adapt to the application requirements, and have high efficiency and low conduction losses. These devices are present in multiple applications like power supplies for portable electronics, uninterruptible power supplies for servers, inverters for wind and solar sources, and motor drives for automotive/railroad/naval applications, among others. Advances in semiconductor technology have allowed achieving blocking voltages/conduction currents up to thousands of volts/amperes. Also, advances in converter topologies have allowed using more mature medium voltage semiconductor devices in cascaded configurations that allow them to operate at higher power levels.

The different semiconductor devices present in a power converter must be activated in a coordinated way to achieve the performance objectives defined by the application. This requires the design of controllers that must satisfy performance objectives such as stability, reference tracking, disturbance rejection, harmonic distortion, efficiency, response time, etc. The highly nonlinear characteristics of the semiconductor devices used in power converters increase the complexity in the design of these controllers. One of the usual approaches to control design is to obtain a mathematical model of the plant/system to be controlled. Power converters can be represented using switched systems. These models represent systems where dynamics change abruptly over time and have different configuration modes. These kinds of systems have been investigated in the field of control theory, yielding interesting results regarding the stability, controllability, and observability of switched systems.

Some of the main challenges present in the operation of power converters are:

Cette thèse est accessible à l'adresse : http://theses.insa-lyon.fr/publication/2019LYSEI123/these.pdf
© [G. J. Becerra], [2019], INSA de Lyon, tous droits réservés

1. The nonlinearities present in switching devices produce complex behaviors.

2. Power converters have a fast dynamical behavior, leaving a small time window for acting on the system.

3. The use of unidirectional semiconductor switches may produce the existence of discontinuous conduction modes (DCM) which produce drastic changes in the system dynamics.

The main objective of this thesis is to propose novel control and observation methods with stability guarantees, fast closed-loop response, and suitable for application in continuous/discontinuous conduction modes and with practical implementation. To achieve this we capture ideas and theoretical results recently developed for switched and nonlinear systems and extend them to solve the control and observation problems in general for switched systems, and in particular for power converters. The advantage of this approach is that the developed methods do not depend on the particular details of the converter topology, but are abstracted to the structure of the switched model, allowing them to be applied to different converter topologies.

1.2 Organization

The thesis is divided into the chapters described below. Chapter 2 presents an overview of the application context and the particular problems in power converters that motivate this research. Also, the general model that will be used for switched systems is introduced. The basic converter topologies used for testing the proposed methods are shown, discussing their main properties. Then, a brief introduction to the main concepts in four theoretical subjects is presented. These subjects will provide the basic ideas for the proposed methods in the following chapters.

Chapter 3 introduces the proposed approach to the problem of modeling. Moment relaxations provide equivalent models for the switched systems of interest. These models will be useful in chapter 4 for solving the control problem. An example is provided, and a discussion on the properties of the operation regions of these models is included.

Chapter 4 deals with the control problem of switched systems. The approach is based on Lyapunov's theory of stability and is extended by defining parameterized Lyapunov functions. Two different approaches are discussed. In the first approach, the case of fixed parameters is studied and a stabilizing control law is proposed. Results obtained are discussed for the case of one converter topology, and an analysis of the control structure is presented. In the second approach, the case of trajectory dependent Lyapunov functions is discussed. Here, the results from chapter 2 are used to extend this method to the case of switched systems. Results are shown for three different converter topologies.

Cette thèse est accessible à l'adresse : http://theses.insa-lyon.fr/publication/2019LYSEI123/these.pdf
© [G. J. Becerra], [2019], INSA de Lyon, tous droits réservés

Chapter 5 deals with the observation problem for switched systems. The proposed approach is based on methods from the theory of system identification, allowing to build state estimators based on measurements obtained from the system. This approach allows to solve the problem of state estimation for converters operating in continuous and discontinuous modes. Two application examples are developed for one converter topology, illustrating the case of single and full state estimation.

In chapter 6 the general results of the thesis are discussed and perspectives for future work are outlined. Finally, the bibliography and notation are included.

1.3 Contribution

The main contribution of this thesis is in the development of two novel approaches to the control and observation problems of power converters. The basic ideas on which this work is based have been tested before for other types of systems (linear, nonlinear, piece-wise affine), but not for switched systems. The methods proposed here take these theoretical ideas and extend them, allowing to obtain practical implementations that solve the problems of interest in the context of power converters. The two novel approaches are the following:

- Synthesis of trajectory-dependent control Lyapunov functions for switched systems. This method allows to obtain less conservative (more general) Lyapunov functions by using varying parameters, which are computed on-line by solving a mathematical programming problem. The extension to the case of switched systems is achieved by using moment relaxations to formulate and solve the mathematical problem in the moments domain, and then by recovering the control signal for the original system. This approach is general, meaning that it can be applied to different converter topologies.

- Direct filtering for state estimation in power converters operating in continuous and discontinuous modes. This approach allows to obtain estimates of the state variables in power converters without *a-priori* knowledge on the system model, but based on datasets obtained from experiments carried on in the plant. The approach allows to obtain estimates during continuous and discontinuous mode operation, without having to rely on complicated mathematical models that try to capture the dynamics of these differing conditions. Also, this algorithm has a parallel structure, allowing the use of a multiprocessor architecture to improve the computation performance. Details of the ideas used to achieve a parallel implementation, as well as the results obtained for one converter topology are shown.

One of the main advantages of these methods is that the algorithms are formulated for the general switched model, allowing the application to different converter topologies without any significant modifications. The main

Cette thèse est accessible à l'adresse : http://theses.insa-lyon.fr/publication/2019LYSEI123/these.pdf
© [G. J. Becerra], [2019], INSA de Lyon, tous droits réservés

difficulty in applying these methods is the computational cost. This drawback was solved for the case of the estimation method by using specialized hardware and by making optimizations to the algorithm, which allowed to obtain simulation and experimental results. In the case of the control algorithm simulation results are presented.

1.4 Publications

The contents of this thesis are based on published material, as well as material awaiting for publishing.

Published material:

- G. Becerra, D. Patino, M.T. Pham, and X. LinShi. *Algebraic and geometric properties of equilibria in cyclic switched dynamic systems*. Int. J. Robust. Nonlinear Control, 27: 2218 2233. 2017. doi: 10.1002/rnc.3679.
- G. Becerra, A. R. Meghnous, M. T. Pham, X. Lin-Shi and D. Patino, *A unified hybrid control for DC/DC power converters using port-Hamiltonian formulation*, IECON 2017 - 43rd Annual Conference of the IEEE Industrial Electronics Society, Beijing, 2017, pp. 4851-4856. doi: 10.1109/IECON.2017.8216837
- G. Becerra, A. R. Meghnous, M. T. Pham, X. Lin-Shi, D. Patino and J. Y. Gauthier, *Hybrid Lyapunov based control of multicellular converters using Port-Hamiltonian modeling*, IECON 2017 - 43rd Annual Conference of the IEEE Industrial Electronics Society, Beijing, 2017, pp. 8213-8218. doi: 10.1109/IECON.2017.8217441

In preparation:

- G. Becerra, D. Patino, M.T. Pham, and X. LinShi. *Trajectory-dependent Control Lyapunov Functions for Switched Systems*.
- G. Becerra, F. Ruiz, D. Patino, M.T. Pham, and X. LinShi. *Direct Filtering for Current Estimation in Power Converters Operating in Continuous and Discontinuous Conduction Modes*.

Cette thèse est accessible à l'adresse : http://theses.insa-lyon.fr/publication/2019LYSEI123/these.pdf
© [G. J. Becerra], [2019], INSA de Lyon, tous droits réservés

Chapter 2

Background

2.1 Power Converters

Power converters can be viewed as power processing units [1], with an input port from which the device draws power, an output port for delivering power and a control input which determines the behavior of the system. The type of device in which we are interested is the switching power converter, which uses semiconductor devices to perform the switching operations. The semiconductor devices are operated in the cutoff and saturation regions, where the power consumption is negligible compared to the active region. Ideally, a power converter should have a small size/weight, and process power at high efficiency. The power processing is performed by changing the voltage/current waveforms from input to output. Depending on the different input - output waveforms a power converter classification can be established:

- DC-DC: These converters take as input a DC level and transform it into another DC level. The output level can be higher, lower or with inverse polarity with respect to the input level. These are commonly used for supplying power to electronic circuits from batteries, and also for storing the energy supplied by photo-voltaic cells. There are different circuit topologies such as Buck, Buck-Boost, SEPIC, Ćuk, etc.

- AC-DC: These converters take an AC waveform and produce an output DC level. One of the circuit topologies belonging to this category is the controlled rectifier. In this circuit the timing of the switching events with respect to the periodic input waveform determine the output DC level. These converters are used for supplying power from the AC grid to equipment operating with DC power.

- DC-AC: These converters transform a DC level to an AC waveform, and are commonly known as power inverters. In this case the DC level may be supplied by batteries, a AC-DC converter or the HVDC power lines. These are used extensively in applications like uninterruptible power supplies (UPS), photo-voltaic systems or power inverters. In this configuration, the semiconductor devices switch in a way that produces an output waveform which is more or less a sinusoidal.

- AC-AC: These converters transform directly an AC waveform to another AC waveform of lower frequency, without the need of a DC link

Cette thèse est accessible à l'adresse : http://theses.insa-lyon.fr/publication/2019LYSEI123/these.pdf
© [G. J. Becerra], [2019], INSA de Lyon, tous droits réservés

(that is, having in cascade an AC-DC with a DC-AC converter). This kind of converter is usually used in motor control applications where it is convenient to control the speed by changing the output frequency of the converter.

In all the previous cases one of the most important requirements for a proper operation of the power converter is the generation of suitable switching signals for controlling the semiconductor devices. These signals are usually provided by a controller, whose design depends on the particular control objectives. The control design problem is one of the main themes of this work. Also, in order to implement a control scheme able to compensate the effects of transient disturbances while maintaining stability and efficiency, it is required to measure some or all the system state variables. However, it is not always practical or feasible to use sensors to obtain this information. In this situation, it is required to design an observation/estimation strategy to obtain information on the unmeasurable state variables. The observer/estimator design problem is another main theme in this work.

2.1.1 Control and Observation of Power Converters

Classical control theory gives solutions to the control and observation problems of linear systems. However, this theory can not be directly extended to the case of switched power converters because of their inherently discontinuous behavior. In order to overcome this difficulty, the principle of averaging was introduced [2], allowing the study of the low frequency behavior of the converter, obtain small signal models by linearization and design linear feedback control laws. This model is correct under the assumption of slow system dynamics with respect to the switching frequency. There are advantages in this approach, like ease in implementation and well developed analysis tools. However, these approaches are limited when better system performance is required.

There are two general approaches for control and observation of switched power converters, shown in Fig. 2.1. The first comes from power systems engineering, based on classical methods like linear and hysteresis control [3], [4], or more recent ones like sliding modes [5], [6], neuro/fuzzy [7], [8], and predictive control [9], [10]. A common aspect of these methods is the focus on practical aspects like simplicity, ease of implementation and performance.

The second approach comes from the theory and practice of control systems, which puts greater emphasis on theoretical results related to stability, controllability and observability of switched systems. Some methods taking this approach are optimal control [11], [12], [13], robust control [14], [15], passivity based control [16], [17], Lyapunov control [18], [19], and polynomial control [20]. The latter approach usually yields results that have theoretical guarantees, but in practice may be harder to implement.

One of the main goals of the present work is to bridge the gap between these two approaches by taking recent advances in control systems and deriving practical implementations that can be used in real power converter test benches.

Cette thèse est accessible à l'adresse : http://theses.insa-lyon.fr/publication/2019LYSEI123/these.pdf
© [G. J. Becerra], [2019], INSA de Lyon, tous droits réservés

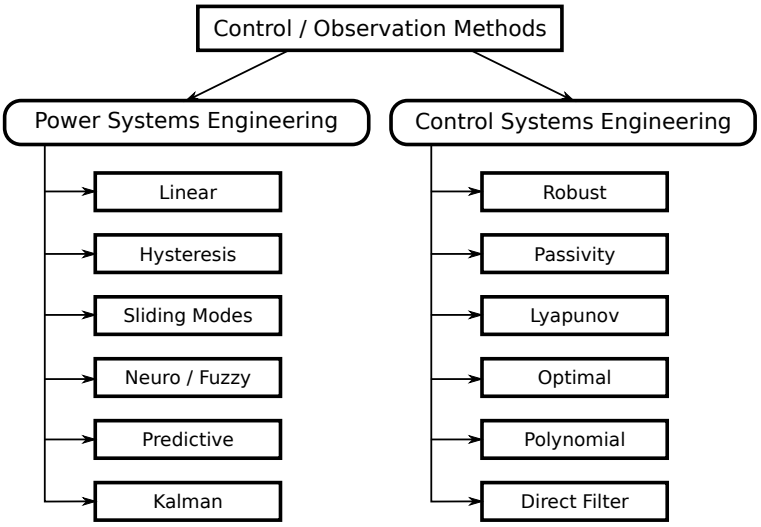

FIGURE 2.1 – Control and observation methods for switched power converters.

2.1.2 Continuous and Discontinuous Modes in Power Converters

Passive elements are used as intermediate stages in power converters for storing the energy and filtering the waveforms, while semiconductor devices are used to perform the switching operations. In PWM power converters, the circuit topology is repeatedly switched according to the conduction state of these devices by the action of a switching signal. However, some devices (typically diodes) can switch spontaneously depending on the circuit conditions. This characteristic is the reason for the existence of continuous and discontinuous conduction modes in power converters.

Consider the case of PWM converters with two switches, like the SEPIC shown in Fig. 2.3. Continuous conduction mode (CCM) happens when the two switches are operated in a synchronous, complementary way. This means that when one of them is turned on the other is turned off, and vice-versa. This can be observed in Fig. 2.2(a), which shows the typical current and voltage waveforms of the SEPIC converter in CCM operation. During the first half of the PWM period T_{PWM} the switching signal turns on the MOSFET, and turns it off during the second half.

When the diode switches asynchronously with respect to the MOSFET due to particular circuit conditions, discontinuous conduction modes (DCM) arise. In Fig. 2.2(b), when the current I_{L1} falls causing the diode current I_D to fall to zero before the end of the PWM period T_{PWM} the diode stops conducting while the MOSFET is turned off, producing discontinuous inductor current mode (DICM). Notice that in this case both currents I_{L1} and I_{L2} become equal. When the voltage V_{C1} falls and becomes negative enough to match the output voltage the diode becomes forward biased and starts conducting while the MOSFET is turned on, producing discontinuous capacitor voltage mode (DCVM). This can be observed in Fig. 2.2(c). Notice that in this case both voltages V_{C1} and V_{C2} become equal, with opposite polarity. This

Cette thèse est accessible à l'adresse : http://theses.insa-lyon.fr/publication/2019LYSEI123/these.pdf
© [G. J. Becerra], [2019], INSA de Lyon, tous droits réservés

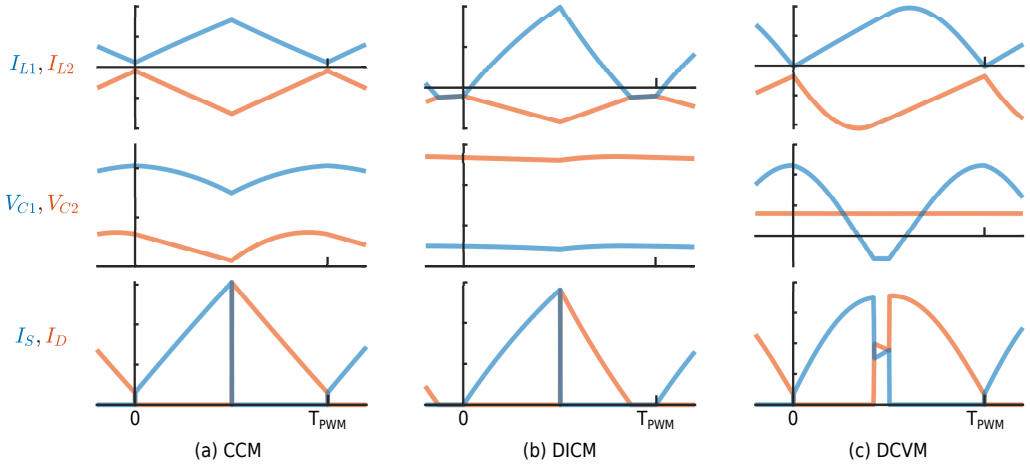

FIGURE 2.2 – Typical current and voltage waveforms for the different conduction modes in the SEPIC converter: inductor currents I_{L1} and I_{L2} (top), capacitor voltages V_{C1} and V_{C2} (center), MOSFET and diode currents I_S and I_D (bottom). PWM duty cycle equal to 50%.

behavior may be caused by the presence of a big ripple in the signals I_{L1} for DCIM or V_{C1} for DCVM, causing the diode to change state before the end of the current semi-cycle. The big ripple may be caused by having small capacitor or inductance values. Also, depending on the circuit parameters it may be the case that driving the converter with a PWM signal with sufficiently small duty cycle may produce discontinuous modes.

Notice that in order to obtain the average value for I_{L1} and V_{C1} in DCM, it is required to know the time instants when the autonomous switching events happen. This is why the usual assumptions used for computing the average model are no longer applicable and an estimator has to be designed to obtain these times [21]. For additional details on the operation and dynamical properties of power converters operating in DCM, the reader can refer to [1], [22], [23].

2.1.3 Models for Power Converters

A switched power converter can be modeled by considering all possible circuit topologies obtained from the different conducting and blocking states of the semiconductor devices. These configurations are represented by a system of switched linear differential-algebraic equations:

$$\mathcal{P}_{\sigma(t)}\dot{x}(t) = \mathcal{A}_{\sigma(t)}x(t) + \mathcal{B}_{\sigma(t)}u(t) \tag{2.1a}$$

$$y(t) = \mathcal{C}_{\sigma(t)}x(t) + \mathcal{D}_{\sigma(t)}u(t) \tag{2.1b}$$

where $x(t) \in \mathbb{R}^{n_x}$ corresponds to the state, $u(t) \in \mathbb{R}^{n_u}$ the input, $y(t) \in \mathbb{R}^{n_y}$ the measurable output. Notice that the system state is continuous and evolves without jumps. The matrix $\mathcal{P}_\sigma$ depends on the energy storage parameters, and is associated to the presence of discontinuous conduction modes. When DCM is present, this matrix will eliminate one of the state variable

Cette thèse est accessible à l'adresse : http://theses.insa-lyon.fr/publication/2019LYSEI123/these.pdf
© [G. J. Becerra], [2019], INSA de Lyon, tous droits réservés

derivatives, generating an algebraic relation between variables. The consequence is that one of the state variables becomes linearly dependent on another, effectively reducing the system dimension. This will be illustrated in the following section for the case of the SEPIC converter.

The system matrices $\{\mathcal{P}_\sigma, \mathcal{A}_\sigma, \mathcal{B}_\sigma, \mathcal{C}_\sigma, \mathcal{D}_\sigma\}$ are selected depending on the system mode $\sigma(t) \in \mathcal{I}$, where $\mathcal{I}$ is a finite index set. Only one system mode $\sigma(t)$ is active at each time instant t, and it depends on the controlled switch states $s(t)$ and uncontrolled switch states $\delta(t)$: $\sigma(t) = g(s(t), \delta(t))$, $s(t) \in \{0,1\}^{n_s}$, $\delta \in \{0,1\}^{n_\delta}$. n_s and d_δ are the number of controlled and uncontrolled switches, respectively. The state of the uncontrolled switches depends on the system states $x(t)$ and inputs $u(t)$: $\delta(t) = h(x(t), u(t))$. This interaction between the continuous and discrete variables in system (2.1) produces a hybrid dynamical system [24]. The control and observation of these systems is quite involved, and currently is subject of active research efforts.

Assumption 2.1.1. *The modes σ in system (2.1) are activated in sequence $\mathcal{I} = \{1, 2, \ldots, 2^{n_s+n_\delta}\}$, each with a duration of $d_\sigma T$, where T is the total switching period.*

Under assumption 2.1.1, an average model approximation of system (2.1) can be obtained:

$$P\dot{x}(t) = Ax(t) + Bu(t) \tag{2.2a}$$
$$y(t) = Cx(t) + Du(t) \tag{2.2b}$$

where $M \in \{P, A, B, C, D\}$, $\mathcal{M}_\sigma \in \{\mathcal{P}_\sigma, \mathcal{A}_\sigma, \mathcal{B}_\sigma, \mathcal{C}_\sigma, \mathcal{D}_\sigma\}$, $M = \sum_{\sigma\in\mathcal{I}} d_\sigma \mathcal{M}_\sigma$. d_σ corresponds to the proportion of the total switching period duration T that mode σ is active: $\sum_{\sigma\in\mathcal{I}} d_\sigma = 1$.

Notice that a difficulty in obtaining this model is that the mode transitions due to uncontrolled switching would need to be measured directly or estimated indirectly. For instance, in [25] an adaptive control law is designed for the boost converter operating in DCM, based on the computation of the switching times for the sequence of modes, assuming exact knowledge of the system model. When no uncontrolled switching events are present, model (2.2) corresponds to the classical average model widely used in the context of power converters. This model works under the assumption of slow state space dynamics compared to the period of one switching cycle [26]. However, this assumption is not always satisfied in practice, leading to inaccuracies in the model.

2.1.4 DC-DC Converter Topologies

SEPIC Converter

The single-ended primary-inductor converter (SEPIC) is a DC-DC power converter that allows to have an output voltage with a higher, equal or lower level than the input voltage. A PWM signal with controlled duty cycle is used to drive the semiconductor device, usually a MOSFET. The typical schematic diagram is shown in Fig. 2.3. This converter has 4 state variables: $x = \left[I_{L_1}, V_{C_1}, I_{L_2}, V_{C_2}\right]^\intercal$. One of its main advantages it that the obtained output

Cette thèse est accessible à l'adresse : http://theses.insa-lyon.fr/publication/2019LYSEI123/these.pdf
© [G. J. Becerra], [2019], INSA de Lyon, tous droits réservés

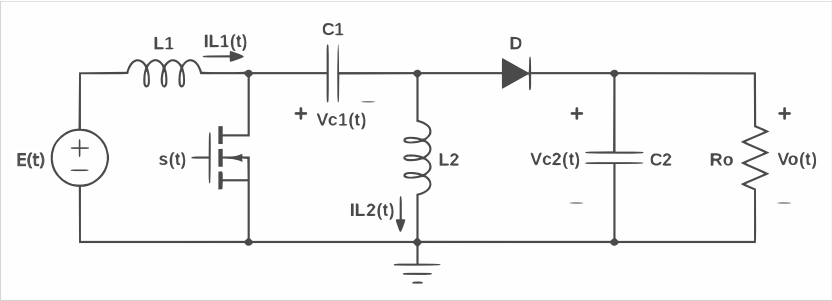

FIGURE 2.3 – Schematic diagram of the SEPIC converter.

voltage has the same polarity as the input voltage [1]. The switched linear model of the SEPIC converter in Eq. (2.1) is represented by the following matrices:

$$A_{s(t),\delta(t)} = \begin{bmatrix} -R_{L1} - R_{L2}(1-s-\delta+s\delta) & s-1 & 0 & (s-1)\delta \\ 1-s & s\delta & s(1-\delta) & s\delta \\ 1-s-\delta+s\delta & -s & (1-s)(1-\delta) - R_{L2}(s+\delta-s\delta) & \delta(1-s) \\ \delta(1-s) & 0 & -\delta & -1/R_o \end{bmatrix}, \tag{2.3}$$

$$B_{s(t),\delta(t)} = \begin{bmatrix} 1 \\ 0 \\ 0 \\ 0 \end{bmatrix}, C_{s(t),\delta(t)} = \begin{bmatrix} 0 & 0 & 0 & 1 \end{bmatrix}, D_{s(t),\delta(t)} = 0, \tag{2.4}$$

$$P_{s(t),\delta(t)} = \begin{bmatrix} L_1 & 0 & (1-s-\delta+s\delta)L_1 & 0 \\ 0 & (1-s\delta)C_1 & 0 & 0 \\ 0 & 0 & (s+\delta-s\delta)L_2 & 0 \\ 0 & s\delta C_1 & 0 & C_2 \end{bmatrix}, \tag{2.5}$$

where $s(t) \in \{0,1\}$ is the binary signal that controls the switching of the MOSFET, and $\delta(t) \in \{0,1\}$ is a binary variable that represents the uncontrolled state of the diode. R_{L1}, R_{L2} are the equivalent internal inductor resistances and R_o is the load resistance. Notice that if the converter operates in CCM, the MOSFET and the diode will be activated complementarily (i.e. $s = 1, \delta = 0$ and $s = 0, \delta = 1$). In this case the off-diagonal elements in matrix $\mathcal{P}_{s(t),\delta(t)}$ become zero, and the diagonal consists of the storage element values. In this case the model (2.1) is determined by a system of differential equations.

However, under DCM operation the MOSFET and the diode will be both turned on or off, depending on the type of discontinuity (i.e. $s = 0, \delta = 0$ or $s = 1, \delta = 1$). In this case the matrix $\mathcal{P}_{s(t),\delta(t)}$ will have nonzero elements in the off-diagonal, and one of the differential equations will become an algebraic equation. For example, when the SEPIC converter is operating in discontinuous inductor current mode both the MOSFET and diode are turned off ($s = 0, \delta = 0$). Observing the circuit diagram for this configuration, both inductors are in a series configuration, forcing them to have the same current value. The equivalent inductance will determine the dynamics during the duration of the discontinuous mode, and the system will have three state

Cette thèse est accessible à l'adresse : http://theses.insa-lyon.fr/publication/2019LYSEI123/these.pdf
© [G. J. Becerra], [2019], INSA de Lyon, tous droits réservés

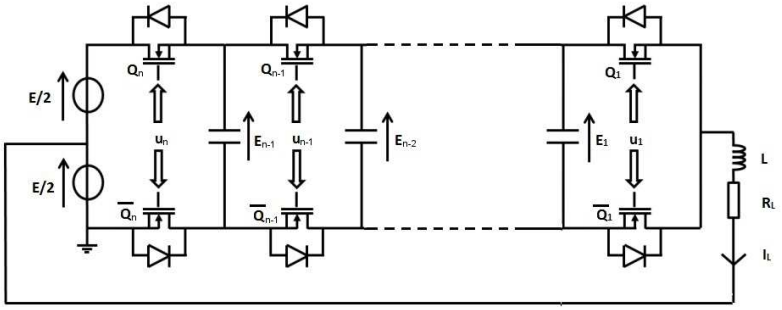

FIGURE 2.4 – Multicellular converter with n cells.

variables: $I_{L_{eq}}$, V_{C_1} and V_{C_2}. In discontinuous capacitor voltage mode the MOSFET and diode are turned on at the same time ($s = 1, \delta = 1$), forcing both capacitors in a parallel configuration, yielding a system with three state variables: $V_{C_{eq}}$, I_{L_1}, I_{L_2}.

Using the averaging principle, $s(t)$ and $\delta(t)$ can be redefined as continuous variables in the interval $[0, 1]$ representing the duty cycle of PWM signals with a sufficiently high constant frequency f_{PWM}. These duty cycles will represent the fraction of time period that each operation mode is active. This assumes that there is a way to measure or estimate the uncontrolled state of the diode. Table 2.1 shows the parameters used for the SEPIC converter in this work for simulation and in the experimental test bench available at *Laboratoire Ampère, INSA de Lyon*.

Multicellular Converter

Multicellular converters have recently gained popularity because of their modularity and reliability. Its main characteristic is that they can supply high output power while using mature medium-power semiconductor technology [27]. This is achieved by distributing the voltages in a series of cells formed by passive storage elements interconnected by switching semiconductor devices. Because of this configuration, it is important to maintain a balanced voltage distribution across all cells. The typical schematic diagram for the n-cell converter is shown in Fig. 2.4. The switched model (2.1) can be rewritten in the case of the multicellular converter as

$$P\dot{x}(t) = (J_{s(t)} - R)x(t) + B_{s(t)}u(t), \tag{2.6}$$

where $x(t) \in \mathbb{R}^n$ is the state vector, defined as

$$x(t) = [V_{C_1}(t), V_{C_2}(t), \cdots, V_{C_{n-1}}, I_L(t)]^\mathsf{T},$$

with $V_{C_1}, V_{C_2}, \ldots, V_{C_{n-1}}$ the voltages of the flying capacitors and I_L is the load current. The input $u(t) \in \mathbb{R}$ corresponds to the supply voltage and $s(t) \in \mathbb{R}^n$ corresponds to the vector of switching inputs. $J_{s(t)} \in \mathbb{R}^{n\times n}$ is the skew-symmetric structure matrix corresponding to the power interconnections in

Cette thèse est accessible à l'adresse : http://theses.insa-lyon.fr/publication/2019LYSEI123/these.pdf
© [G. J. Becerra], [2019], INSA de Lyon, tous droits réservés

the system. $B_{s(t)} \in \mathbb{R}^{n\times 1}$ is the input matrix and $P \in \mathbb{R}^{n\times n}$ is a diagonal matrix that contains the parameter values of the storage elements. $R \in \mathbb{R}^{n\times n}$ is the dissipation matrix that contains the values of the circuit resistors. Matrices J and B are defined by the variable structure associated to the switching of the semiconductor devices. These can be written as:

$$J_{s(t)} = J_0 + \sum_{i=0}^{n} J_i s_i(t) \tag{2.7a}$$

$$B_{s(t)} = B_0 + \sum_{i=0}^{n} B_i s_i(t) \tag{2.7b}$$

Eq. (2.6) is written in the form of a *port-Hamiltonian* system [28]. This framework focuses on modeling and analysis of physical systems formed by the interaction of elements that supply, store and dissipate energy, using a network of interconnected ports. In this equation, matrix B is associated to the energy supply, P to the energy storage, R to the energy dissipation and J to the network of ideal connections between elements.

It is assumed that there are no jumps in the state variables, because the switches in each cell are operated in a complementary way. The switching inputs are $s_i \in \{0,1\}$, $i = 1,\dots,n$. Those inputs represent the on/off control signals of the switching devices (IGBT, MOSFET, etc). It is also assumed that there is a finite number of switching events in any finite time interval. The control vector $s(t)$ is defined as $s(t) = [s_1(t), s_2(t), \cdots, s_n(t)]^\intercal$. Notice that this converter does not exhibit DCM operation, because there are not uncontrolled switching devices present, such as diodes. The matrices P, R, $J_{s(t)}$, $B_{s(t)}$ are given by

$$P = \begin{bmatrix} C_1 & 0 & \dots & 0 & 0 \\ 0 & C_2 & \dots & 0 & 0 \\ \vdots & \vdots & \ddots & \vdots & \vdots \\ 0 & 0 & \cdots & C_{n-1} & 0 \\ 0 & 0 & \dots & 0 & L \end{bmatrix}, \tag{2.8a}$$

$$R = \begin{bmatrix} 0 & \dots & 0 & 0 \\ \vdots & \ddots & \vdots & \vdots \\ 0 & \dots & 0 & 0 \\ 0 & \dots & 0 & R_L \end{bmatrix}, \tag{2.8b}$$

$$J_{s(t)} = \begin{bmatrix} 0 & 0 & \dots & 0 & s_2 - s_1 \\ 0 & 0 & \dots & 0 & s_3 - s_2 \\ \vdots & \vdots & \ddots & \vdots & \vdots \\ 0 & 0 & \dots & 0 & s_n - s_{n-1} \\ s_1 - s_2 & s_2 - s_3 & \dots & s_{n-1} - s_n & 0 \end{bmatrix}, \tag{2.8c}$$

Cette thèse est accessible à l'adresse : http://theses.insa-lyon.fr/publication/2019LYSEI123/these.pdf
© [G. J. Becerra], [2019], INSA de Lyon, tous droits réservés

$$B_{s(t)} = \begin{bmatrix} 0 \\ 0 \\ \vdots \\ 0 \\ s_n - \frac{1}{2} \end{bmatrix}, \tag{2.8d}$$

where $C_1, C_2, \cdots, C_{n-1}$ correspond to the flying capacitors, L to the load inductor and R_L to the load resistor. Notice that the voltage in the output resistor is constrained by the input source:

$$-\frac{u(t)}{2} \leq R_L I_L \leq \frac{u(t)}{2}. \tag{2.9}$$

The meaning of this constraint is that there is a physical limit imposed on the output current determined by the input voltage and the load resistance, for operation in steady state. This fact can be proved by observing Fig. 2.4. When all the switches $s_1, s_2, \ldots, s_n$ are on, the output current will converge to $E/(2R_L)$, and when the complementary switches $\bar{s}_1, \bar{s}_2, \ldots, \bar{s}_n$ are on, the output current will converge to $-E/(2R_L)$. Table 2.1 shows the parameters in the 3-cell converter used for simulation and in the experimental test bench available at *Laboratoire Ampère, INSA de Lyon*.

Converter	Parameters
SEPIC converter	$u(t) = 20$ V, $L_1 = 2.3$ mH, $C_1 = 190$ μF, $L_2 = 330$ μH, $C_2 = 190$ μF, $R_{L1} = 2.134$ Ω, $R_{L2} = 0.234$ Ω, $R_o = 22$ Ω.
2-cell Multicellular converter	$u(t) = 60$ V, $L = 50$ mH, $C = 33$ μF, $R_L = 33$ Ω.
3-cell Multicellular converter	$u(t) = 60$ V, $L = 50$ mH, $C_1 = 33$ μF, $C_2 = 33$ μF, $R_L = 33$ Ω.

TABLE 2.1 – Parameters used in the application examples.

2.2 Lyapunov Stability

The methods developed by Lyapunov to address the problem of stability of nonlinear systems are widely used in applications such as stability analysis, synthesis of stabilizing controllers and synthesis of asymptotically stable observers. These methods rely on the existence and construction of suitable Lyapunov functions (LF) or control Lyapunov functions (CLF). The classical approach for continuous-time systems (known as Lyapunov's direct method) consists in finding a candidate LF or CLF such that its time derivatives are negative along trajectories of the system. In the particular case of physical systems the LF can be interpreted as the system's energy. In this context if the energy is strictly decreasing the system should follow a trajectory that converges towards a certain equilibrium point. For the case of switched systems, different stability conditions can be derived for the cases when the switching signal is or not time-constrained.

Cette thèse est accessible à l'adresse : http://theses.insa-lyon.fr/publication/2019LYSEI123/these.pdf
© [G. J. Becerra], [2019], INSA de Lyon, tous droits réservés

Stability under arbitrary switching: A necessary condition for stability of switched systems under arbitrary switching is that all individual subsystems are asymptotically stable. A sufficient condition for asymptotic stability is the existence of a common quadratic Lyapunov function (CQLF) for all subsystems. The existence of a CQLF can be recast as linear matrix inequalities (LMI) which can in turn be solved numerically using interior point methods. However, as the number of modes in the switching system increases, also increases the difficulty in finding a numerical solution. This is why the development of algebraic methods has been an important research subject. For instance, it is known [29] that there are necessary and sufficient conditions for the existence of a CQLF for a two-mode switched system based on the convex combination of the subsystem matrices. Unfortunately, this kind of condition does not extend to the general case. [30] presents an approach based on the properties of the Lie Algebra generated by the system matrices. If the Lie algebra is solvable and other conditions on the system matrices are satisfied, then the switched system is globally uniformly exponentially stable. These conditions have been extended to the nonlinear case [30]. [31] has introduced necessary and sufficient conditions for the asymptotic stability of switched linear systems showing that this problem is equivalent to the case of robust asymptotic stability for polytopic uncertain linear time variant systems [31].

Stability under constrained switching: It is known that fast switching may produce instabilities, even when all subsystems are stable. Therefore, if the switching is sufficiently slow, the transient switching effects have a chance to disappear, and the system is stable. This slow switching frequency condition is expressed as the dwell time, which corresponds to the minimum time the system has to stay in each mode before the next switching event. This requirement may be too hard on certain situations, so the concept of average dwell time can be used for relaxing the constraint by requiring the system to stay in each system mode, on average, a minimum time [32]. The main approach to study the case of constrained switching is the use of multiple Lyapunov functions (MLF). In this case, each Lyapunov function is associated with each subsystem or with a region in state space, and these are concatenated in a way such that the value of each Lyapunov function at the beginning of its activation period is less than the value in the previous activation period. Then it can be guaranteed that the system is asymptotically stable [33]. However, it is not always easy to find the appropriate Lyapunov functions to achieve this.

2.2.1 Parameterized Control Lyapunov Functions (pCLF)

Most of the classical methods described in the previous section yield overconservative LFs for switched systems, due to the strong sufficient conditions for Lyapunov asymptotic stability. One approach to relax these conditions is the use of piecewise quadratic (PWQ) LFs, allowing each quadratic function to be positive definite and satisfy the decreasing conditions only on a subset

Cette thèse est accessible à l'adresse : http://theses.insa-lyon.fr/publication/2019LYSEI123/these.pdf
© [G. J. Becerra], [2019], INSA de Lyon, tous droits réservés

of the state-space. These conditions can be recast as a semidefinite problem (SDP). However, when this approach is applied for the synthesis of CLFs, nonlinear matrix inequalities appear in the mathematical program making it harder to solve. An alternative approach proposed in [18] and [19] allows to find less conservative CLFs for discrete-time nonlinear systems. The reduction in conservatism is achieved by considering a more general class of CLFs, where these depend on a set of varying parameters that are computed on-line by solving an optimization problem. The solution of the optimization problem also gives the control signal. A brief summary of this approach is presented next. Consider the discrete-time autonomous system

$$x_{k+1} = \phi(x_k) \tag{2.10}$$

where $x_k \in \mathbb{R}^n$ is the state at time k and $\phi : \mathbb{R}^n \to \mathbb{R}^n$ is an arbitrary map with $\phi(0) = 0$.

Definition 2.2.1. *[19] Let $\mathbb{X}$ with $0 \in int(\mathbb{X})$ be a subset of $\mathbb{R}^n$. We call system (2.10) asymptotically stable in $\mathbb{X}$ if there exists a $\mathcal{KL}$ function $\beta(\cdot,\cdot)$ such that, for each $x_0 \in \mathbb{X}$ it holds that the corresponding state trajectory of (2.10) satisfies $\|x_k\| \leq \beta(\|x_0\|, k)$, $\forall k \in \mathbb{Z}_+$. We call system (2.10) exponentially stable in $\mathbb{X}$ if $\beta(s,k) := \theta\mu^k s$ for some $\theta \in \mathbb{R}_{\geq 1}$, $\mu \in \mathbb{R}_{[0,1)}$.*

Theorem 2.2.1. *[19] Let $\mathbb{X} \subset \mathbb{R}^n$ be a positive invariant (PI) set for (2.10) with $0 \in int(\mathbb{X})$. Furthermore, let $\alpha_1, \alpha_2 \in \mathcal{K}_\infty, \rho \in \mathbb{R}_{[0,1)}$ and let $V : \mathbb{R}^n \to \mathbb{R}_+$ be a function such that:*

$$\alpha_1(\|x\|) \leq V(x) \leq \alpha_2(\|x\|), \forall x \in \mathbb{X} \tag{2.11a}$$
$$V(\phi(x)) \leq \rho V(x), \forall x \in \mathbb{X} \tag{2.11b}$$

Then, system (2.10) is asymptotically stable on $\mathbb{X}$.

A function V that satisfies (2.11) is called a Lyapunov function (LF), and ρ is the decrease rate of V.

Let $\mathbb{Q}$ denote a set of parameter sets, where each element of $\mathbb{Q}$ contains a finite number of parameters with an arbitrary structure (for instance, a matrix of certain fixed dimensions). Define a function $V : \mathbb{R}^n \times \mathbb{Q} \to \mathbb{R}_+$, $V(0, Q) = 0\ \forall Q \in \mathbb{Q}$. Consider the discrete time system

$$x_{k+1} = \phi(x_k, u_k) \tag{2.12}$$

where $x_k \in \mathbb{X} \subseteq \mathbb{R}^n$ is the state, $u_k \in \mathbb{U} \subseteq \mathbb{R}^m$ is the input, $\phi : \mathbb{R}^n \times \mathbb{R}^m \to \mathbb{R}^n$ is an arbitrary map with $\phi(0,0) = 0$ and $\mathbb{X}$, $\mathbb{U}$ contain the origin in their interior.

Definition 2.2.2. *The set $\mathbb{X} \subseteq \mathbb{R}^n$ is constrained control invariant with respect to $\mathbb{U}$ (CCI($\mathbb{X}, \mathbb{U}$)) for system (2.12) if $\forall x \in \mathbb{X}$, $\exists u \in \mathbb{U}$ such that $\phi(x,u) \in \mathbb{X}$.*

Given some $x \in \mathbb{X}$, consider the following inequalities:

$$\alpha_1(\|x\|) \leq V(x, Q_1) \leq \alpha_2(\|x\|), \tag{2.13a}$$
$$V(\phi(x,u), Q_2) \leq \rho V(x, Q_1). \tag{2.13b}$$

Cette thèse est accessible à l'adresse : http://theses.insa-lyon.fr/publication/2019LYSEI123/these.pdf
© [G. J. Becerra], [2019], INSA de Lyon, tous droits réservés

Consider the set-valued map $\mathcal{Q} \rightrightarrows \mathbb{Q} \times \mathbb{Q}$

$$\mathcal{Q}(x) := \{(Q_1, Q_2) \in \mathbb{Q}^2 \mid \exists u \in \mathbb{U} \text{ s.t. } (2.13) \text{ holds}\}. \tag{2.14}$$

For any $x \in \mathbb{X}$, $\mathcal{Q} \neq \emptyset$ indicates that there exists at least one pair $(Q_1, Q_2) \in \mathbb{Q}^2$ that satisfies (2.13). $[\mathcal{Q}(x)]_1$ and $[\mathcal{Q}(x)]_2$ denote the sets where the first and second component of a pair $(Q_1, Q_2) \in \mathbb{Q}^2$ that satisfies (2.13) take values, respectively. $[\mathcal{Q}(x)]_\bullet$ represents an element of $\mathcal{Q}(x)$.

Definition 2.2.3. *A function $V(x, Q(x))$ with $Q(x) \in [\mathcal{Q}(x)]_1$ is called a weak parameterized CLF (pCLF) in $\mathbb{X}$ for system (2.12) if*

$$\mathcal{Q}(x) \neq \emptyset, \forall x \in \mathbb{X}, \tag{2.15a}$$

$$\forall [\mathcal{Q}(x)]_\bullet \in \mathcal{Q}(x), \exists u \in \pi(x, [\mathcal{Q}(x)]_\bullet)$$

$$s.t.\ [\mathcal{Q}(x)]_2 \cap [\mathcal{Q}(\phi(x,u))]_1 \neq \emptyset, \forall x \in \mathbb{X} \tag{2.15b}$$

The following optimization problem can be solved at each time k to obtain a trajectory-dependent pCLF.

Problem 2.2.1. *Let $x_k \in \mathbb{R}$ be known at each k. Let $x_k^+ := \phi(x_k, u_k)$ for all k. Consider the following optimization problem:*

$$\inf_{u_k, Q(x_k^+)} \quad J(x_k, u_k, Q(x_k^+)) := \rho V(x_k, Q(x_k)) - V(x_k^+, Q(x_k^+)) \tag{2.16a}$$

$$s.t. \quad x_k^+ \in \mathbb{X}, u_k \in \mathbb{U}, \tag{2.16b}$$

$$\alpha_1(\|x_k\|) \leq V(x_k, Q(x_k)) \leq \alpha_2(\|x_k\|) \tag{2.16c}$$

$$\alpha_1(\|x_k^+\|) \leq V(x_k^+, Q(x_k^+)) \leq \alpha_2(\|x_k^+\|) \tag{2.16d}$$

$$V(x_k^+, Q(x_k^+)) \leq \rho V(x_k, Q(x_k)) \tag{2.16e}$$

If $k = 0$, find a $u(0)$ and a $(Q(x_0^+), Q(x_0)) \in \mathbb{Q}^2$ that satisfy (2.16). If $k \geq 1$ set $Q(x_k) = Q(x_{k-1}^+)$ and find $u_k \in \mathbb{U}$ and $Q(x_k^+) \in \mathbb{Q}$ that satisfy (2.16a), (2.16c), (2.16d).

Theorem 2.2.2. *Suppose that $\mathbb{X} \subseteq \mathbb{R}^n$ is CCI($\mathbb{X}, \mathbb{U}$) set for system (2.12). Also, assume the existence of a weak pCLF in $\mathbb{X}$. Moreover, let $Q(x_0)$ take any value in $[\mathcal{Q}(x_0)]_1$. Then the difference equation*

$$x_{k+1} = \phi(x_k, u_k^*) \tag{2.17}$$

is asymptotically stable in $\mathbb{X}$.

Proof. [19]. □

Cette thèse est accessible à l'adresse : http://theses.insa-lyon.fr/publication/2019LYSEI123/these.pdf
© [G. J. Becerra], [2019], INSA de Lyon, tous droits réservés

Assuming that the system (2.12) is affine in u_k and considering quadratic pCLFs, problem (2.16) can be written as the following SDP:

$$\min_{u_k, Q(x_k), Z_k} \quad \varepsilon_k \tag{2.18a}$$

$$\text{s.t.} \quad \phi(x_k, u_k) \in \mathbb{X}, \quad u_k \in \mathbb{U} \tag{2.18b}$$

$$x_k^\intercal \left(Q(x_k) - \gamma I_n\right) x_k \geq 0 \tag{2.18c}$$

$$x_k^\intercal \left(\Gamma I_n - Q(x_k)\right) x_k \geq 0 \tag{2.18d}$$

$$Z_k - \Gamma^{-1} I_n \succeq 0, \quad \gamma^{-1} I_n - Z_k \succeq 0 \tag{2.18e}$$

$$\begin{bmatrix} \rho x_k^\intercal Q(x_k) x_k & \phi(x_k, u_k) \\ \phi(x_k, u_k) & Z_k \end{bmatrix} \succeq 0 \tag{2.18f}$$

$$\varepsilon_k I_{n+1} - \begin{bmatrix} \rho x_k^\intercal Q(x_k) x_k & \phi(x_k, u_k) \\ \phi(x_k, u_k) & Z_k \end{bmatrix} \succeq 0 \tag{2.18g}$$

Lemma 2.2.1. *Let $k \in \mathbb{Z}_+$ and let $x(k) \in \mathbb{X}$, γ, Γ, and ρ be known. Suppose that $\{u_k, Q(x_k), Z_k\}$ are a feasible solution of problem (2.18). Then, $V(x_k, Q(x_k)) = x_k^\intercal Q(x_k) x_k$, $Q(x_k^+) = Z_k^{-1}$ and u_k are a solution for problem (2.16) with $\alpha_1(s) := \gamma s^2$ and $\alpha_2(s) := \Gamma s^2$.*

Proof. See [19]. □

The solution of problem (2.18) at each time k yields a control signal u_k that asymptotically stabilizes the system $x_{k+1} = \phi(x_k, u_k)$ towards the equilibrium point at the origin. It also yields the values of the varying parameters that determine the values of the CLFs $Q(x_k)$ and $Q(x_k^+)$ at each time k.

2.3 Method of Moments

The method of moments emerges from the study of the classical problem of finding a map that takes a sequence of real numbers $\{m_0, m_1, m_2, \ldots\}$ to a measure μ such that

$$m_i = \int_{\mathbb{R}} s^n d\mu(s), \quad \text{for } i = \{0, 1, 2, \ldots\}. \tag{2.19}$$

The number m_i corresponds to the i^{th} moment of μ, and the sequence $\{m_i\}$ is the moment sequence of μ. The basic idea of this method is that, under certain conditions, a given non-linear non-convex optimization problem can be expressed as a linear convex problem. This method is based on results introduced by [34] for the global optimization of polynomials based on results from the problem of moments. A brief summary or the method is presented next.

Lemma 2.3.1. *Let $f(s) = \sum_{k=0}^{L-1} \Gamma_k s^k$, $f(s) \in \mathbb{R}[s]$ be an even degree polynomial whose leading coefficient is positive. The convex hull of the graph of f is given by*

$$co(graph(f)) = \left\{ \int_{\mathbb{R}} (s, f(s))\, d\mu(s) : \mu \in P(\mathbb{R}) \right\} \tag{2.20}$$

Cette thèse est accessible à l'adresse : http://theses.insa-lyon.fr/publication/2019LYSEI123/these.pdf
© [G. J. Becerra], [2019], INSA de Lyon, tous droits réservés

where $P(\mathbb{R})$ corresponds to the family of all probability measures supported on the real line.

From this lemma it can be seen that the convex hull of a set has a relationship with measure theory, particularly with probability measures. Obtaining the convex hull of a polynomial function can be stated as the optimization problem of finding a measure μ supported on the real numbers such that it minimizes the Lebesgue integral of the function.

Theorem 2.3.1. *Assume that f is a coercive polynomial with a single global minimum at s^*, then the optimization problem*

$$\min_{\mu \in P(\mathbb{R})} \int_{\mathbb{R}} f(s) d\mu(s) \tag{2.21}$$

has a unique solution given by the Dirac measure δ_s^*.

The problem of determining if a given sequence (finite or infinite) of numbers correspond to the moments of a representing measure and whether it is unique is known as the moment problem. There are certain positivity conditions on the sequence of moments that are sufficient and necessary for a measure to be representative of these.

Theorem 2.3.2 (The full moment problem)**.** *Let $m = (m_\beta) \subset \mathbb{R}$ be an infinite sequence where $\beta \in \mathbb{N}^n$. The sequence m has a representing Borel measure on $\mathbb{R}$ if and only if the Hankel matrix $H_n(m)(i,j) = (m_{i+j}(t))_{i,j=0}^{L/2} \succeq 0$, $m_0(t) = 1$ for all $n \in \mathbb{N}$.*

The optimization problem in Eq. (2.21) can be transformed into a new optimization problem

$$\min_{m \in M} \sum_{k=0}^{L} \alpha_k m_k \tag{2.22}$$

where M is the convex set of all vectors in $\mathbb{R}^{L+1}$ whose entries are the algebraic moments of a probability measure supported on the real line.

Theorem 2.3.3. *Let $f(s) = \sum_{k=0}^{L-1} \alpha_k s^k$ be a coercive polynomial with a single global minimum s^*. The solution of the mathematical problem*

$$\min_{m \in M} \sum_{k=0}^{L} \alpha_k m_k \;\; s.t. \;\; H_n(m)(i,j) = (m_{i+j})_{i,j=0}^{L/2} \succeq 0, \; m_0 = 1 \tag{2.23}$$

is the vector $m^* \in \mathbb{R}^{L+1}$ which is composed of the algebraic moments of the Dirac measure δ_{s^*}. That is $m_k^* = (s^*)^k$, for $k = 0, 1, \ldots, L$.

2.4 Varieties, Ideals and Groebner Basis

Algebraic geometry deals with the relation between certain classes of algebraic and geometric objects. The geometric objects are called *affine varieties*,

Cette thèse est accessible à l'adresse : http://theses.insa-lyon.fr/publication/2019LYSEI123/these.pdf
© [G. J. Becerra], [2019], INSA de Lyon, tous droits réservés

which correspond to curves and surfaces or similar higher dimensional objects. These geometric objects are defined by sets of polynomial equations. These polynomials generate the algebraic objects known as *ideals*. The importance of ideals is that they provide a language for computing with affine varieties. Also, there is a correspondence between ideals and varieties that allows to draw conclusions on the structure of varieties by examining the structure of ideals. A brief introduction to the main concepts in algebraic geometry is presented next.

Definition 1 (Affine Variety)**.** Let K be a field, $f_1, \ldots, f_s$ be polynomials in the ring $K[x_1, \ldots, x_n]$. The set

$$\mathbf{V}(f_1, \ldots, f_s) = \{(a_1, \ldots, a_n) \in K^n : f_i(a_1, \ldots, a_n) = 0,\ \forall i \in \{1, \ldots, s\}\}$$

is called the affine variety defined by $f_1, \ldots, f_s$.

Thus, an affine variety corresponds to the set of points in n-dimensional affine space K^n where all f_i polynomial functions vanish simultaneously. Familiar geometric objects such as the line, the plane, the circle and the ellipse correspond to affine varieties. The set of defining equations $f_1 = \cdots = f_s = 0$ define an implicit representation of the affine variety. An alternative representation for the set of solutions known as a parametrization may also be available. In this representation the variables $x_1, \ldots, x_n$ are defined explicitly as functions of some parameters: $x_1 = p_1(t_1, t_2, \ldots, t_m), \ldots, x_n = p_n(t_1, t_2, \ldots, t_m)$, where each p_i is a polynomial or rational polynomial function defined for the set of parameters $\{t_1, t_2, \ldots, t_m\}$. It is not always possible to obtain a parametric representation for an affine variety, given its defining implicit equations. However, the opposite process of finding the implicit representation given a parametrization can be done using elimination theory. Before reviewing this, the main algebraic object must be introduced, which is related to the parametric and implicit representations just discussed.

Definition 2 (Ideal)**.** A subset $I \subset K[x_1, \ldots, x_n]$ is an ideal if it satisfies:

1. $0 \in I$ (The zero polynomial is in the ideal)
2. If $f, g \in I$, then $f + g \in I$ (Closure property under addition for the elements of the ideal)
3. If $f \in I$ and $h \in K[x_1, \ldots, x_n]$, then $hf \in I$ (Absorbent property for multiplication by an element in the ideal)

The ideal generated by the set of polynomials $f_1, \ldots, f_s$ is represented by

$$\langle f_1, \ldots, f_s \rangle = \left\{ \sum_{i=1}^{s} h_i f_i : h_1, \ldots, h_s \in K[x_1, \ldots, x_n] \right\}. \tag{2.24}$$

Notice here that a set of polynomials $f_1, \ldots, f_s$ can be used both for defining the locus of an affine variety (Definition 1) or for specifying the generating set for an ideal (Definition 2). This fact represents just a small part in the deep relationship existing between affine varieties and ideals.

Cette thèse est accessible à l'adresse : http://theses.insa-lyon.fr/publication/2019LYSEI123/these.pdf
© [G. J. Becerra], [2019], INSA de Lyon, tous droits réservés

Theorem 2.4.1 (Ideal-Variety Correspondence). *Let K be an arbitrary field. If $I_1 \subset I_2$ are ideals, then $\mathbf{V}(I_1) \supset \mathbf{V}(I_2)$ and similarly, if $V_1 \subset V_2$ are varieties, then $\mathbf{I}(V_1) \supset \mathbf{I}(V_2)$.*

Proof. See [35], Ch. 4. □

The properties presented in this lemma are a direct consequence of the *Nullstellensatz*. Another important result known as the Hilbert Basis Theorem states that every ideal in $K[x_1, \ldots, x_n]$ is generated by a finite set (a basis) of polynomials. There can be many different bases for a given ideal, but there is a special one known as the *Groebner basis* whose properties are very useful for characterizations and computations with ideals.

Definition 3 (Groebner Basis). Given a monomial order on $K[x_1, \ldots, x_n]$, a finite subset $G = \{g_1, \ldots, g_t\}$ of an ideal I is said to be a Groebner basis if and only if the leading term on any element of I is divisible by the leading term of one of the g_i.

This definition may not clearly illustrate the importance of these bases as good generating sets for ideals. When a polynomial f is divided by a Groebner basis as $f = a_1 g_1 + \cdots + a_t g_t + r$, the remainder r is uniquely determined. The condition that the remainder r is zero if and only if $f \in I$ is useful for testing the membership of the polynomial f to the ideal I. Another application for Groebner bases is in finding the implicit representation of a set of parametric equations by eliminating the parameter variables. The concept of an elimination ideal becomes relevant here.

Definition 4 (Elimination ideal). Given $I = \langle f_1, \ldots, f_s \rangle \subset K[x_1, \ldots, x_n]$, the l^{th} elimination ideal I_l is the ideal of $K[x_{l+1}, \ldots, x_n]$ defined by $I_l = I \cap K[x_{l+1}, \ldots, x_n]$.

We present now the theorem that allows to perform the elimination step for obtaining the implicit representation for an affine variety.

Theorem 2.4.2 (Elimination Theorem). *Let $I \subset K[x_1, \ldots, x_n]$ be an ideal and let G be a Groebner basis of I with respect to lexicographic order where $x_1 > x_2 > \cdots > x_n$. Then, for every $0 \leq l \leq n$, the set $G_l = G \cap K[x_{l+1}, \ldots, x_n]$ is a Groebner basis of the l^{th} elimination ideal I_l.*

Proof. See [35], Ch. 3. □

The relevance of this theorem is that by computing a Groebner basis an elimination ideal can be found that does not involve any of the parameters that are to be eliminated. Eliminating the parameters is called implicitization, that is, obtaining a set of implicit defining equations given a parametric representation.

Cette thèse est accessible à l'adresse : http://theses.insa-lyon.fr/publication/2019LYSEI123/these.pdf
© [G. J. Becerra], [2019], INSA de Lyon, tous droits réservés

2.5 Direct Filtering for State Estimation of Unknown Systems

In the present work, we make use of a direct approach for designing state estimators directly from data, without identifying a mathematical model for the system. This approach is based on the set membership (SM) framework introduced by [36] and later expanded by [37] and [38]. While the traditional identification methods require *a priori* assumptions on the system class (linear, bilinear, polynomial, etc), the SM approach does require less restrictive assumptions, in the form of bounds on the function gradients. Consider the discrete-time nonlinear system

$$\begin{aligned} x^{t+1} &= F(x^t, \tilde{u}^t, \tilde{d}^t, w^t) \\ \tilde{y}^t &= G(x^t, \tilde{u}^t, \tilde{d}^t, w^t) \\ v^t &= H(x^t, \tilde{u}^t, \tilde{d}^t) \end{aligned} \tag{2.25}$$

where $x^t \in \mathbb{R}^{n_x}$ corresponds to the state, $\tilde{d}^t \in \mathbb{R}^{n_d}$ the controlled input, $\tilde{u}^t \in \mathbb{R}^{n_u}$ the measurable but uncontrolled input, $\tilde{y}^t \in \mathbb{R}^{n_y}$ the measurable output, $v^t \in \mathbb{R}$ the variable we want to estimate and w^t the noise. A causal estimator for v^t is a function f mapping the past m values for inputs $\tilde{d}$, $\tilde{u}$ and output $\tilde{y}$ into an estimate $\hat{v}^t$:

$$\hat{v}^t = f(\tilde{d}^t, \tilde{y}^t, \tilde{u}^t, \tilde{d}^{t-1}, \tilde{y}^{t-1}, \tilde{u}^{t-1}, \ldots, \tilde{d}^{t-m+1}, \tilde{y}^{t-m+1}, \tilde{u}^{t-m+1}) \tag{2.26}$$

The objective is to obtain a causal filter with small estimation error $v^t - \hat{v}^t$. The filter structure in this case is non-linear finite impulse response (NFIR). This method is optimal in the sense of approximating a filter function f such that the worst case estimation error is minimized. This provides a means to compute not only the estimate but the tightest error bounds, allowing to quantify the uncertainty associated to the estimation process. One of the advantages of this method is that the considered NFIR estimators are guaranteed to be bounded input - bounded output (BIBO) stable. The following assumptions are considered:

1. The system functions F, G, H are unknown.
2. The system is n-step observable [38].
3. The noise w^t is unknown, but known to be bounded in l_p-norm.
4. A dataset $\mathcal{D} = \{(\tilde{\boldsymbol{\varphi}}^t, \tilde{v}^t), t = 1, 2, \ldots, N\}$ is available, where

$$\tilde{\boldsymbol{\varphi}}^t = [\tilde{\mathbf{d}}^{t,m}; \tilde{\mathbf{y}}^{t,m}; \tilde{\mathbf{u}}^{t,m}] \tag{2.27}$$

corresponds to a column vector concatenation of the last m measured values at time t for each variable $(\tilde{d}, \tilde{y}, \tilde{u})$. $\tilde{v}^t = v^t + \xi^t$ is the noise corrupted measurement of v^t, with ξ^t the unknown but bounded measurement noise. Notice that each of the N regressors $\tilde{\boldsymbol{\varphi}}^t$ is associated with a value $\tilde{v}^t$.

Cette thèse est accessible à l'adresse : http://theses.insa-lyon.fr/publication/2019LYSEI123/these.pdf
© [G. J. Becerra], [2019], INSA de Lyon, tous droits réservés

The design process allows to find an approximation $\hat{f}$ of the unknown optimal filter f_0 from the dataset $\mathcal{D}$. This dataset is obtained for different input sequences which should provide sufficient exploration of the regressor domain. Consider the filter with NFIR structure $\hat{v}^t = f(\tilde{\boldsymbol{\varphi}}^t)$. Let us assume that the filter function f belongs to the set of Lipschitz continuous functions

$$\mathcal{F}(\gamma) = \left\{ f \in C^1 : \left\| f'(\boldsymbol{\varphi}) \right\| \leq \gamma, \forall \boldsymbol{\varphi} \in \mathfrak{R} \right\} \tag{2.28}$$

where f' is the gradient of f and $\mathfrak{R} \subseteq \mathbb{R}^{(n_d+n_y+n_u)m}$ is the regressor domain. Regarding the noise assumptions let us define

$$e^t \doteq \tilde{v}^t - f_0(\tilde{\boldsymbol{\varphi}}^t) = \xi^t + e_0^t \tag{2.29}$$

where $\xi^t = \tilde{v}^t - v^t$ is the measurement error and $e_0^t = v^t - \hat{v}_0^t$ is the estimation error of the optimal filter f_0. Assuming that ξ^t is bounded, it follows that e^t is bounded:

$$|e^t| \leq \varepsilon, t = 1, 2, \ldots, N. \tag{2.30}$$

Based on these assumptions, the Feasible Filter Set (FFS) is defined as:

$$FFS \doteq \left\{ f \in \mathcal{F}(\gamma) : \left| \tilde{v}^t - f(\tilde{\boldsymbol{\varphi}}^t) \right| \leq \varepsilon, t = 1, \ldots, N \right\} \tag{2.31}$$

This set corresponds to the smallest set containing f_0, or equivalently, the set of all systems consistent with prior information and measured data. The problem here consists on choosing γ and ε such that the set FFS is not empty. Let us define the following functions:

$$\overline{f}_c(\tilde{\boldsymbol{\phi}}^t) = \min_{k=1,\ldots,N} \left(\tilde{v}^k + \varepsilon + \gamma \left\| \tilde{\boldsymbol{\phi}}^t - \tilde{\boldsymbol{\varphi}}^k \right\| \right) \tag{2.32}$$

$$\underline{f}_c(\tilde{\boldsymbol{\phi}}^t) = \max_{k=1,\ldots,N} \left(\tilde{v}^k - \varepsilon - \gamma \left\| \tilde{\boldsymbol{\phi}}^t - \tilde{\boldsymbol{\varphi}}^k \right\| \right) \tag{2.33}$$

The following result is useful for checking the validity of prior assumptions:

Theorem 2.5.1.

1. *A necessary condition for the FFS to be non-empty is* $\overline{f}\left(\tilde{\boldsymbol{\varphi}}^k\right) \geq \tilde{v}^k - \varepsilon$, $k = 1, \ldots, N$.
2. *A sufficient condition for the FFS to be non-empty is* $\overline{f}\left(\tilde{\boldsymbol{\varphi}}^k\right) > \tilde{v}^k - \varepsilon$, $k = 1, \ldots, N$.

Proof. See [36]. □

Using these conditions, the values γ and ε can be properly chosen. A procedure for achieving this is presented in [36]. Specifically, for each ε value, a boundary value of γ^* separating the region $FFS = \emptyset$ from the region $FFS \neq \emptyset$ can be found. Therefore, if an estimate for ε is available, it is reasonable to choose γ as a slightly higher value than $\gamma^*(\varepsilon)$. Using these

Cette thèse est accessible à l'adresse : http://theses.insa-lyon.fr/publication/2019LYSEI123/these.pdf
© [G. J. Becerra], [2019], INSA de Lyon, tous droits réservés

parameters, the direct filter is defined in terms of the optimal tightest bounds in Eqs (2.32),(2.33):

$$\hat{v}^t = f_c\left(\tilde{\boldsymbol{\varphi}}^t\right) \doteq \frac{1}{2}\left[\overline{f}\left(\tilde{\boldsymbol{\varphi}}^t\right) + \underline{f}\left(\tilde{\boldsymbol{\varphi}}^t\right)\right] \tag{2.34}$$

The main advantage of this approach is that the optimal bounds provide a measure of confidence on the obtained estimates, which is not available in other approaches like the well known Kalman filter.

2.6 Conclusion

A brief review of the main themes in this work has been presented. An introduction to power converters, their basic properties and some modeling approaches for different topologies have been discussed. These devices constitute the main application for the developed control and observation approaches for switched systems. The existence of discontinuous conduction modes in power converters has also been discussed.

Lyapunov's stability theory is the main tool used in this work for developing a novel control approach for switched systems. This method was originally developed for control-affine nonlinear systems and depends on the formulation of parameterized control Lyapunov functions. The method of moments is used as a means to translate the control problem for the switched system into a new relaxed form suitable for computation using numerical methods. These developments are presented in chapter 4.

Basic concepts and tools from algebraic geometry are introduced. These tools allow to study the relationship between the equilibrium regions for different models derived from the switched system. These methods are described in chapter 3.

Finally, a data-based estimation approach for systems with unknown model was introduced. This method is extended here for solving the state estimation problem for power converters. The practical implementation of this approach is described in chapter 5.

Cette thèse est accessible à l'adresse : http://theses.insa-lyon.fr/publication/2019LYSEI123/these.pdf
© [G. J. Becerra], [2019], INSA de Lyon, tous droits réservés

Cette thèse est accessible à l'adresse : http://theses.insa-lyon.fr/publication/2019LYSEI123/these.pdf
© [G. J. Becerra], [2019], INSA de Lyon, tous droits réservés

Chapter 3

Moment Relaxations of Switched Systems

3.1 Introduction

A starting point for the study of dynamic systems usually involves studying the set of steady solutions that do not have a temporal evolution, which is called the equilibria. These steady solutions provide valuable information for performing further analysis such as evaluating the stability of the system. Thus, a unifying approach for analyzing the properties of the set of equilibrium points of switched systems, regardless of the dimension or the number of operation modes, is needed.

One of the main applications of equilibrium point analysis is to find admissible references in switched dynamic systems but also to address the problem of no common equilibrium points of some systems. This chapter deals with the equilibrium of switched systems using relaxed representations. A density theorem in infinite time [39] shows that switching laws exist such that the trajectories of a relaxed switched system can be approached as close as desired by a switched system. It has been shown that relaxed representations of switched systems can be used in the solution of optimal control problems [40] [41].

This chapter presents an analysis of the equilibria regions for different models derived from the switched system, using tools from algebraic geometry. The analysis of the set of equilibrium points is achieved by defining it as a region in state space defined by a set of polynomial equations. Tools from algebraic geometry are used for making inferences on the geometry of the equilibrium regions by analyzing the corresponding algebraic parameterizations. This method can be used to study switched systems with more than two dimensions and more than two modes. It also allows to find relationships between the different switched system formulations introduced here, revealing an underlying common structure in them. With this new approach, information about the geometry of the equilibrium region is obtained without explicitly computing all equilibrium points.

3.2 Contribution

The main original contributions in this chapter are:

Cette thèse est accessible à l'adresse : http://theses.insa-lyon.fr/publication/2019LYSEI123/these.pdf
© [G. J. Becerra], [2019], INSA de Lyon, tous droits réservés

1. Formulation of the switched system as a polynomial system using Lagrange polynomials (Section 3.4).
2. Derivation of model relaxations for the polynomial system using the method of moments introduced in section 2.3 (Section 3.4).
3. Analysis of the geometric properties of the equilibrium regions for the average, polynomial and relaxed models using Groebner bases introduced in section 2.4 (Section 3.5).

3.3 Linear Switched Dynamic Systems

Consider a linear switched dynamic system (LSDS) characterized by a family of linear differential equations

$$\dot{x}(t) = A_{\sigma(t)}x(t) + B_{\sigma(t)} \tag{3.1}$$

where $x(t) \in \mathbb{R}^n$ corresponds to the continuous state, $\sigma(t) : [0, \infty) \to \mathcal{S} = \{s_1, s_2, \ldots, s_p\}$ is a piecewise constant input, with $\mathcal{S}$ a set of numerical labels associated to the different operation modes and $\mathcal{I} = \{1, 2, \ldots, p\}$ the set of corresponding indexes for those operation modes. $A_\sigma \in \mathbb{R}^{n\times n}$ and $B_\sigma \in \mathbb{R}^{n\times m}$ are matrices with appropriate dimensions. The signal $\sigma(t)$ is the control input that will be used to select the active mode, and $u(t)$ is an uncontrolled exogenous measurable input. In general $u(t)$ will be constant, but can be a source of disturbances. Notice that we assume no explicit dependence of time in the equations.

The family of linear differential equations (3.1) can be written in a single expression using a set of *switching functions* $h_j(\cdot)$:

$$\dot{x}(t) = \sum_{j=1}^{p} h_j(\sigma(t)) \left[A_{s_j}x(t) + b_{s_j}\right], \qquad h_j(\sigma) = \begin{cases} 1 & \text{if } \sigma = s_j \\ 0 & \text{if } \sigma \neq s_j \end{cases} \tag{3.2}$$

Eq. (3.2) guarantees that only one mode is active at any time because $h_j \in \{0, 1\}$. For the trivial case when $\sigma(t) = s_j$, $\forall t$, where s_j is one of the system modes, the behavior is that of the single selected mode with the system state approaching the unique equilibrium point $\bar{x}$ determined by $A_{s_j}\bar{x} + b_{s_j} = 0$ (assuming A_{s_j} is nonsingular).

The equilibrium points for all individual subsystems may be different. If some or all the system modes are selected alternatively in a certain periodic sequence during predetermined time intervals, the system state will show a cyclic behavior, approaching a steady cycle. We will refer to this periodic sequence of modes as a switching regime.

Assumption 3.3.1. *The modes σ in system (3.2) are activated in sequence $\{i_1, i_2, \ldots, i_p\}$, $i_j \in \mathcal{I}$, each with a duration of $d_{i_j}T$, where T is the total switching period.*

Notice that if the switching period T is decreased, the limit cycle will converge towards a single point equal to the average of $x(t)$ over the time

Cette thèse est accessible à l'adresse : http://theses.insa-lyon.fr/publication/2019LYSEI123/these.pdf
© [G. J. Becerra], [2019], INSA de Lyon, tous droits réservés

period. This fact is the basis for the approximation used for deriving average models for switched systems.

3.4 Polynomial and Relaxed Models for Linear Switched Dynamic Systems

Let us define the average $\bar{x}$ of $x(t)$, as follows:

$$\bar{x}(t) = \frac{1}{T_p} \int_{t-T_p}^{t} x(\tau) d\tau \tag{3.3}$$

where T_p is the period of the cycle. the dynamical model of $\bar{x}(t)$ is obtained by differentiating (3.3). Nevertheless, this derivative is generally intractable or unusable because of its non-linear form. It can be proven that if T_p is small compared to the system dynamics, the state x corresponding to the average model approximates $\bar{x}$ [26][39].

The dynamics of the switched system can be approximated by an average model computed as the weighted sum of the switched system modes. In this case the equilibrium points of the average model will approximate the operation points of the switched system. A convex combination of subsystems is obtained, where the convexity characteristic refers to weighting each system mode by its corresponding activation time interval.

Definition 5 (Average Model)**.** The system defined by the differential equation

$$\dot{x}(t) = \sum_{j=1}^{p} d_j(t) \left[A_{s_j} x(t) + b_{s_j} \right] \tag{3.4}$$

is an average model of (3.2), where the switching functions $h_j(\cdot)$ are replaced by $d_j(t)$ constrained by the convexity conditions

$$\sum_{j=1}^{p} d_j(t) = 1,\ d_j(t) \in [0,1],\ \forall t \tag{3.5}$$

Remark 3.4.1. Notice that the value of each parameter d_j lies in the convex hull $co(\{0,1\})$ of the range set for the switching functions $h_j(\cdot)$ in Eq. (3.2), and equals the duty cycle of the switching function $h_j(\cdot)$ for the corresponding mode. Therefore, the variables d_j are the control signals for system (3.4).

An alternative formulation for the switched system can be obtained in terms of a polynomial basis. In this context these polynomials are used as switching functions to select the active subsystem.

Definition 6 (Lagrange Interpolating Polynomial)**.** Let $\{(s_1, b_1), (s_2, b_2), \ldots, (s_Q, b_Q)\}$ be a set of data points with $s_i \neq s_j,\ \forall i, j = 1, 2, \ldots, Q,\ i \neq j$. The

Cette thèse est accessible à l'adresse : http://theses.insa-lyon.fr/publication/2019LYSEI123/these.pdf
© [G. J. Becerra], [2019], INSA de Lyon, tous droits réservés

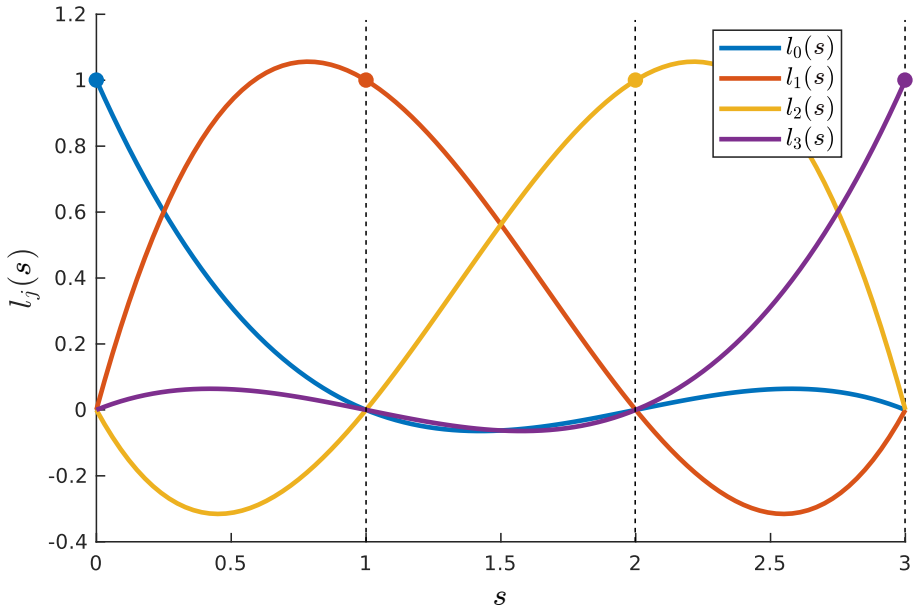

FIGURE 3.1 – Basis of Lagrange polynomials in Eq. (3.7) for the set of points $(s, b) \in \{(0,1),(1,1),(2,1),(3,1)\}$.

interpolating polynomial in the Lagrange form is a linear combination of Lagrange basis polynomials as

$$L(s) = \sum_{j=1}^{Q} b_j l_j(s) \tag{3.6}$$

where the basis polynomials $l_j(s)$ take the form

$$\begin{aligned} l_j(s) &= \prod_{\substack{i=1 \\ i \neq j}}^{Q} \frac{s - s_i}{s_j - s_i} \\ &= \frac{s - s_0}{s_j - s_0} \cdot \frac{s - s_1}{s_j - s_1} \cdots \frac{s - s_{j-1}}{s_j - s_{j-1}} \cdot \frac{s - s_{j+1}}{s_j - s_{j+1}} \cdots \frac{s - s_Q}{s_j - s_Q} \end{aligned} \tag{3.7}$$

The condition $i \neq j$ is necessary to guarantee that none of the terms in the product have a vanishing denominator. Fig. 3.1 shows an example of the basis of Lagrange polynomials obtained for 4 equally spaced points in the interval $[0, 3]$.

The following lemma states an important property of the basis of Lagrange polynomials.

Lemma 3.4.1. *Given a basis of Lagrange polynomials as defined in Eq. (3.7), the following condition is always satisfied:*

$$\sum_{j=1}^{Q} l_j(a) = 1, \ \forall \ a \in \mathbb{R}$$

Cette thèse est accessible à l'adresse : http://theses.insa-lyon.fr/publication/2019LYSEI123/these.pdf
© [G. J. Becerra], [2019], INSA de Lyon, tous droits réservés

Proof. Given the function $f(x) = 1$, any set of points $\{x_1, x_2, \ldots, x_n\}$ such that $f(x_1) = f(x_2) = \cdots = f(x_n) = 1$ perfectly interpolates the $f(\cdot)$ function by the 0^{th}-order polynomial $p(x) = 1$. The Lagrange form for the interpolating polynomial is given by

$$p(x) = \sum_{j=1}^{k} f(x_j) l_j(x) = \sum_{j=1}^{k} l_j(x)$$

Since the interpolating polynomial for a set of points is unique,

$$p(x) = \sum_{j=1}^{k} l_j(x) = 1$$

for all $x \in \mathbb{R}$ □

Thus, a basis of Lagrange polynomials verifies the first condition given by Eq. (3.5). Another interesting property, related to the fact that these polynomials can be used for exactly interpolating a set of points, is that for any given a_i

$$l_j(a_i) = \begin{cases} 1 & \text{if } i = j \\ 0 & \text{if } i \neq j \end{cases}$$

which can be viewed as a switching function similar to Eq. (3.2), where only one of the basis functions is active. This is used as the mode selection mechanism for a polynomial formulation of the switched system.

Definition 7 (Polynomial Model)**.** Given a finite set of system modes $\mathcal{S} = \{s_1, s_2, \ldots\ s_p\}$, $s_j \in \mathbb{R}$, the system described by

$$\dot{x}(t) = \sum_{j=1}^{p} l_j(s(t)) \left[A_{s_j} x(t) + b_{s_j} \right] \tag{3.8}$$

is the polynomial model of (3.2) where the $l_j(\cdot)$ functions correspond to a basis of Lagrange polynomials

$$l_j(s(t)) = \prod_{\substack{i=1 \\ i \neq j}}^{p} \frac{s(t) - s_i}{s_j - s_i},\ s(t) \in co(\mathcal{S}) \tag{3.9}$$

The system is represented as a combination of the different modes, but in this case the weighting parameters are given by the basis of Lagrange polynomials. Notice that $s(t)$ corresponds to the control signal for the polynomial model, and is defined in the convex hull of the set $\mathcal{S}$. This means that when $s(t) \in co(\mathcal{S}) \backslash \mathcal{S}$ more than one Lagrange polynomial will have nonzero value, representing the concept of allowing partial activation of system modes during a switching period. The difference with respect to the average model is that only variable $s(t)$ determines the activation status of the modes. After distributing and reorganizing terms as powers of $s(t)$, Eq.

Cette thèse est accessible à l'adresse : http://theses.insa-lyon.fr/publication/2019LYSEI123/these.pdf
© [G. J. Becerra], [2019], INSA de Lyon, tous droits réservés

(3.9) yields a polynomial of $p-1$ order in the s variable as follows:

$$\dot{x}(t) = \sum_{i=0}^{p-1} \left[\sum_{j=1}^{p} c_{ij} \left[A_{s_j} x(t) + b_{s_j} \right] \right] s^i(t), \tag{3.10}$$

where c_{ij} are constants. Since the terms in the inner sum are functions depending only on the system state $x(t)$, Eq. (3.10) can be rewritten as

$$\dot{x}(t) = \sum_{i=0}^{p-1} \alpha_i(x(t)) s^i(t) \tag{3.11}$$

Notice that the nonlinearity of the model (3.11) is due to the presence of powers of the control variable $s(t)$. In section 2.3 a method for transforming a non-linear, non-convex optimization problem into an equivalent linear, convex problem was introduced. This method is used here for obtaining a moment relaxation for the polynomial model in definition 7. The obtained form is more suitable for performing numerical computations such as obtaining an optimal control, as shown in [41].

Theorem 3 in [42] is used for transforming the polynomial model (3.11) into a new relaxed formulation, where the nonlinear terms introduced by the powers s^i of the control signal are replaced by new variables m_i corresponding to the algebraic moments of a measure supported on $\mathbb{R}$. This alternative form is presented next.

Definition 8 (Relaxed Model)**.** Given a finite set of system modes $\mathcal{S} = \{s_1, s_2, \ldots, s_p\}$, the system described by

$$\dot{x}(t) = \sum_{i=0}^{p-1} \alpha_i(x(t)) m_i(t) \tag{3.12}$$

is the relaxed model of (3.11), where $\{m_i\}$ corresponds to a sequence of algebraic moments representing a probability measure supported on the real line. This sequence is constrained to form a positive semidefinite Hankel matrix $H_n(m) \succeq 0$ with $m_0(t) = 1$.

In this formulation, $m_i(t)$ are the control variables. The relaxed form (3.12) is an affine function of the control variables m_i. Furthermore, the positivity constraint on the sequence of algebraic moments yields a convex set in the parameter space $(m_0, m_1, \ldots, m_{p-1}) \in \mathbb{R}^p$. The convexity of the feasible set is a desirable property when performing numerical computations such as those required for obtaining an optimal control.

3.5 Equilibrium Points for Average, Polynomial and Relaxed Models

The properties of the equilibrium regions for each of the formulations introduced in the previous section can be studied using the tools introduced

Cette thèse est accessible à l'adresse : http://theses.insa-lyon.fr/publication/2019LYSEI123/these.pdf
© [G. J. Becerra], [2019], INSA de Lyon, tous droits réservés

in [43]. This is important in the context of the control problem, because it provides information on the regions in state space that can be reached and maintained by the system for a particular switching regime. Consider the set of equilibrium points for the average model (3.4):

$$\mathbb{X}_a = \left\{ \bar{x} \in \mathbb{R}^n \;\middle|\; 0 = \sum_{j=1}^{p} \bar{d}_j \left[A_{s_j} \bar{x} + b_{s_j} \right],\ \bar{d}_j \in [0,1] \right\}, \tag{3.13}$$

for the polynomial model (3.9):

$$\mathbb{X}_p = \left\{ \bar{x} \in \mathbb{R}^n \;\middle|\; 0 = \sum_{i=0}^{p-1} \alpha_i(\bar{x}) \bar{s}^i,\ \bar{s} \in co(\mathcal{S}) \right\}, \tag{3.14}$$

and for the relaxed model (3.12):

$$\mathbb{X}_r = \left\{ \bar{x} \in \mathbb{R}^n \;\middle|\; 0 = \sum_{i=0}^{p-1} \alpha_i(\bar{x}) \bar{m}_i,\ H_n(\bar{m}) \succeq 0 \right\}. \tag{3.15}$$

Notice that in (3.13) and (3.15) the expressions contain bilinear terms $\bar{x}\bar{d}$ and $\bar{x}\bar{m}$, respectively. On the other hand, (3.14) contains powers of $\bar{s}$ multiplied by $\bar{x}$. In each of these cases, the equation can be solved explicitly to obtain a parametrization of $\bar{x}$ as functions of the control parameters $\bar{d}_j$, $\bar{s}$ and $\bar{m}_i$, assuming that the required matrix inversion can be computed.

An alternative approach to study the structure of the equilibrium regions is to compute a Groebner basis for these polynomials. This basis represents a minimal algebraic representation of the equilibrium region. This allows to use the elimination theorem 2.4.2 to compute an explicit representation of the equilibria by eliminating the parameters d_j, s and m_i in the equations. This approach allows to make inferences on the geometric properties of the equilibria based on the algebraic properties of the generating polynomials. As an illustrating example, consider the following three-mode switched system:

$$A_{s_1} = \begin{bmatrix} -5 & -2 & -2 \\ -3 & -4 & 1 \\ 4 & 1 & -2 \end{bmatrix}, \quad A_{s_2} = \begin{bmatrix} -1 & 3 & -3 \\ -2 & -5 & 4 \\ -2 & -5 & -1 \end{bmatrix}, \quad A_{s_3} = \begin{bmatrix} -2 & -5 & 4 \\ 3 & -5 & -1 \\ 0 & 2 & -5 \end{bmatrix},$$
$$b_{s_1} = \begin{bmatrix} -2 & -2 & -2 \end{bmatrix}^\intercal, \quad b_{s_2} = \begin{bmatrix} -2 & 0 & 1 \end{bmatrix}^\intercal, \quad b_{s_3} = \begin{bmatrix} 2 & -2 & 1 \end{bmatrix}^\intercal.$$

The associated average models is:

$$\dot{x} = \sum_{j=1}^{3} d_j \left[A_{s_j} x + b_{s_j} \right] = \begin{bmatrix} p_{A,1}(x_1, x_2, x_3, d_1, d_2, d_3) \\ p_{A,2}(x_1, x_2, x_3, d_1, d_2, d_3) \\ p_{A,3}(x_1, x_2, x_3, d_1, d_2, d_3) \end{bmatrix} \tag{3.16}$$

Cette thèse est accessible à l'adresse : http://theses.insa-lyon.fr/publication/2019LYSEI123/these.pdf
© [G. J. Becerra], [2019], INSA de Lyon, tous droits réservés

where the polynomials $p_{A,1}$, $p_{A,3}$, $p_{A,2}$, are

$$\begin{aligned} p_{A,1}(x_1,x_2,x_3,d_1,d_2,d_3) =& -2d_1-2d_2+2d_3-5d_1x_1-d_2x_1-2d_3x_1-2d_1x_2 \\ &+3d_2x_2-5d_3x_2-2d_1x_3-3d_2x_3+4d_3x_3 \quad (3.17a) \\ p_{A,2}(x_1,x_2,x_3,d_1,d_2,d_3) =& -2d_1-2d_3-3d_1x_1-2d_2x_1+3d_3x_1-4d_1x_2 \\ &-5d_2x_2-5d_3x_2+d_1x_3+4d_2x_3-d_3x_3 \quad (3.17b) \\ p_{A,3}(x_1,x_2,x_3,d_1,d_2,d_3) =& -2d_1+d_2+d_3+4d_1x_1-2d_2x_1+d_1x_2-5d_2x_2 \\ &+2d_3x_2-2d1x_3-d_2x_3-5d_3x_3 \quad (3.17c) \end{aligned}$$

The set of equilibrium points for the average model (3.16) is defined by the vanishing of these three polynomials, while also satisfying the constraint $q_a = d_1 + d_2 + d_3 - 1 = 0$. In the context of algebraic geometry, these four polynomials generate the ideal

$$I_A = \langle p_{a,1}, p_{a,2}, p_{a,3}, q_a \rangle. \quad (3.18)$$

Recall from the brief introduction in section 2.4 that, using elimination theory, a Groebner basis can be used to compute an implicit representation of the ideal where the parameters d_1, d_2, d_3 have been eliminated. The result may inform us on some of the properties of the equilibrium region in state space for the different models. Using a computer algebra system, the 4-th elimination ideal I_A^4 obtained by computing the Groebner basis consists of a single generating polynomial:

$$\begin{aligned} I_A^4 = \langle & 20-22x_1-54x_1^2+70x_1^3-4x_2-152x_1x_2+130x_1^2x_2-202x_2^2 \\ & +138x_1x_2^2+46x_2^3+4x_3+3x_1x_3-16x_1^2x_3+170x_2x_3 \\ & -137x_1x_2x_3-151x_2^2x_3-95x_3^2-61x_1x_3^2+39x_2x_3^2-49x_3^3\rangle. \quad (3.19) \end{aligned}$$

Now, consider the polynomial model

$$\dot{x} = \sum_{i=0}^{2} \alpha_i(x) s^i = \begin{bmatrix} p_{L,1}(x_1,x_2,x_3,s) \\ p_{L,2}(x_1,x_2,x_3,s) \\ p_{L,3}(x_1,x_2,x_3,s) \end{bmatrix}. \quad (3.20)$$

Assuming $s_1 = 1$, $s_2 = 2$, $s_3 = 3$, the polynomials in (3.20) are:

$$\begin{aligned} p_{L,1}(x_1,x_2,x_3,s) =& 2-6s+2s^2-14x_1+23/2sx_1-5/2s^2x_1-20x_2 \\ &+49/2sx_2-13/2s^2x_2+7x_3-13sx_3+4s^2x_3 \quad (3.21a) \\ p_{L,2}(x_1,x_2,x_3,s) =& -8+8s-2s^2-5sx_1+2s^2x_1-2x_2-5/2sx_2 \\ &+1/2s^2x_2-10x_3+15sx_3-4s^2x_3 \quad (3.21b) \\ p_{L,3}(x_1,x_2,x_3,s) =& -8+15/2s-3/2s^2+18x_1-18sx_1+4s^2x_1+20x_2 \\ &-51/2sx_2+13/2s^2x_2-8x_3+17/2sx_3-5/2s^2x_3 \\ & \quad (3.21c) \end{aligned}$$

Cette thèse est accessible à l'adresse : http://theses.insa-lyon.fr/publication/2019LYSEI123/these.pdf
© [G. J. Becerra], [2019], INSA de Lyon, tous droits réservés

The ideal generated by the vanishing of these polynomials is

$$I_L = \langle p_{L,1}, p_{L,2}, p_{L,3} \rangle. \tag{3.22}$$

After computing the 2nd elimination ideal, we obtain a Groebner basis with 7 polynomials:

$$\begin{aligned} I_L^2 = &\langle g_1(x_1, x_2, x_3), g_2(x_1, x_2, x_3), g_3(x_1, x_2, x_3), g_4(x_1, x_2, x_3), \\ &g_5(x_1, x_2, x_3), g_6(x_1, x_2, x_3), g_7(x_1, x_2, x_3) \rangle \end{aligned} \tag{3.23}$$

where

$$\begin{aligned} g_1(x_1, x_2, x_3) = &\, 20 - 22x_1 - 54x_1^2 + 70x_1^3 - 4x_2 - 152x_1x_2 + 130x_1^2x_2 - 202x_2^2 \\ &+ 138x_1x_2^2 + 46x_2^3 + 4x_3 + 3x_1x_3 - 16x_1^2x_3 + 170x_2x_3 - 137x_1x_2x_3 \\ &- 151x_2^2x_3 - 95x_3^2 - 61x_1x_3^2 + 39x_2x_3^2 - 49x_3^3 \end{aligned} \tag{3.24}$$

The rest of the polynomials in I_L^2 are not reproduced here since the coefficients are too big. However, notice that the first polynomial in I_L^2 is the same as the one in I_A. The relaxed model can be written as

$$\dot{x} = \sum_{i=0}^{2} \alpha_i(x) m_i = \begin{bmatrix} p_{R,1}(x_1, x_2, x_3, m_1, m_2) \\ p_{R,2}(x_1, x_2, x_3, m_1, m_2) \\ p_{R,3}(x_1, x_2, x_3, m_1, m_2) \end{bmatrix} \tag{3.25}$$

with the polynomials

$$\begin{aligned} p_{R,1}(x_1, x_2, x_3, m_1, m_2) = &\, 2 - 6m_1 + 2m_2 - 14x_1 + 23/2m_1x_1 - 5/2m_2x_1 - 20x_2 \\ &+ 49/2m_1x_2 - 13/2m_2x_2 + 7x_3 - 13m_1x_3 + 4m_2x_3 \end{aligned} \tag{3.26}$$

$$\begin{aligned} p_{R,2}(x_1, x_2, x_3, m_1, m_2) = &\, -8 + 8m_1 - 2m_2 - 5m_1x_1 + 2m_2x_1 - 2x_2 - 5/2m_1x_2 \\ &+ 1/2m_2x_2 - 10x_3 + 15m_1x_3 - 4m_2x_3 \end{aligned} \tag{3.27}$$

$$\begin{aligned} p_{R,3}(x_1, x_2, x_3, m_1, m_2) = &\, -8 + 15/2m_1 - 3/2m_2 + 18x_1 - 18m_1x_1 + 4m_2x_1 \\ &+ 20x_2 - 51/2m_1x_2 + 13/2m_2x_2 - 8x_3 + 17/2m_1x_3 - 5/2m_2x_3 \end{aligned} \tag{3.28}$$

the ideal I_M is generated by the polynomials

$$I_R = \langle p_{m,1}, p_{m,2}, p_{m,3} \rangle \tag{3.29}$$

The third elimination ideal obtained consists of a single polynomial:

$$\begin{aligned} I_R^3 = \langle &20 - 22x_1 - 54x_1^2 + 70x_1^3 - 4x_2 - 152x_1x_2 + 130x_1^2x_2 - 202x_2^2 \\ &+ 138x_1x_2^2 + 46x_2^3 + 4x_3 + 3x_1x_3 - 16x_1^2x_3 + 170x_2x_3 \\ &- 137x_1x_2x_3 - 151x_2^2x_3 - 95x_3^2 - 61x_1x_3^2 + 39x_2x_3^2 - 49x_3^3 \rangle. \end{aligned} \tag{3.30}$$

Notice that, after eliminating the control variables for each model, all the Groebner basis obtained have one polynomial in common. This fact has several implications in the geometry of the equilibrium regions for each model.

Cette thèse est accessible à l'adresse : http://theses.insa-lyon.fr/publication/2019LYSEI123/these.pdf
© [G. J. Becerra], [2019], INSA de Lyon, tous droits réservés

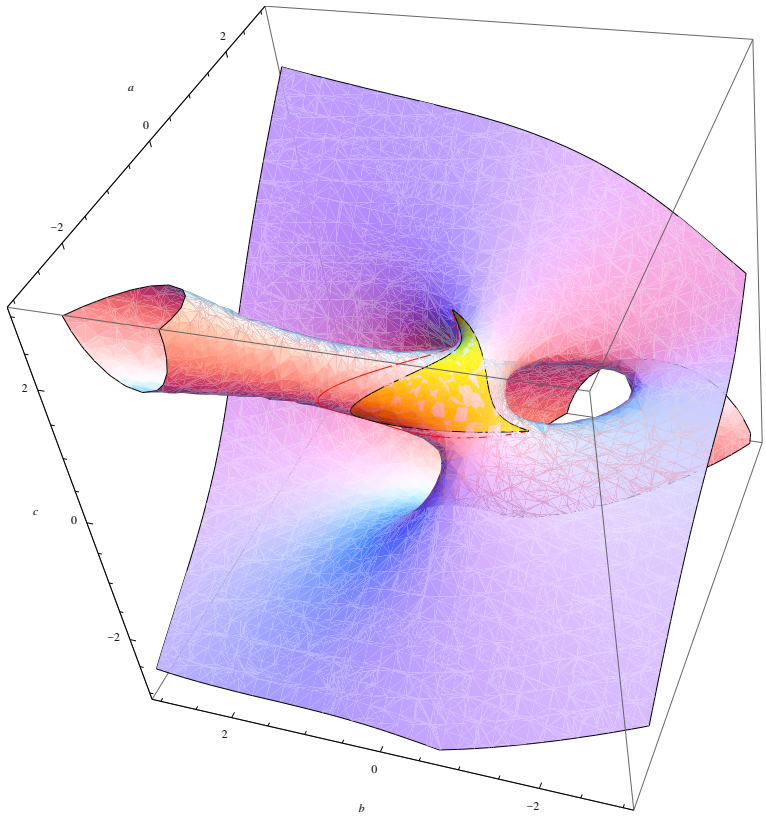

FIGURE 3.2 – Equilibria for the average (yellow) and polynomial (red) models, embedded in the same affine variety.

First, the polynomials in a basis can be interpreted like constraints in state space: as you add more of them, the set may become smaller. Fig.3.2 shows the equilibria regions for the average and polynomial models. Notice that the equilibria for the average model is a surface in $\mathbb{R}^3$, because there are three free parameters d_1, d_2, d_3 with the constraint $d_1 + d_2 + d_3 = 1$, yielding two degrees of freedom. In the case of the polynomial model, the equilibria is a curve in $\mathbb{R}^3$, which is a consequence of having a single parameter s. Notice that both sets are subsets of a bigger set, which is the affine variety associated to the ideal generated by the single polynomial that both I_A and I_L have in common. Clearly, the polynomial model is more constrained and can not reach the same regions in state space as the average model, except on three points when $s = s_1$, $s = s_2$, $s = s_3$. The difference between both regions is that the parameters used to *span* them have different characterizations: the yellow region is defined by all combinations of d_1, d_2 and d_3 that satisfy $d_1 + d_2 + d_3 = 1$, while the red region is defined by $s \in [1, 3]$.

Second, the fact that both the average and relaxed models have the same Groebner basis means that the equilibrium points for both systems are a subset of the same *affine variety*, which is generated by the single polynomial in these bases. This can be observed in Fig. 3.3, where the equilibria for the relaxed model is shown for three different mode orders. Notice that in all cases the relaxed equilibria region is a subset of the same affine variety as the previous cases. The difference here is that the parameters m_1, m_2 that define

Cette thèse est accessible à l'adresse : http://theses.insa-lyon.fr/publication/2019LYSEI123/these.pdf
© [G. J. Becerra], [2019], INSA de Lyon, tous droits réservés

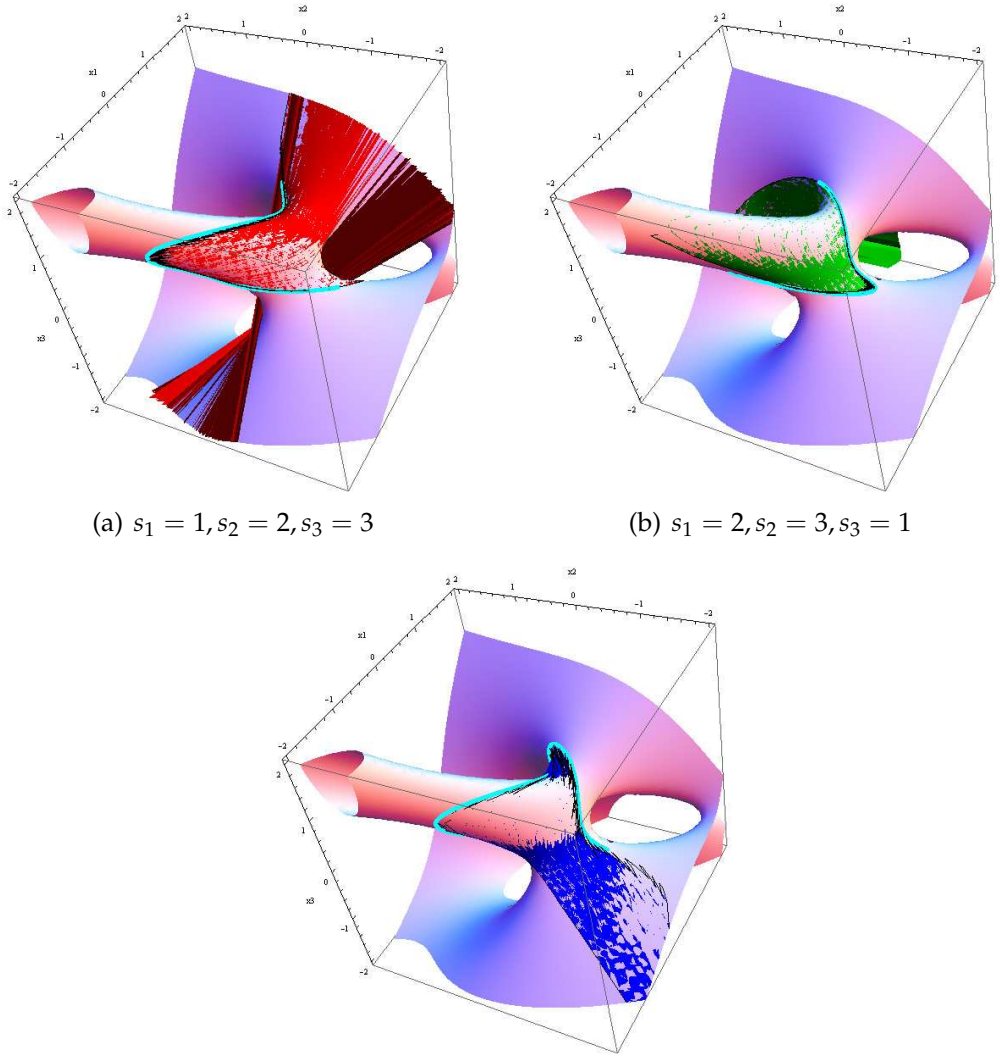

(a) $s_1 = 1, s_2 = 2, s_3 = 3$

(b) $s_1 = 2, s_2 = 3, s_3 = 1$

(c) $s_1 = 3, s_2 = 1, s_3 = 2$

FIGURE 3.3 – Equilibria for the polynomial (cyan) and relaxed (red,green,blue) models for three different mode label orders.

the surface are characterized by the condition $H(m) \succeq 0$.

These results show that a relaxed model can be obtained from a switched model such that the the equilibria region spanned by the parameters m_i in the relaxed model is the same as the region spanned by the parameters d_j in the average model, which is an approximation of the limit cycles reached by the switched model under a particular switching regime. This suggests that the control problem for the switched system can be solved using moment relaxations. The basic idea is to obtain a relaxed model, compute a control law $m_i(t)$ for it and then map this control back to the original switched control $\sigma(t)$. The benefit of this approach is that the relaxed model is easier to deal with than the switched model when a mathematical program is formulated to solve the optimal control problem [41] or the Lyapunov control problem that will be introduced in chapter 4.

Cette thèse est accessible à l'adresse : http://theses.insa-lyon.fr/publication/2019LYSEI123/these.pdf
© [G. J. Becerra], [2019], INSA de Lyon, tous droits réservés

3.6 Conclusion

The structure of a switched system imposes difficulties in its treatment, due to the nonlinearity and non-convexity associated with the presence of a switching behavior. By finding convex relaxations of these nonlinear dynamics, models with better properties for numerical computation can be found. Furthermore, a relaxation approximation enabled by the method of moments allows to find a linear model determined by convex constraints. These characteristics are desirable for performing computations based on semidefinite programming, such as finding an optimal control.

The utility of the modeling approach using moment relaxations is that the nonlinearities present in the switched system control signal σ can be mapped to a different control space m (a space of moments) where the system becomes linear, while maintaining the dynamic properties of the original switched system. It was shown that the operation points reached by the switched system under sufficiently fast sequential switching can also be reached by the relaxed system. The approach presented here will be used in the following chapter for solving the control problem for switched systems by formulating a semidefinite optimization problem that can be solved using highly efficient numerical methods.

Cette thèse est accessible à l'adresse : http://theses.insa-lyon.fr/publication/2019LYSEI123/these.pdf
© [G. J. Becerra], [2019], INSA de Lyon, tous droits réservés

Chapter 4

Parameterized Control Lyapunov Functions

4.1 Introduction

Lyapunov's stability theory has been used extensively in the analysis of system stability, and in the synthesis of asymptotically stable controllers - observers for different kinds of systems. The main approach considers a proposed candidate Lyapunov function that has the property of having a decreasing value along the system trajectories. This condition allows to compute the control laws or observer gains required to guarantee a stabilizing behavior. Usually, the conditions derived from this approach are too conservative, yielding a performance that is far from optimal. On the other hand, other approaches like optimal or predictive control may give solutions with better performance, but without stability guarantees.

In an attempt to find a middle ground between these approaches, the use of parameterized Lyapunov functions has been proposed. The basic idea is to define parameterized functions that can be tuned to obtain improvements in the performance, while maintaining the stability guarantees provided by Lyapuonv's theory. The difficulty in this approach lies in the decision needed to select the values of these parameters.

In the present chapter we present a general approach for the synthesis of a parameterized control law using the Lyapunov conditions for the case of the multicellular converter introduced in section 2.1.4. This approach is developed using the port Hamiltonian model, and a diagonal matrix is used to parameterize the Lyapunov function. An analysis of the resulting decision surfaces depending on these parameters is presented. Also, a new approach to the use of parameterized Lyapunov functions for switched systems is presented in section 4.4. This method can be applied to different converter topologies and shows good control performance results. A discussion on the computational complexity is also presented.

4.2 Contribution

The main original contributions in this chapter are:

Cette thèse est accessible à l'adresse : http://theses.insa-lyon.fr/publication/2019LYSEI123/these.pdf
© [G. J. Becerra], [2019], INSA de Lyon, tous droits réservés

1. Formulation of a basic approach to solve the control problem using parameterized control Lyapunov functions with fixed parameters (Section 4.3).

2. Derivation of model relaxations for the switched system using the methods introduced in chapter 3 (Section 4.4.2).

3. Extension of the semidefinite problem introduced in section 2.2.1 to include the relaxed model and the moment sequence constraint (Section 4.4.2).

4. Definition of a synthesis procedure for the switched system control signal from the recovered measure (Section 4.4.4).

5. Formulation of the control algorithm for switched systems using the proposed tdCLF approach (Section 4.4.5).

4.3 Parameterized Control Lyapunov Functions with Fixed Parameters

The use of parameterized Lyapunov functions for analyzing the stability of systems or synthesizing control laws has been shown to reduce the conservativeness of solutions. For instance, these have been used in [44], [45] to define conditions in the form of LMIs for checking the stability of systems with time varying uncertainty. These methods have been extended for the case of piecewise affine (PWA) [46] and nonlinear [19] systems.

The main objective in this section is to obtain a parameter-dependent control law for switched systems that can be tuned to improve the closed-loop system performance. This performance is measured as the tracking error for the state variables with respect to piecewise-constant references. The port Hamiltonian model is used to formulate the control problem for switched systems. Lyapunov's direct method is then used to obtain an explicit expression for a parameterized control law. The port Hamiltonian model in Eq. (2.6) can be written in the following control-affine form

$$\begin{aligned} P\dot{x}(t) &= f(x(t)) + \sum_{i=1}^{n} g_i(x(t))s_i(t), \\ f(x(t)) &= (J_0 - R)x(t) + B_0 E, \\ g_i(x(t)) &= J_i x(t) + B_i E. \end{aligned} \tag{4.1}$$

We proceed now to formulate the control problem.

Problem 4.3.1. *Consider the port-Hamiltonian system in Eq. (4.1). Given a constant reference x^{ref}, obtain a feedback control law $s \in \mathcal{S}^n, s(t) = h(x, x^{ref})$ such that x follows x^{ref} as closely as possible.*

Cette thèse est accessible à l'adresse : http://theses.insa-lyon.fr/publication/2019LYSEI123/these.pdf
© [G. J. Becerra], [2019], INSA de Lyon, tous droits réservés

Let us define the tracking error as $\tilde{x}(t) = x(t) - x^{ref}$. The error dynamics are determined by

$$\dot{\tilde{x}}(t) = P^{-1}\left[(J_0 - R)(\tilde{x}(t) + x^{ref}) + B_0 E + \sum_{i=1}^{n}\left[J_i(\tilde{x}(t) + x^{ref}) + B_i E\right] s_i(t)\right] \tag{4.2}$$

Then, we can reformulate problem 4.3.1 in terms of the $\tilde{x}$ variable.

Problem 4.3.2. *Consider the port-Hamiltonian system (4.2). Given a constant reference x^{ref}, obtain a control law $s \in \mathcal{S}^n, s(t) = h(\tilde{x}(t), x^{ref})$ such that $\tilde{x}(t)$ converges to zero.*

Problem 4.3.2 can be interpreted in terms of system energy. In this case, tracking a reference signal is equivalent to decreasing the energy of the error dynamics. This can be represented by the Hamiltonian function of system (4.2):

$$\mathcal{H}(\tilde{x}) = \frac{1}{2}\tilde{x}^{\intercal} P \tilde{x}. \tag{4.3}$$

Then, the derived Lyapunov control will be based on Eq. (4.3). Let $V(t)$ be a parameterized Lyapunov function candidate given by

$$V(\tilde{x}, Q) := \frac{1}{2}\tilde{x}^{\intercal}(t) Q P \tilde{x}(t), \tag{4.4}$$

with Q a diagonal, positive definite matrix. Computing $\dot{V}(\tilde{x}, Q)$ along the trajectories of system in Eq. (4.2) we obtain

$$\begin{aligned}\dot{V}(\tilde{x}, Q) &= \tilde{x}^{\intercal}(t) Q P \dot{\tilde{x}}(t) \\ &= \tilde{x}^{\intercal}(t) Q\left[(J_0 - R)(\tilde{x}(t) + x^{ref}) + B_0 E\right] + \sum_{i=1}^{n}\tilde{x}^{\intercal}(t) Q\left[J_i(\tilde{x}(t) + x^{ref}) + B_i E\right] s_i(t).\end{aligned} \tag{4.5}$$

Using Lyapunov's direct method, a control law can be computed for the switched system. We show this for the case of the multicellular converter.

Proposition 4.3.1. *Consider the port-Hamiltonian system in Eq. (4.2) with matrices (2.8). Then, for any $\epsilon > 0$ there exists $\delta > 0$ such that if $||\tilde{x}(t_0)|| < \delta$, then $||\tilde{x}(t)|| < \epsilon$, for all $t > t_0$, if the feedback control law is defined as*

$$s_i(\tilde{x}, x^{ref}) = \frac{1 - sign\left(\phi_i(\tilde{x}(t), x^{ref})\right)}{2}, \tag{4.6}$$

$$\phi_i(\tilde{x}(t), x^{ref}) = \tilde{x}^{\intercal}(t) Q\left[J_i(\tilde{x}(t) + x^{ref}) + B_i E\right], \tag{4.7}$$

$$i = 1, 2, \ldots, n.$$

Cette thèse est accessible à l'adresse : http://theses.insa-lyon.fr/publication/2019LYSEI123/these.pdf
© [G. J. Becerra], [2019], INSA de Lyon, tous droits réservés

Proof. Using the explicit representation of matrices P, R, $J_{s(t)}$, $B_{s(t)}$ defined in Eq. (2.8), $\dot{V}$ can be written as:

$$\dot{V} = -\sum_{k=1}^{n-1} A_k(s_k - s_{k+1}) - A_n\left[R_L I_L - E\left(s_n - \frac{1}{2}\right)\right], \tag{4.8}$$

$$A_k = -q_n(I_L - I_L^{ref})E_k + q_k(E_k - E_k^{ref})I_L, \tag{4.9}$$

$$A_n = q_n(I_L - I_L^{ref}), \tag{4.10}$$

with $Q = \text{diag}[q_1, q_2, \ldots, q_n]$. The switching functions ϕ_i in Eq. (4.7) are rewritten as:

$$\phi_1 = q_n(I_L - I_L^{ref})E_1 - q_1(E_1 - E_1^{ref})I_L, \tag{4.11a}$$

$$\phi_2 = -\phi_1 + q_n(I_L - I_L^{ref})E_2 - q_2(E_2 - E_2^{ref})I_L, \tag{4.11b}$$

$$\phi_3 = -\phi_1 - \phi_2 + q_n(I_L - I_L^{ref})E_3 - q_3(E_3 - E_3^{ref})I_L, \tag{4.11c}$$

$$\vdots$$

$$\phi_k = -\sum_{i=1}^{k-1}\phi_i + q_n(I_L - I_L^{ref})E_k - q_k(E_k - E_k^{ref})I_L, \tag{4.11d}$$

$$\vdots$$

$$\phi_n = -\sum_{i=1}^{n-1}\phi_i + q_n(I_L - I_L^{ref})E. \tag{4.11e}$$

It can be seen from Eqs. (4.9), (4.11a) that $A_1 = -\phi_1$, and from Eqs. (4.9), (4.11d) that $\sum_{i=1}^{k-1}\phi_i = -A_k$. It is important to notice that each term in (4.8) is related to a cell of the power converter and, in order to guarantee the condition $\dot{V} \leq 0$, the adjacent switch configuration in the terms $-A_k(s_k - s_{k-1})$ must be properly selected. The strategy for the proof is to show that each term in Eq. (4.8) is negative or null for any switch combination. We will consider three different cases:

1. The first cell is related to the term $-A_1(s_1 - s_2)$ and the switching function ϕ_1. The control signal of the first cell s_1 is chosen in order to satisfy $-A_1(s_1 - s_2) \leq 0$ for any value of the control signal in the second cell s_2. In other terms, we need to set $s_1 = 0$ when $\phi_1 = -A_1 > 0$ and $s_1 = 1$ when $\phi_1 = -A_1 < 0$. These conditions are represented by the control law given in Eq. (4.6). Therefore the term corresponding to A_1 is always negative or null in $\dot{V}$.

2. Each k^{th} cell, $k = 2, \ldots, n-1$, is related to a term of the form $-A_k(s_k - s_{k+1})$ in Eq. (4.8) and the switching function ϕ_k. Similarly to the first cell, the k^{th} control signal s_k is chosen to guarantee $-A_k(s_k - s_{k+1}) \leq 0$ for any value of the control signal s_{k+1}. So we need to set $s_1 = 0$ when $\sum_{i=1}^{k}\phi_i = -A_k > 0$ and $s_1 = 1$ when $\sum_{i=1}^{k}\phi_i = -A_k < 0$. These conditions are represented by the control law in Eq. (4.6). Therefore each k^{th} term, $k = 2, \ldots, n-1$, is always negative or null in $\dot{V}$.

Cette thèse est accessible à l'adresse : http://theses.insa-lyon.fr/publication/2019LYSEI123/these.pdf
© [G. J. Becerra], [2019], INSA de Lyon, tous droits réservés

3. The last cell is related to the term $-A_n\left[R_L I_L - E\left(s_n - 1/2\right)\right]$ in Eq. (4.8) and to the switching function ϕ_n. The control signal s_n is chosen to guarantee $-A_n\left[R_L I_L - E\left(s_n - 1/2\right)\right] < 0$. If we set $s_n = 0$, the term becomes $-A_n(R_L I_L + E/2)$, and if we set $s_n = 1$, the term becomes $-A_n(R_L I_L - E/2)$. Taking into account the constraint given in Eq. (2.9), it can be shown that these two expressions are negative or null.

□

Control law in Eq. (4.6) is simple to implement, since it depends only on the system state, the reference vector and the structure matrix. Notice that the control does not depend on the non dissipative system parameters contained within the matrix P.

Remark 4.3.1. Notice that the proof provided for proposition 4.3.1 is presented only for the case of the multicellular converter. In [47] we show that the same control law can be used for other converter topologies, such as buck, buck-boost, SEPIC and uk.

4.3.1 Three-Cell Multicellular Converter

In this subsection, the Lyapunov control is designed for a three-cell converter. The obtained control law is validated in simulation and in experimentation. Furthermore, the proposed technique is compared to the two Lyapunov control benchmark methods proposed in [48], [49] and tested in the same experimental environment.

Modeling and Control Design

According to the model given by Eq. (2.6), the port Hamiltonian model of the three-cell converter has the following form

$$\begin{aligned} P\dot{x}(t) =& (J_0 + J_1 s_1(t) + J_2 s_2(t) + J_3 s_3(t) - R)x(t) \\ &+ P(B_0 + B_1 s_1(t) + B_2 s_2(t) + B_3 s_3(t))E \end{aligned} \tag{4.12}$$

with $x(t) = [E_1(t), E_2(t), I_L(t)]^\intercal$ and

$$J_0 = \begin{bmatrix} 0 & 0 & 0 \\ 0 & 0 & 0 \\ 0 & 0 & 0 \end{bmatrix}, J_1 = \begin{bmatrix} 0 & 0 & -1 \\ 0 & 0 & 0 \\ 1 & 0 & 0 \end{bmatrix}, J_2 = \begin{bmatrix} 0 & 0 & 1 \\ 0 & 0 & -1 \\ -1 & 1 & 0 \end{bmatrix},$$

$$J_3 = \begin{bmatrix} 0 & 0 & 0 \\ 0 & 0 & 1 \\ 0 & -1 & 0 \end{bmatrix}, R = \begin{bmatrix} 0 & 0 & 0 \\ 0 & 0 & 0 \\ 0 & 0 & R_L \end{bmatrix}, P = \begin{bmatrix} C_1 & 0 & 0 \\ 0 & C_2 & 0 \\ 0 & 0 & L \end{bmatrix},$$

$$B_0 = \begin{bmatrix} 0 \\ 0 \\ -1/2 \end{bmatrix}, B_1 = \begin{bmatrix} 0 \\ 0 \\ 0 \end{bmatrix}, B_2 = \begin{bmatrix} 0 \\ 0 \\ 0 \end{bmatrix}, B_3 = \begin{bmatrix} 0 \\ 0 \\ 1 \end{bmatrix}$$

Cette thèse est accessible à l'adresse : http://theses.insa-lyon.fr/publication/2019LYSEI123/these.pdf
© [G. J. Becerra], [2019], INSA de Lyon, tous droits réservés

Define the reference vector $x^{ref} = [E_1^{ref}, E_2^{ref}, I_L^{ref}]^\intercal$. The Q matrix can be defined as diagonal, where each parameter is associated with one variable:

$$Q = \begin{bmatrix} q_1 & 0 & 0 \\ 0 & q_2 & 0 \\ 0 & 0 & q_3 \end{bmatrix} \tag{4.13}$$

with q_1, q_2, q_3 positive. Then, the control law for each cell can be written as:

$$s_i = \frac{1 - \text{sign}\,(\phi_i)}{2}, i = 1, 2, 3. \tag{4.14}$$

$$\phi_1 = -q_1(E_1 - E_1^{ref})I_L + q_3(I_L - I_L^{ref})E_1 \tag{4.15}$$

$$\phi_2 = q_1(E_1 - E_1^{ref})I_L - q_2(E_2 - E_2^{ref})I_L - q_3(I_L - I_L^{ref})(E_1 - E_2) \tag{4.16}$$

$$\phi_3 = q_2(E_2 - E_2^{ref})I_L + q_3(I_L - I_L^{ref})(E - E_2) \tag{4.17}$$

The use of a parameterized Lyapunov function depending on Q allows the designer to modify the shape of the control Lyapunov function, hence changing the dynamic properties of the closed loop, which could in turn be used to improve the response performance. However, the problem of choosing appropriate values for Q is not trivial. This problem is analyzed in the following section.

State Trajectory Dependence on the Control Lyapunov Parameterization

We explore the dependence of the decision surfaces determined by the control law in Eqs. (4.15)-(4.17) and the state trajectory performance with respect to the parameters in the Lyapunov function. The shapes of the surfaces are determined by the parameterization, which in turn determine the trajectories followed by the system in state space. A performance measure is defined as a function of the system trajectory in order to choose the best set of parameters for a given initial condition. This is illustrated for two particular cases: capacitors with a non-zero initial condition (representing the normal operation of the converter), and with zero initial condition (representing the converter startup). This analysis is performed running noiseless simulations of the multicellular converter in Matlab - Simulink, with a fixed step time of 50 μs.

In the first case, the capacitor voltages are maintained constant in $E_1 = 20$ V, $E_2 = 40$ V, while there is a change in current reference from -0.5 A to 0.5 A. This is a common scenario in practice, because one of the usual requirements is to maintain voltage balance in the converter cells, while tracking a reference waveform in the output current. Fig. 4.1 presents simulation results of the system trajectory, and also the decision surfaces defined by Eqs. (4.15)-(4.17) with $[q_1, q_2, q_3] = [1, 1, 1]$. These surfaces provide a partition of the state space, where each region is associated to a particular on-off combination in the switch states. The system follows a direct vertical trajectory

Cette thèse est accessible à l'adresse : http://theses.insa-lyon.fr/publication/2019LYSEI123/these.pdf
© [G. J. Becerra], [2019], INSA de Lyon, tous droits réservés

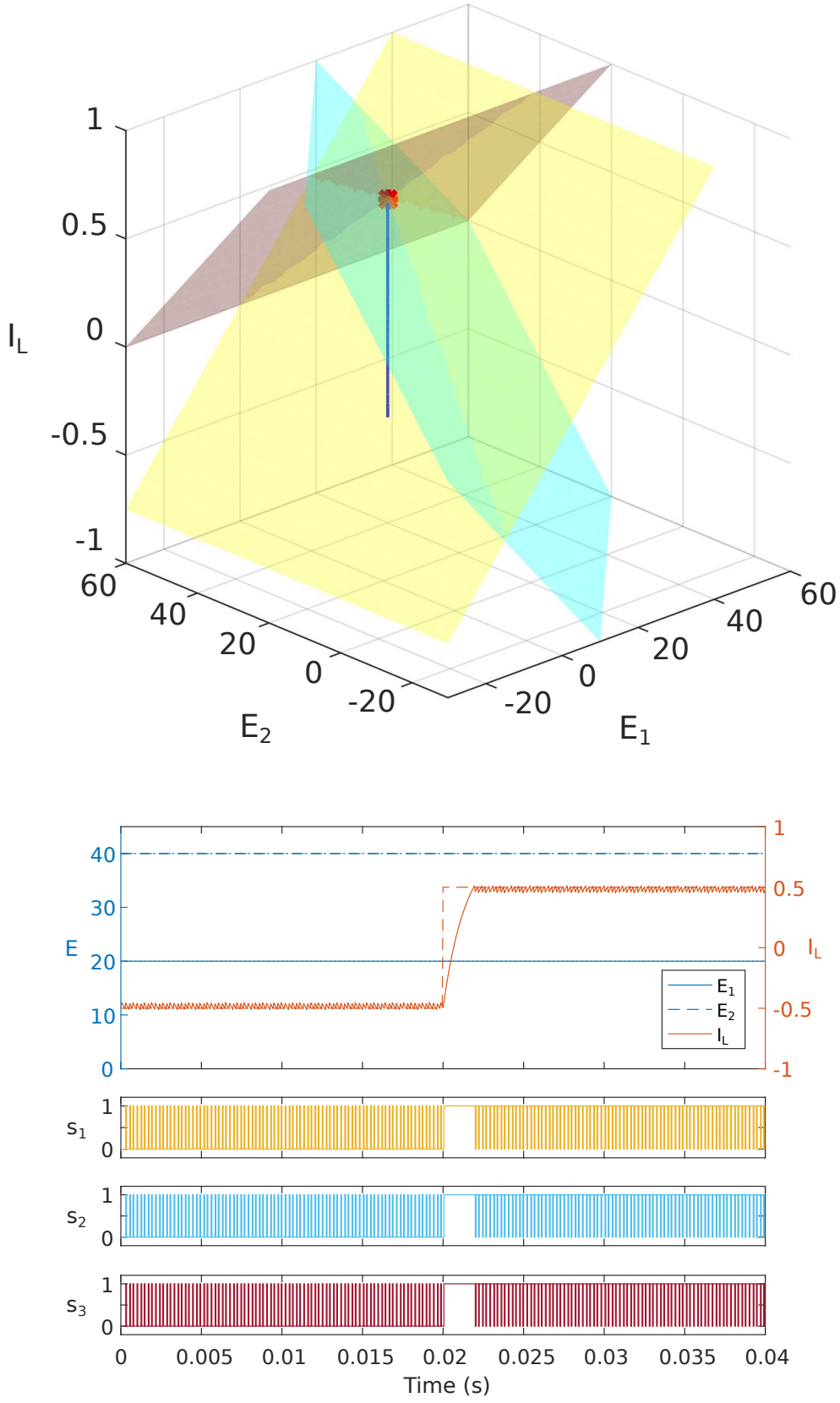

FIGURE 4.1 – Simulation response for a step change in current I_L and constant capacitor voltages E_1, E_2, with $[q_1, q_2, q_3] = [1, 1, 1]$. (a) Decision surfaces. (b) Control signals.

Cette thèse est accessible à l'adresse : http://theses.insa-lyon.fr/publication/2019LYSEI123/these.pdf
© [G. J. Becerra], [2019], INSA de Lyon, tous droits réservés

without meeting any of the surfaces, and no switching events are produced during this part of the trajectory. When the state reaches the reference, the control starts a switching behavior which maintains the state near the reference.

For the second case, the voltages start on 0 V. This can represent the startup conditions for the converter, when the capacitors are discharged. Fig. 4.2 presents a simulation of the system response in this case, with an initial condition $x_0 = [0, 0, -0.5]^\intercal$. When the trajectory reaches both the yellow and blue surfaces, the switch configuration changes and the system continues evolving with the new vector flow. Later, it meets again the blue surface, starting a sliding behavior along it, until it meets the yellow surface, driving the sliding over the intersection of both planes. It finally reaches the red surface and the switching behavior maintains the state in the neighborhood of the reference.

Now, when the parameters in the weight matrix Q are changed, the shape of the decision surfaces will change and the resulting trajectories will be different. Fig. 4.3 illustrates this for $[q_1, q_2, q_3] = [5, 5, 1]$.

Taking these weights as design parameters, it is desired to assign them values such that a performance measure is optimized. For instance, the normalized total error e_{tot} with respect to the change in each reference Δx_i^{ref} can be formulated as the optimality criterion:

$$e_{tot} = \frac{e_1}{\Delta x_1^{ref}} + \frac{e_2}{\Delta x_2^{ref}} + \frac{e_3}{\Delta x_3^{ref}}, \tag{4.18}$$

where e_i is the RMS tracking error in each state variable with respect to its reference, computed as follows:

$$e_i = \sqrt{\frac{1}{N}\sum_{k=1}^{N}\left(x_i(k) - x_i^{ref}\right)^2}, i \in \{1, 2, 3\} \tag{4.19}$$

with N the number of measured samples. Table 4.1 shows the errors for the two trajectories presented in Figs. 4.2 and 4.3.

Cette thèse est accessible à l'adresse : http://theses.insa-lyon.fr/publication/2019LYSEI123/these.pdf
© [G. J. Becerra], [2019], INSA de Lyon, tous droits réservés

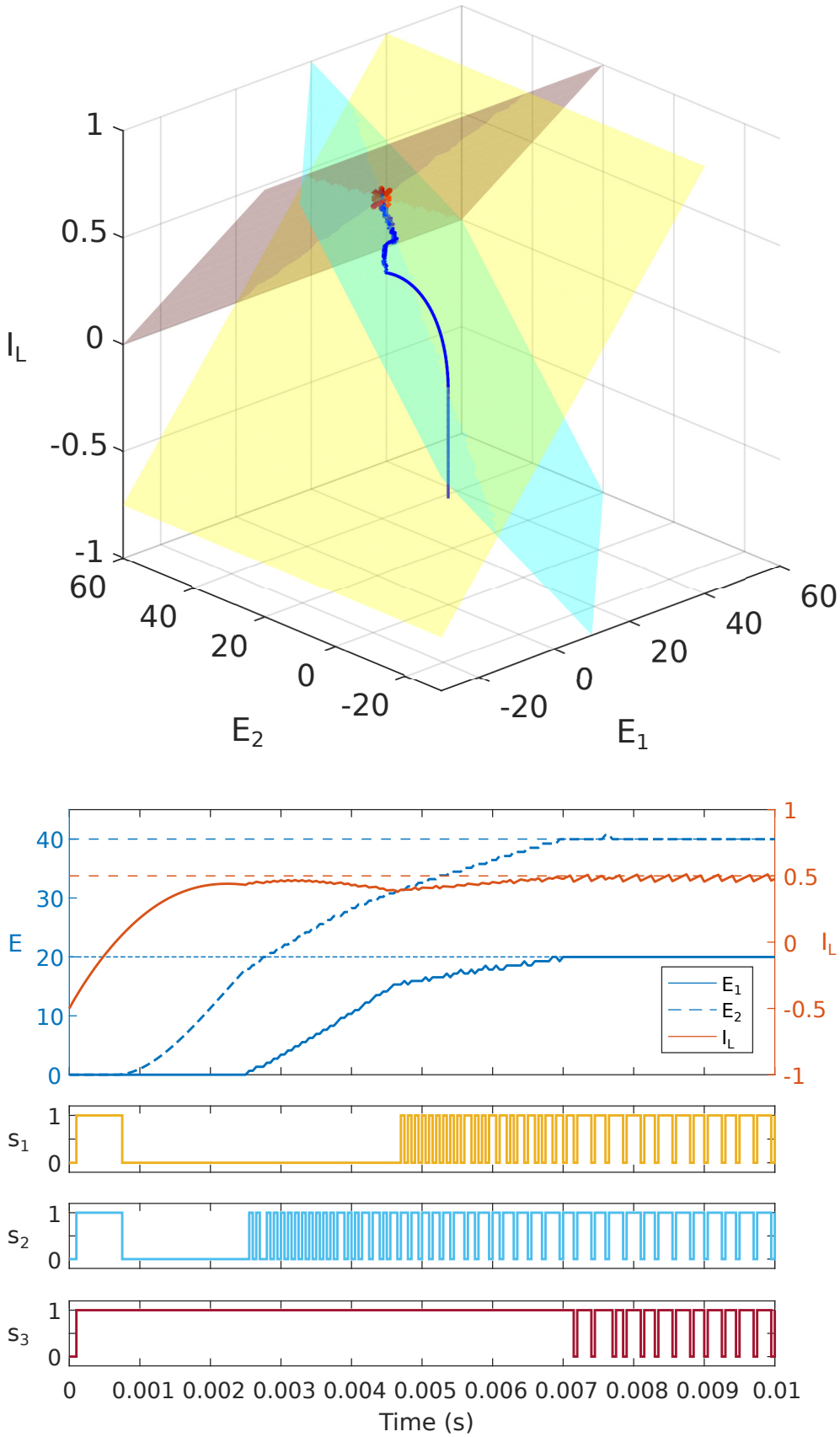

FIGURE 4.2 – Simulation response for a step change in current I_L and initial capacitor voltages E_1, E_2 equal to zero, with $[q_1, q_2, q_3] = [1, 1, 1]$. (a) Decision surfaces. (b) Control signals

Cette thèse est accessible à l'adresse : http://theses.insa-lyon.fr/publication/2019LYSEI123/these.pdf
© [G. J. Becerra], [2019], INSA de Lyon, tous droits réservés

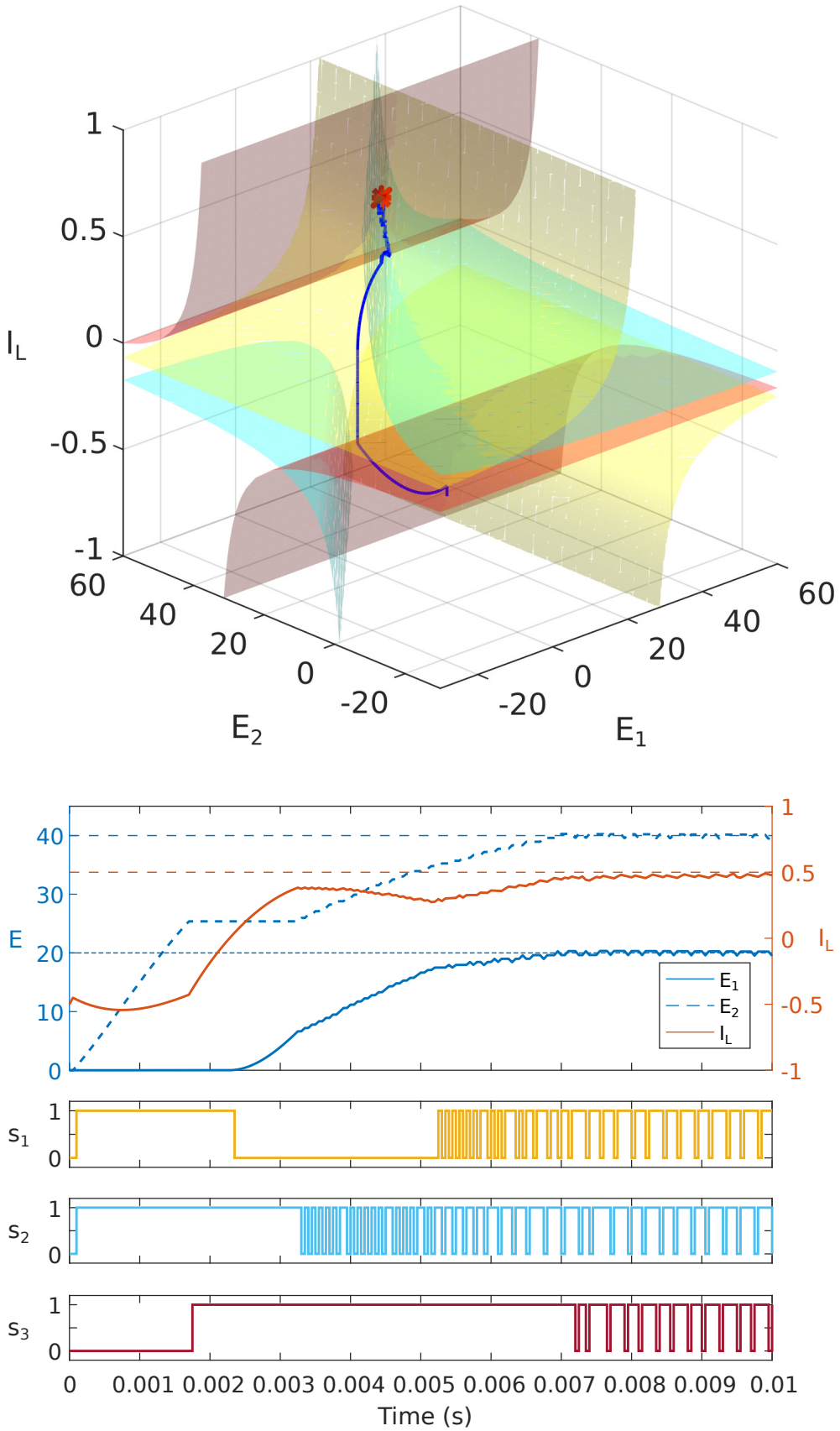

FIGURE 4.3 – Simulation response for a step change in current I_L and initial capacitor voltages E_1, E_2 equal to zero, with $[q_1, q_2, q_3] = [5, 5, 1]$. (a) Decision surfaces. (b) Control signals.

Cette thèse est accessible à l'adresse : http://theses.insa-lyon.fr/publication/2019LYSEI123/these.pdf
© [G. J. Becerra], [2019], INSA de Lyon, tous droits réservés

4.3.2 Simulation and Experimental Results

The proposed control is tested on a three-cell converter and simulation results are compared to experimental data using Matlab. The converter parameters are presented in Table 2.1. It is standard practice to define the references for the flying capacitor voltages as $E_1^{ref} = E/3 = 20$ V and $E_2^{ref} = 2E/3 = 40$ V. This configuration yields a balanced voltage distribution on the switches, allowing to use semiconductor devices with the same electrical characteristics. The current refererence is piecewise constant in the interval $[-1, 1]$. In addition to simulation, an experimental validation is performed on the test-bench shown in Fig. 4.4. The converter is manufactured with 6 IRF740 MOSFET. It is supplied by 2 Xantrex voltage sources with capacitors. The component values are the same as those for the simulation. The drivers for the transistors are controlled by optical fibers coming from a Field-Programmable Gate Array (FPGA) that ensures a non-optimized dead-time of $6\mu s$. The inputs of the FPGA board were connected to three digital outputs of a DS1104 dSPACE board. Measurements of the two capacitor voltages and the load current are made by using probes. The sampling frequency of 20 kHz and the reference signals are identical in simulation and in practice. The characteristics of this power converter are not industry-grade, because it was designed as a small test bench for comparing different control approaches.

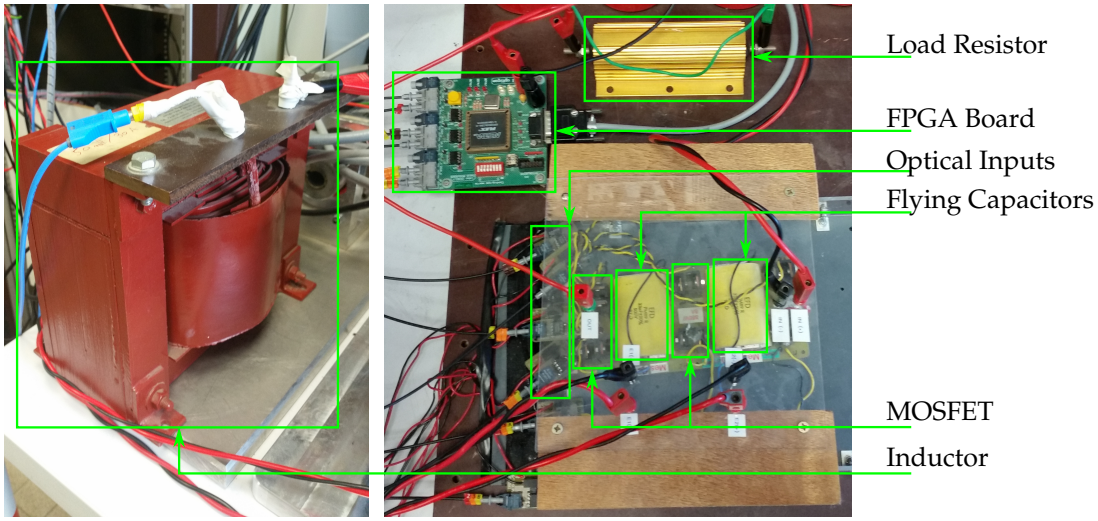

FIGURE 4.4 – Multicellular converter Test-bench.

To have a preliminary idea of how the criterion changes depending on the weights, a series of simulation and experimental tests have been performed for the multicellular converter described in section 2.1.4. A grid of 21 values was defined for $q_i \in [1, 100]$, $i = \{1, 2, 3\}$ with a total of 9261 experiments carried out. For each experiment, a pulse signal with period of 0.02 s is applied to each reference, and the system response is recorded for three periods with a sampling time of 50 μs. In order to reduce the noise, the final signal for each state variable is obtained by averaging the three periods. Then, for each experiment, the total error is computed using Eqs. (4.18),(4.19).

Cette thèse est accessible à l'adresse : http://theses.insa-lyon.fr/publication/2019LYSEI123/these.pdf
© [G. J. Becerra], [2019], INSA de Lyon, tous droits réservés

Fig. 4.5 shows the best trajectory found in simulation and experiment, corresponding to the weight parameters $[q_1, q_2, q_3] = [85, 15, 50]$. When comparing it with respect to the trajectory obtained for the base case shown in Fig. 4.2 it can be observed that this criterion will favor a trajectory whose variables begin increasing right from the beginning in order to obtain an overall faster convergence to the reference. Notice that in the base case the current will start increasing for a period of time during which each voltage will remain in 0 V. The chosen criterion penalizes this behavior and tends to produce surfaces which allow sliding much sooner than the base case.

Table 4.1 shows the errors for the best parameters $[q_1, q_2, q_3] = [85, 15, 50]$, in simulation and experiment. These are compared with the errors computed for the trajectories produced by the related Lyapunov control methods described in [48] and [49], tested under exactly the same conditions. Fig. 4.6 shows the comparison of the time responses in simulation and experiment. Notice that the chosen parameters produce an improvement in the total tracking error when compared with these benchmark methods in simulation (last column, italicized) and experiment (last column, bold), suggesting that a proper choice of a time varying parameterization of the Lyapunov function can provide even further improvements. This will be the subject of future studies.

$[q_1, q_2, q_3]$	Fig.	Test	$e_1/\Delta x_1^{ref}$	$e_2/\Delta x_2^{ref}$	$e_3/\Delta x_3^{ref}$	e_{tot}
$[1, 1, 1]$	4.2	Simulation	0.2940	0.2387	0.1103	0.6431
$[5, 5, 1]$	4.3	Simulation	0.2831	0.1711	0.2320	0.6861
$[85, 15, 50]$	4.5,4.6	Simulation	0.2104	0.2662	0.1086	*0.5852*
	4.5,4.6	Experiment	0.1973	0.2729	0.1134	**0.5836**
Defoort et al.	4.6	Simulation	0.3173	0.2323	0.1112	*0.6608*
	4.6	Experiment	0.3236	0.2419	0.1181	**0.6836**
Buisson et al.	4.6	Simulation	0.2279	0.2675	0.1128	*0.6082*
	4.6	Experiment	0.3055	0.2462	0.1299	**0.6816**

TABLE 4.1 – Normalized RMS errors and total error for different trajectories.

Robustness Tests

Two types of robustness tests were carried out on simulation: a change in the output resistance R_L and a change in the input voltage E, occurring at $t = 0.005$ s in steady state, while keeping all the references constant. In the first case R_L changed from 33 Ω to 3.3 Ω, and on the second case E changed from 60 V to 42 V. Fig. 4.7 shows the resulting behavior for the control law in Eqs. (4.15)-(4.17) using the best parameters found in the previous subsection. This behavior is compared with respect to the responses obtained using the benchmark methods in [48] and [49]. It is clear from the figures that the three approaches exhibit a similar robust response and similar switching patterns. The small differences are due to the local properties of the decision surfaces in the neighborhood of the equilibrium point.

Cette thèse est accessible à l'adresse : http://theses.insa-lyon.fr/publication/2019LYSEI123/these.pdf
© [G. J. Becerra], [2019], INSA de Lyon, tous droits réservés

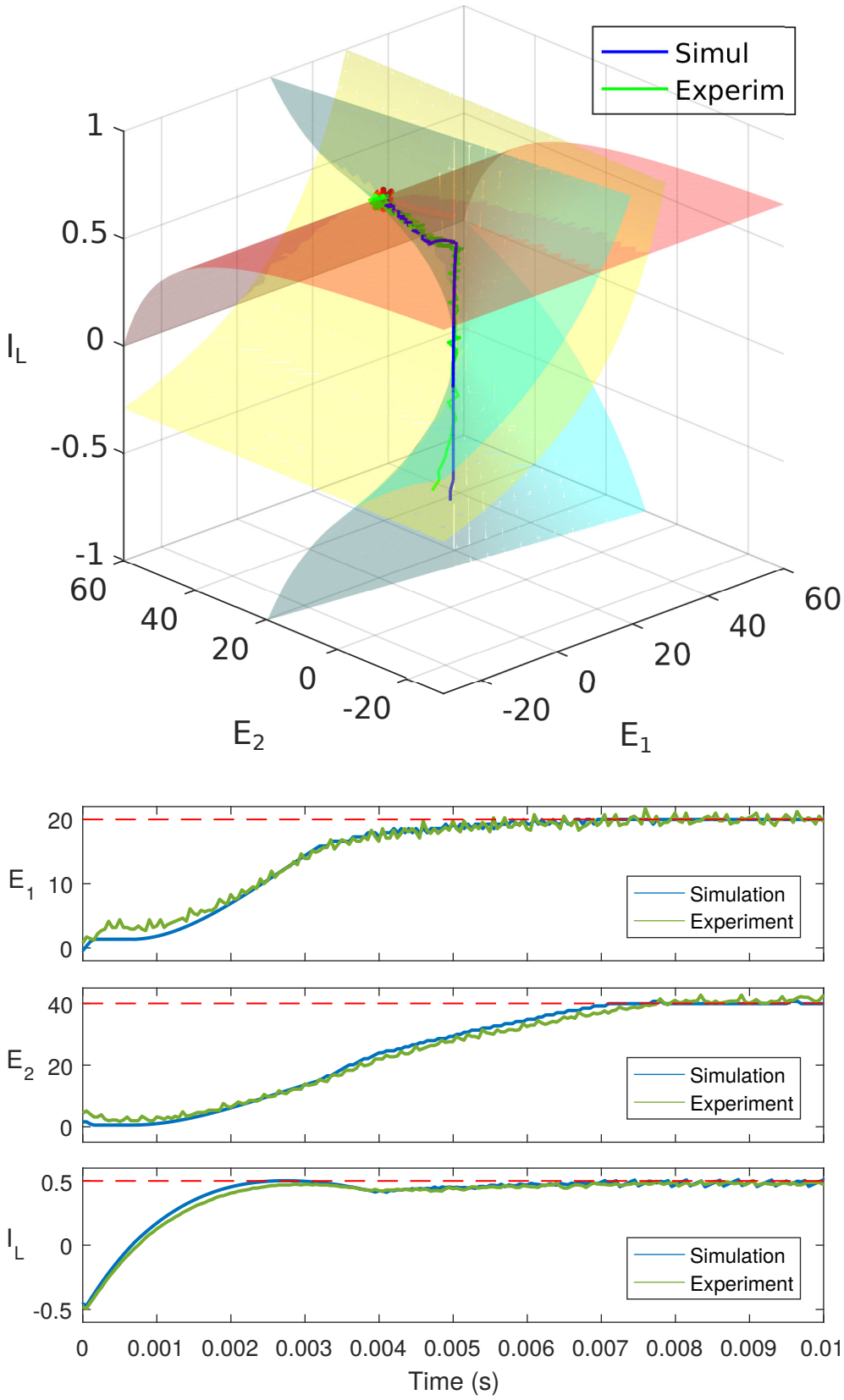

FIGURE 4.5 – Simulation and experimental response for a step change in current I_L and initial capacitor voltages E_1, E_2 equal to zero, with $[q_1, q_2, q_3] = [85, 15, 50]$. (a) System trajectory. (b) Time response.

Cette thèse est accessible à l'adresse : http://theses.insa-lyon.fr/publication/2019LYSEI123/these.pdf
© [G. J. Becerra], [2019], INSA de Lyon, tous droits réservés

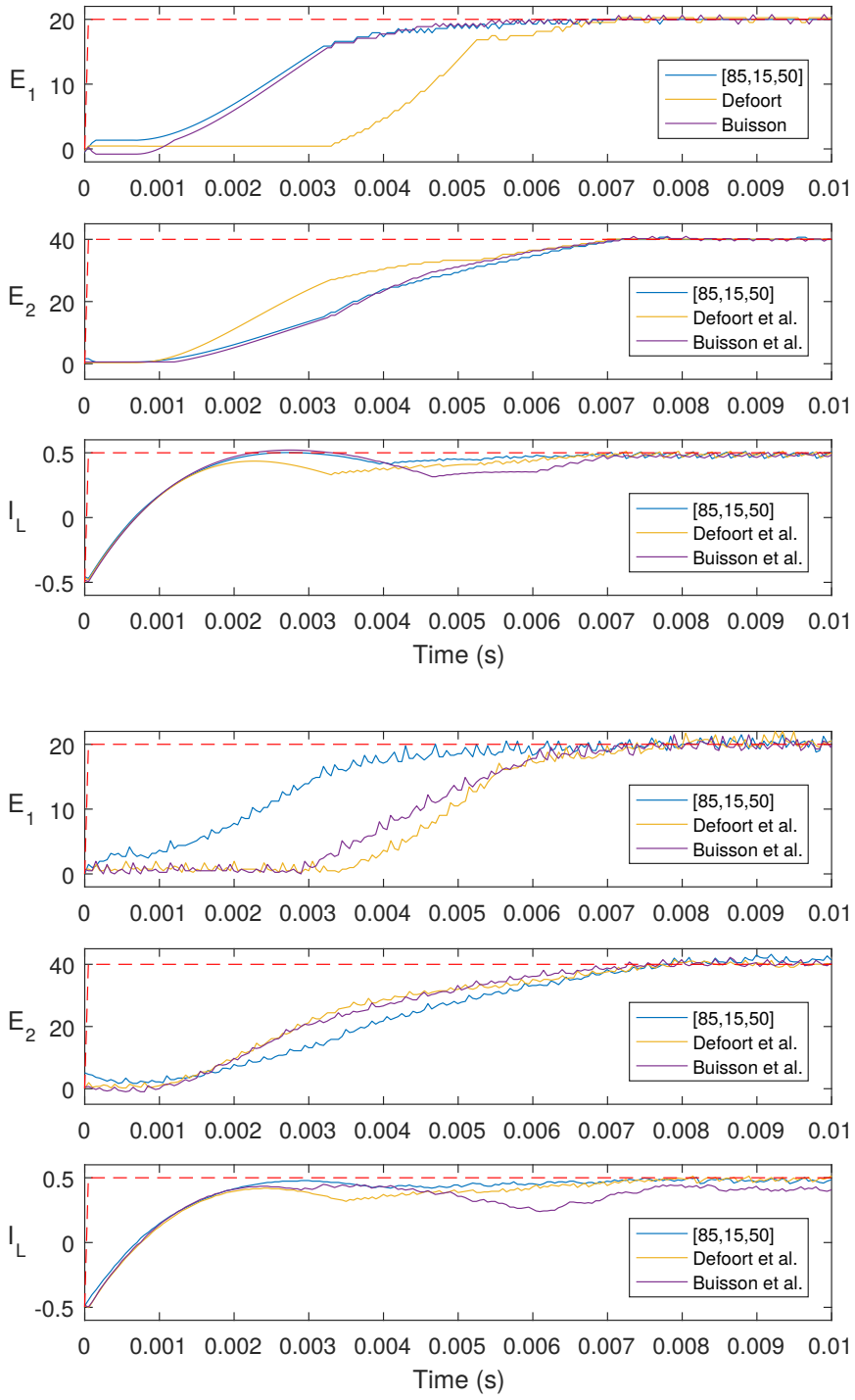

FIGURE 4.6 – Comparison between the best trajectory found for the parameterized control law in Eqs. (4.15)-(4.17) and the methods proposed by [48] and [49]. Simulation results (top). Experimental results (bottom).

Cette thèse est accessible à l'adresse : http://theses.insa-lyon.fr/publication/2019LYSEI123/these.pdf
© [G. J. Becerra], [2019], INSA de Lyon, tous droits réservés

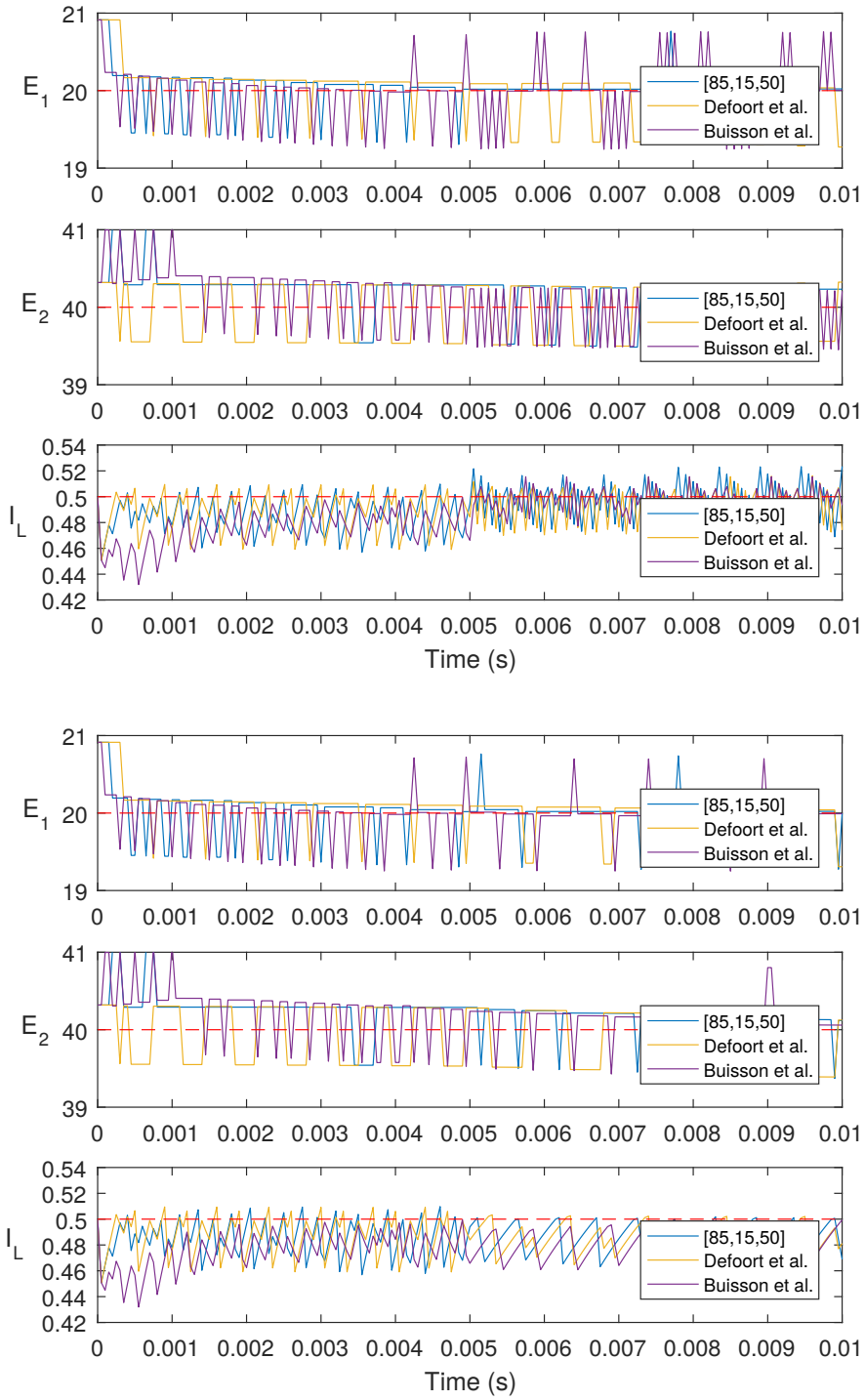

FIGURE 4.7 – Steady state response under a disturbance occurring at $t = 0.005s$ for the control law in Eqs. (4.15)-(4.17) with the best parameters found, and the methods proposed by [48] and [49], in simulation. Disturbance in output resistance R_L (top). Disturbance in input voltage E (bottom).

Cette thèse est accessible à l'adresse : http://theses.insa-lyon.fr/publication/2019LYSEI123/these.pdf
© [G. J. Becerra], [2019], INSA de Lyon, tous droits réservés

4.3.3 Discussion on the Fixed-Parameter Approach

The approach presented in this section allows to modify the system response by choosing the parameters that define the decision surfaces. The resulting control law is simple to implement and provides stability guarantees. However, there are several shortcomings to this method:

1. It is not easy to define a criterion for appropriately selecting the values that parameterize the decision surfaces.
2. The parameters are fixed along the trajectory.
3. The choice of the diagonal structure for matrix Q constrains the set of candidate Lyapunov functions, limiting the possibilities for obtaining less conservative solutions to the control problem.

In the next section we present an approach with the aim of solving these problems for the general switched system case, regardless of the converter topology used.

4.4 Trajectory Dependent Control Lyapunov Functions (tdCLF) for Switched Systems

We now introduce a new method for the control of switched systems using parameterized Lyapunov functions. It is based on developments introduced in [18] and later expanded by [19], where the existence of parameterized control Lyapunov functions (pCLF) for non-linear control-affine systems is proven and proposes a method to synthesize these functions. This approach solves the problems discussed in the previous section as follows:

1. The control problem is recast as an optimization problem that defines the parameters of the Lyapunov function as decision variables, along with the control signal.
2. The parameters are computed iteratively at each sample time along the trajectory being traversed by the system.
3. The structure of the parameter matrix provides a riches admissible set of Lyapunov functions than the diagonal matrix used in the fixed case, providing less conservative solutions.

The computed pCLF is trajectory-dependent (tdCLF) in the sense that the sequence of parameters computed are only valid along the particular trajectory being followed. This method allows to obtain non-conservative control Lyapunov functions by solving a low-complexity convex optimization problem. The advantages of the tdCLF approach with respect to the fixed parameter case presented in the previous section come at a cost. This cost is that obtaining the control signal is more expensive computationally, rendering a formulation for the continuous-time system intractable. Therefore, the discrete-time model of the switched system is used in this approach.

Cette thèse est accessible à l'adresse : http://theses.insa-lyon.fr/publication/2019LYSEI123/these.pdf
© [G. J. Becerra], [2019], INSA de Lyon, tous droits réservés

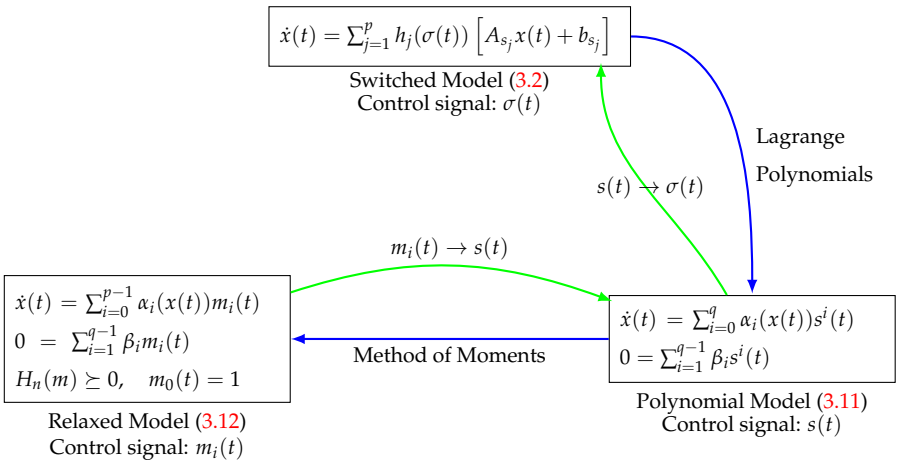

FIGURE 4.8 – From switched to relaxed models and back: reformulation of the switched system as a constrained linear system using Lagrange polynomials and the method of moments (blue arrows) and recovery of the switching control signal (green arrows).

The developed method extends the use of tdCLFs to the case of switched systems. This is achieved in two stages, illustrated in Fig. 4.8:

1. **Offline:** The switched model is transformed into a polynomial model by substituting the switching functions with a basis of Lagrange polynomials. The resulting polynomial model is transformed into a relaxed (constrained linear) model using the method of moments.

2. **Online:** Solve the control problem using the relaxed model. Recover the polynomial control signal and synthesize the switched signal.

These steps are described in detail in the following sections.

4.4.1 Polynomial Model for the Switched System

Consider the discrete-time switched system

$$x_{k+1} = f_{\sigma_k}(x_k, u_k) \tag{4.20}$$

where $x_k \in \mathbb{X} \subseteq \mathbb{R}^n$ is the state, $u_k \in \mathbb{U} \subseteq \mathbb{R}^m$ is the exogenous input and $\sigma_k : \mathbb{Z}_{>=0} \to \mathcal{S} = \{\bar{s}_1, \bar{s}_2, \ldots, \bar{s}_q\}$ is a piecewise constant function indicating the active subsystem at each time k. The constants $\bar{s}_1, \bar{s}_2, \ldots, \bar{s}_q$ are numerical labels assigned to each subsystem. Let us define a set of polynomials $l_{\bar{s}_i}(s)$ with maximum degree p satisfying $l_{\bar{s}_i}(\bar{s}_j) = 0, \forall i \neq j, \bar{s}_i, \bar{s}_j \in \mathcal{S}$ and $l_{\bar{s}_i}(\bar{s}_i) = 1, \forall \bar{s}_i \in \mathcal{S}$. Notice that the set of Lagrange polynomials defined in section 3.4 satisfy this property. Eq. (4.20) can be written as the difference-algebraic

Cette thèse est accessible à l'adresse : http://theses.insa-lyon.fr/publication/2019LYSEI123/these.pdf
© [G. J. Becerra], [2019], INSA de Lyon, tous droits réservés

system

$$x_{k+1} = \sum_{i=1}^{q} l_{\bar{s}_i}(s_k) f_{\bar{s}_i}(x_k, u_k) \tag{4.21a}$$

$$0 = \prod_{i=1}^{q} (s_k - \bar{s}_i) \tag{4.21b}$$

where the algebraic constraint (4.21b) guarantees $s_k \in \mathcal{S}$. The set of polynomials $l_{\bar{s}_i}(s_k)$ are used as switching functions for selecting the active mode in (4.20) depending on the value of the new control variable s_k. This means that setting $s_k = \bar{s}_i$ in (4.21) is equivalent to selecting the i-th mode in (4.20) as $\sigma_k = \bar{s}_i$. Rearranging terms in (4.21) yields a polynomial expression in the variable s_k that can be written in general as

$$x_{k+1} = \sum_{j=0}^{p} \alpha_j(x_k, u_k) s_k^j \tag{4.22a}$$

$$0 = \sum_{j=1}^{p+1} \beta_j s_k^j \tag{4.22b}$$

We refer to system (4.22) as the polynomial model for the switched system (4.20).

4.4.2 Control Lyapunov Function for the Polynomial System

Recall that problem 2.2.1 allows to compute trajectory dependent CLFs and the control signal for a non-linear discrete-time system. Now, the objective is to rewrite this problem for the particular case of the polynomial representation (4.22).

Let us define the Lyapunov function V with a parameterized quadratic form $V(x, Q(x)) := x^\intercal Q(x) x$. Also, assume that the switched system considered in (4.20) is linear: $x_{k+1} = A_{\sigma_k} x_k + B_{\sigma_k} u_k$. Then, function $\alpha_j(\cdot, \cdot)$ in (4.22a) is linear with respect to x_k and u_k. In this case, the only nonlinearity in (4.22) comes from the powers of s_k.

In the present framework, we are interested in the synthesis of control Lyapunov functions for the tracking problem. This means that we want the system state x_k to converge to a predefined reference x_{ref}. Therefore, the optimization objective (2.16a) can be rewritten in terms of the tracking error

Cette thèse est accessible à l'adresse : http://theses.insa-lyon.fr/publication/2019LYSEI123/these.pdf
© [G. J. Becerra], [2019], INSA de Lyon, tous droits réservés

$\tilde{x}_k = x_k - x_{ref}$:

$$\begin{aligned} J &= \rho V(\tilde{x}_k, Q(\tilde{x}_k)) - V(\tilde{x}_k^+, Q(\tilde{x}_k^+)) \\ &= \rho \left[x_k - x_{ref}\right]^\mathsf{T} Q(\tilde{x}_k) \left[x_k - x_{ref}\right] \\ &- \left[\sum_{j=0}^{p} \alpha_j(x_k, u_k) s_k^j - x_{ref}\right]^\mathsf{T} Q(\tilde{x}_k^+) \left[\sum_{j=0}^{p} \alpha_j(x_k, u_k) s_k^j - x_{ref}\right] \\ &= \sum_{j=0}^{2p} \mathcal{J}_j(x_k, x_{ref}, u_k, Q(\tilde{x}_k), Q(\tilde{x}_k^+)) s_k^j \end{aligned} \tag{4.23}$$

The minimization of this polynomial problem is well suited to be solved using the method of moments introduced in section 2.3. The convexified problem obtained is

$$\min_{m_k} \quad J = \sum_{j=0}^{2p} \mathcal{J}_j(x_k, x_{ref}, u_k, Q(\tilde{x}_k), Q(\tilde{x}_k^+)) m_{j,k} \tag{4.24a}$$

$$s.t. \qquad H(m_k) \succeq 0, \;\; m_{0,k} = 1 \tag{4.24b}$$

where $m_k = \{m_{0,k}, m_{1,k}, m_{2,k}, \ldots\}$ corresponds to the sequence of algebraic moments of a probability measure supported in $\mathbb{R}$, and $H(m_k)$ is the Hankel moment matrix associated with the moment sequence. The polynomial system (4.22) can be rewritten in a relaxed form in terms of new control variables m_k as:

$$x_{k+1} = \sum_{j=0}^{p} \alpha_j(x_k, u_k) m_{j,k} \tag{4.25a}$$

$$0 = \sum_{j=1}^{p+1} \beta_j m_{j,k} \tag{4.25b}$$

The solution m_k^* of problem (4.24) corresponds to the algebraic moments of a Dirac measure $\mu_s = \delta_{s_k^*}$, that may have one or more support points.

Rewriting constraints (2.16b), (2.16c), (2.16d), (2.16e) for the convexified problem (4.24) yields the following semi-definite programming problem (SDP):

Cette thèse est accessible à l'adresse : http://theses.insa-lyon.fr/publication/2019LYSEI123/these.pdf
© [G. J. Becerra], [2019], INSA de Lyon, tous droits réservés

$$\min_{m_k, Q(\tilde{x}_k), Z_k} \quad \varepsilon_k \tag{4.26a}$$

$$\text{s.t.} \quad x_k^+ \in \mathbb{X}, u_k \in \mathbb{U} \tag{4.26b}$$

$$\tilde{x}_k^\intercal \left(Q(\tilde{x}_k) - \gamma I_n\right) \tilde{x}_k \geq 0 \tag{4.26c}$$

$$\tilde{x}_k^\intercal \left(\Gamma I_n - Q(\tilde{x}_k)\right) \tilde{x}_k \geq 0 \tag{4.26d}$$

$$Z_k - \Gamma^{-1} I_n \succeq 0, \tag{4.26e}$$

$$\gamma^{-1} I_n - Z_k \succeq 0 \tag{4.26f}$$

$$\begin{bmatrix} \rho \tilde{x}_k^\intercal Q(\tilde{x}_k) \tilde{x}_k & \sum_{j=0}^{p} \alpha_j^\intercal(x_k, u_k) m_{j,k} - x_{ref}^\intercal \\ \sum_{j=0}^{p} \alpha_j(x_k, u_k) m_{j,k} - x_{ref} & Z_k \end{bmatrix} \succeq 0 \tag{4.26g}$$

$$\varepsilon_k I_{n+1} - \begin{bmatrix} \rho \tilde{x}_k^\intercal Q(\tilde{x}_k) \tilde{x}_k & \sum_{j=0}^{p} \alpha_j^\intercal(x_k, u_k) m_{j,k} - x_{ref}^\intercal \\ \sum_{j=0}^{p} \alpha_j(x_k, u_k) m_{j,k} - x_{ref}^\intercal & Z_k \end{bmatrix} \succeq 0 \tag{4.26h}$$

$$H(m_k) \succeq 0, \quad m_{0,k} = 1 \tag{4.26i}$$

$$\sum_{j=1}^{p+1} \beta_j m_{j,k} = 0 \tag{4.26j}$$

Notice that equality constraint (4.26j) can be written using semidefinite constraints $\sum_{j=1}^{p+1} \beta_j m_{j,k} \geq 0$ and $\sum_{j=1}^{p+1} \beta_j m_{j,k} \leq 0$. The SDP in Eq. (4.26) can be solved at each sample time using highly optimized numerical solvers. The solution yields a sequence of moments, satisfying the positivity constraint of its corresponding Hankel matrix. These moments are the control signals for the relaxed system in Eq. (4.25) that solve the reference tracking problem. In section 4.5 a brief discussion on computational aspects of the SDP will be presented.

4.4.3 Measure recovery

In the context of the relaxed SDP (4.26), the process of measure recovery implies to use the obtained moment sequence m_k to find the control signal s_k for the original polynomial problem. This process will yield a nonnegative Dirac measure supported on the real line. The measure may be supported on one or more points, corresponding to values of the control variable s_k. Each support point has an associated weight value.

Given a sequence of moments $\{m_1, \ldots, m_{2r-1}\}$, the associated nonnegative measure of the form $\mu_s = \sum_{i=1}^{p} \omega_i \delta(s - s_i)$ can be obtained, by considering first the following polynomial [50]:

$$p(s) = \begin{vmatrix} 1 & m_1 & m_2 & \ldots & m_r \\ m_1 & m_2 & m_3 & \ldots & m_{r+1} \\ \vdots & \vdots & \vdots & \ddots & \vdots \\ m_{r-1} & m_r & m_{r+1} & \ldots & m_{2r-1} \\ 1 & s & s^2 & \ldots & s^r \end{vmatrix} \tag{4.27}$$

Cette thèse est accessible à l'adresse : http://theses.insa-lyon.fr/publication/2019LYSEI123/these.pdf
© [G. J. Becerra], [2019], INSA de Lyon, tous droits réservés

where $|\cdot|$ corresponds to the matrix determinant. This polynomial has r different real roots which are the support points s_i of the measure μ_s. To find the weights ω_i for all support points, the following linear system is solved:

$$\sum_{i=1}^{r} \omega_i s_i^j = m_j, \ (1 \leq j \leq r) \tag{4.28}$$

To illustrate this procedure, consider an arbitrary measure:

$$\mu_s = 0.2\delta(s-0.1) + 0.5\delta(s-0.3) + 0.3\delta(s-1), \tag{4.29}$$

with $s \in \mathbb{R}$, and δ the Dirac delta function. The n^{th} moment for this measure can be computed as:

$$m_n = \int_{-\infty}^{\infty} s^n \mu_s ds \tag{4.30}$$

Considering $n \in \{1, 2, \ldots, 9\}$, the associated moment sequence is

$$\begin{aligned} m = \{&0.47, 0.347, 0.3137, 0.30407, 0.301217, 0.3003647, \\ &0.30010937, 0.300032807, 0.3000098417\}. \end{aligned}$$

Let us now assume that the measure μ_s in Eq. (4.29) is unknown, and we want to recover it from the knowledge of its moment sequence. The polynomial in Eq. (4.27) corresponding to this moment sequence with $r = 5$ is:

$$\begin{aligned} p(s) = &-1.8037 \times 10^{-36} s^5 + 1.0751 \times 10^{-36} s^4 - 2.8978 \times 10^{-37} s^3 \\ &+ 1.5925 \times 10^{-36} s^2 - 6.2053 \times 10^{-37} s + 4.6328 \times 10^{-38} \end{aligned}$$

The roots of this polynomial yield the support points for the measure μ_s:

$$s = \{0.1, 0.3, 1, -0.4019 \pm 0.8334j\}$$

Since we know the measure is supported on the real line, we take only the real roots. Therefore, the support points are $s_1 = 0.1$, $s_2 = 0.3$, $s_3 = 1$, which correspond to those in Eq. (4.29). To obtain the weights, we solve the following system:

$$\begin{bmatrix} s_1 & s_2 & s_3 \\ s_1^2 & s_2^2 & s_3^2 \\ s_1^2 & s_2^2 & s_3^2 \end{bmatrix} \begin{bmatrix} \omega_1 \\ \omega_2 \\ \omega_3 \end{bmatrix} = \begin{bmatrix} m_1 \\ m_2 \\ m_3 \end{bmatrix}$$

The computed weights are $\omega_1 = 0.2$, $\omega_2 = 0.5$, $\omega_3 = 0.3$, corresponding to those in Eq. (4.29).

4.4.4 Synthesis of the Control Signal for the Switched System

In the previous section, the sequence of moments m_k was used to recover the measure μ_s at each time k. We now present a procedure to obtain the control

Cette thèse est accessible à l'adresse : http://theses.insa-lyon.fr/publication/2019LYSEI123/these.pdf
© [G. J. Becerra], [2019], INSA de Lyon, tous droits réservés

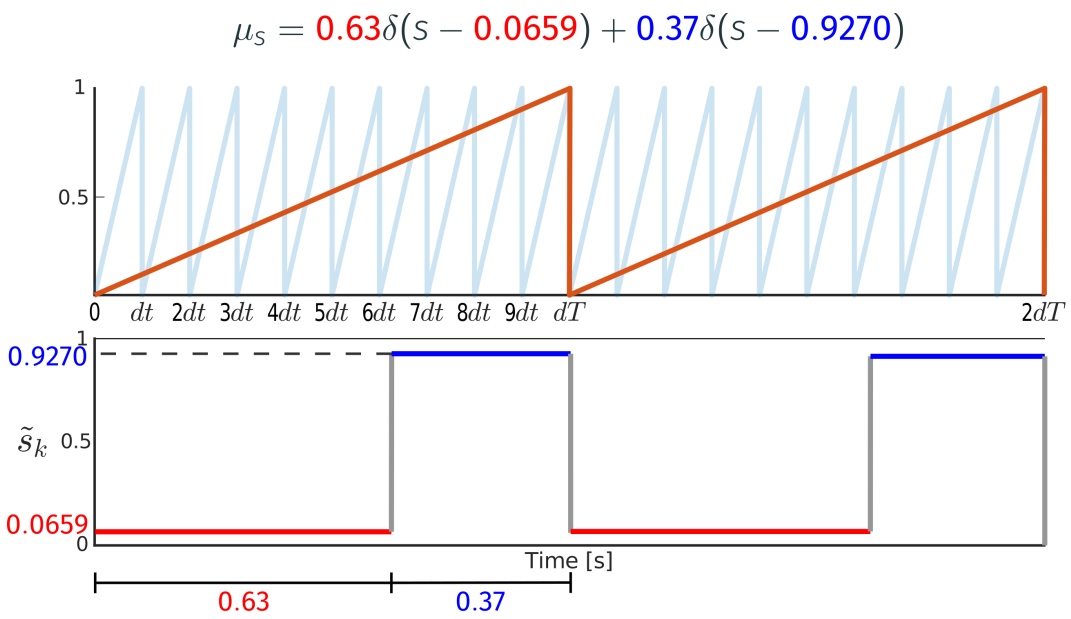

FIGURE 4.9 – Synthesis of control signal: PWM periods τ and T, PWM signal $\tilde{s}_k$ with period T representing the measure μ_s.

signal σ_k for the switched system (4.20), using the information contained in the measure.

As mentioned before, the measure can be supported in one or more points on the real line. The simplest case occurs when the support is a single point, and in this case the control signal for the polynomial system (4.22) is equal to the first moment: $s_k = m_{1,k}$. When the measure is supported in more than one point, there may be different approaches to obtain a value for s_k. One possibility could be to compute the weighted combination of the supports, yielding again $s_k = m_{1,k}$. However, in this case there is a loss of information, because there are infinitely many measures that have the same first moment. The number of support points in a recovered measure μ_s corresponds to the degrees of freedom required to *drive* the system state towards the references and is therefore associated to the controllability of the system.

We propose the following two-step approach to synthesize a control signal for the switched system (4.20). First, the information in the recovered measure μ_s is used to obtain the control signal s_k for the polynomial system (4.22). Then, this signal is used to obtain the indexes of the active subsystems σ_k during a switching period.

Consider first the measure μ_s as a representation of a PWM signal with period T, where the measure supports correspond to the signal values, and the measure weights correspond to the duty cycles. For instance, assume the recovered measure at time k is $\mu_s = 0.63\delta(s - 0.0659) + 0.37\delta(s - 0.9270)$. Notice that this measure has two support points. The PWM signal $\tilde{s}_k$ shown in Fig. 4.9 takes the two values $s_{1,k} = 0.0659$ and $s_{2,k} = 0.9270$ associated to the two support points. Each of these values is active during 63% and 37% of the switching period T, corresponding to the measure weights $\omega_{1,k} = 0.63$ and $\omega_{2,k} = 0.37$.

The obtained PWM signal $\tilde{s}_k$ is then used to evaluate the set of Lagrange

Cette thèse est accessible à l'adresse : http://theses.insa-lyon.fr/publication/2019LYSEI123/these.pdf
© [G. J. Becerra], [2019], INSA de Lyon, tous droits réservés

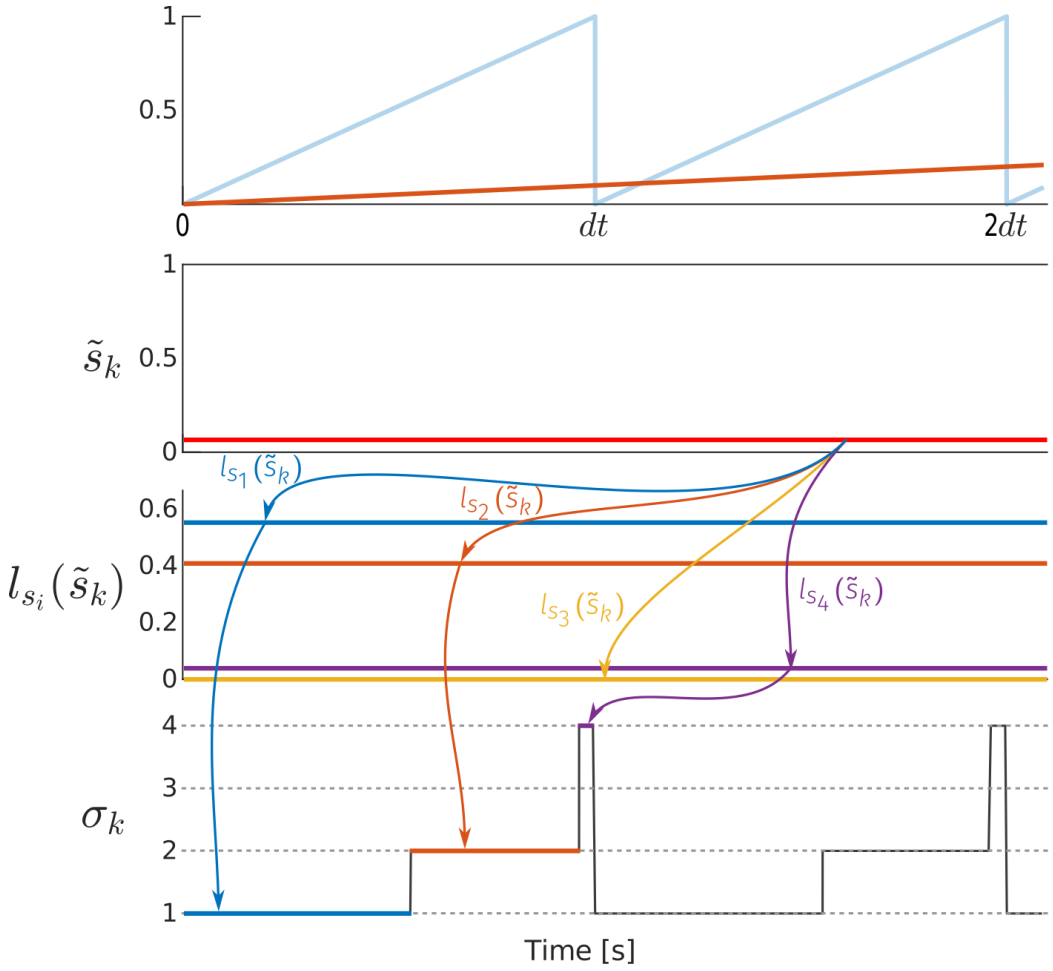

FIGURE 4.10 – Synthesis of control signal: Lagrange functions $l_{s_i}(\tilde{s}_k)$ and switched PWM control signal σ_k with period τ associated to the Lagrange functions.

functions $l_{s_i}(\tilde{s}_k)$ shown in Fig 4.10. The values of the Lagrange functions are interpreted again as the duty cycles of a PWM signal σ_k with period τ. The values this signal takes correspond to the subsystem indices. The resulting signal σ_k is used to select the active subsystem at each sample time.

Notice that evaluating the Lagrange polynomials may yield negative values, as shown in Fig. 3.1, which cannot be associated to *negative duty cycles*. To solve this problem we rescale the obtained values to the interval $[0, 1]$. This approximation introduces an error that could be reduced by using other polynomial bases. The PWM frequencies should be high enough to guarantee that the assumptions of the averaging principle are satisfied.

In the example shown in Figs. 4.9 and 4.10, the switched system has 4 modes. Each T period has 10 τ periods. For each τ period, the subsystem modes $\sigma_k = \{\bar{s}_1, \bar{s}_2, \bar{s}_3, \bar{s}_4\}$ are activated in sequence with a time duration proportional to the values given by the Lagrange functions. This signal is ready to be applied as control input to the switched system.

Cette thèse est accessible à l'adresse : http://theses.insa-lyon.fr/publication/2019LYSEI123/these.pdf
© [G. J. Becerra], [2019], INSA de Lyon, tous droits réservés

4.4.5 tdCLF Algorithm for Switched Systems

Algorithm 1 presents a summary of the proposed tdCLF control method for switched systems. This implementation assumes that the relaxed formulation in Eq. (4.25) has been previously obtained for the switched system, and the constraints in the SDP have been prepared as functions of x_k, x_{ref} and u_k.

Algorithme 1 : Algorithm for closed loop control of switched systems using the tdCLF approach.

Data : Relaxed model (4.25), x_{ref}
while *true* **do**
1. Measure x_k, u_k.
2. Substitute $\tilde{x}_k = x_k - x_{ref}$, u_k in the constraints of Eq. (4.26).
3. Solve the SDP in Eq. (4.26) using an interior-point method to obtain m_k, $Q(\tilde{x}_k)$, Z_k.
4. Recover the measure $\mu_{s,k}$ using Eqs. (4.27) and (4.28).
5. Synthesize the control signal σ_k using the procedure described in section 4.4.4.

end

4.4.6 Application Examples

SEPIC Converter

The approach described in the previous section is used for synthesizing a CLF for the SEPIC converter described in section 2.1.4. Let us assume that the converter operates only in CCM, yielding a switched system with two different modes: $\mathcal{S} = \{\bar{s}_1, \bar{s}_2\} = \{0, 1\}$. We obtain a discrete-time representation of matrices (2.3), (2.4), (2.5) with a complementary activation of s and δ. This means that all the off-diagonal elements in matrix (2.5) are equal to zero. The discretization of each subsystem in the switched model is computed using Tustin's method with a sample time $T_s = 0.1$ ms, obtaining:

$$x_{k+1} = A_{\sigma_k} x_k + B_{\sigma_k} u_k, \quad \sigma_k \in \mathcal{S} \tag{4.31}$$

where A_σ, B_σ correspond to the following matrices:

$$A_0 = \begin{bmatrix} 0.8911 & -0.0411 & 0.0100 & -0.0394 \\ 0.4977 & 0.9892 & 0.0026 & -0.0104 \\ 0.0697 & -0.0015 & 0.8607 & 0.2787 \\ 0.4765 & -0.0104 & -0.4841 & 0.9049 \end{bmatrix}, \quad B_0 = \begin{bmatrix} 0.0411 \\ 0.0108 \\ 0.0015 \\ 0.0104 \end{bmatrix},$$

$$A_1 = \begin{bmatrix} 0.9113 & 0 & 0 & 0 \\ 0 & 0.9258 & 0.4894 & 0 \\ 0 & -0.2818 & 0.8599 & 0 \\ 0 & 0 & 0 & 0.9881 \end{bmatrix}, \quad B_1 = \begin{bmatrix} 0.0416 \\ 0 \\ 0 \\ 0 \end{bmatrix}.$$

Cette thèse est accessible à l'adresse : http://theses.insa-lyon.fr/publication/2019LYSEI123/these.pdf
© [G. J. Becerra], [2019], INSA de Lyon, tous droits réservés

The sample time was determined by running simulations and comparing the responses of the continuous and discrete time systems. It was chosen as the highest time such that the discrete-time system yields a good approximation of the continuous-time system. The set of Lagrange polynomials for a system with two modes are $l_0(s_k) = (1 - s_k)$, $l_1(s_k) = s_k$. Therefore, the polynomial system can be written as

$$x_{k+1} = \sum_{i=1}^{2} l_{\bar{s}_i}(s_k)\left(A_{\bar{s}_i}x_k + B_{\bar{s}_i}u_k\right) = \sum_{j=0}^{1} \alpha_j(x_k, u_k)s_k^j \tag{4.32a}$$

$$0 = \sum_{i=1}^{2}(s_k - \bar{s}_i) = s_k^2 - s_k \tag{4.32b}$$

with the polynomial coefficients given by

$$\alpha_0(x_k, u_k) = \begin{bmatrix} 0.891x_{1,k} - 0.0411x_{2,k} + 0.01x_{3,k} - 0.0394x4 + 0.0411u_k \\ 0.498x_{1,k} + 0.989x_{2,k} + 0.00263x_{3,k} - 0.0104x4 + 0.0108u_k \\ 0.0697x_{1,k} - 0.00152x_{2,k} + 0.861x_{3,k} + 0.279x4 + 0.00152u_k \\ 0.476x_{1,k} - 0.0104x_{2,k} - 0.484x_{3,k} + 0.905x4 + 0.0104u_k \end{bmatrix}, \tag{4.33}$$

$$\alpha_1(x_k, u_k) = \begin{bmatrix} 0.0202x_{1,k} + 0.0411x_{2,k} - 0.01x_{3,k} + 0.0394x4 + 4.4e-4u_k \\ -0.498x_{1,k} - 0.0633x_{2,k} + 0.487x_{3,k} + 0.0104x4 - 0.0108u_k \\ -0.0697x_{1,k} - 0.28x_{2,k} - 7.79e-4x_{3,k} - 0.279x4 - 0.00152u_k \\ -0.476x_{1,k} + 0.0104x_{2,k} + 0.484x_{3,k} + 0.0832x4 - 0.0104u_k \end{bmatrix}. \tag{4.34}$$

The relaxation for the polynomial system is obtained simply by replacing s_k with $m_{1,k}$, and adding the semidefinite constraint

$$H(m_k) = \begin{bmatrix} 1 & m_{1,k} \\ m_{1,k} & m_{2,k} \end{bmatrix} \succeq 0. \tag{4.35}$$

Solving the SDP (4.26) at each sample time k, we obtain the moment sequence m_k, and the matrices $Q(x_k)$ and $Q(x_k^+) = Z_k^{-1}$, which parameterize the Lyapunov functions. In this case there is no need to recover the measure, because its support is a singleton Dirac measure. Therefore, the control signal for the polynomial system is obtained directly as the first moment: $s_k = m_{1,k}$. The tdCLF algorithm is executed at a rate of 10 kHz. The SDP parameter values used are $\gamma = 0.01$, $\Gamma = 100$ and $\rho = 0.9$.

Fig.4.11 shows the simulation results for the polynomial system (4.32a), where the state x_k is tracking a random piecewise constant reference x_{ref} obtained from the equilibrium points of the polynomial system. The control achieves the tracking objective of all the references with a settling time of approximately 10 ms. The control signal s_k is shown in the last subplot, and it can be observed that it also converges to the reference value s_{ref} associated to the tracked equilibrium points.

In order to compute a control signal for the switched system (4.31), s_k is used as the duty cycle of a PWM signal with constant frequency of 50 kHz.

Cette thèse est accessible à l'adresse : http://theses.insa-lyon.fr/publication/2019LYSEI123/these.pdf
© [G. J. Becerra], [2019], INSA de Lyon, tous droits réservés

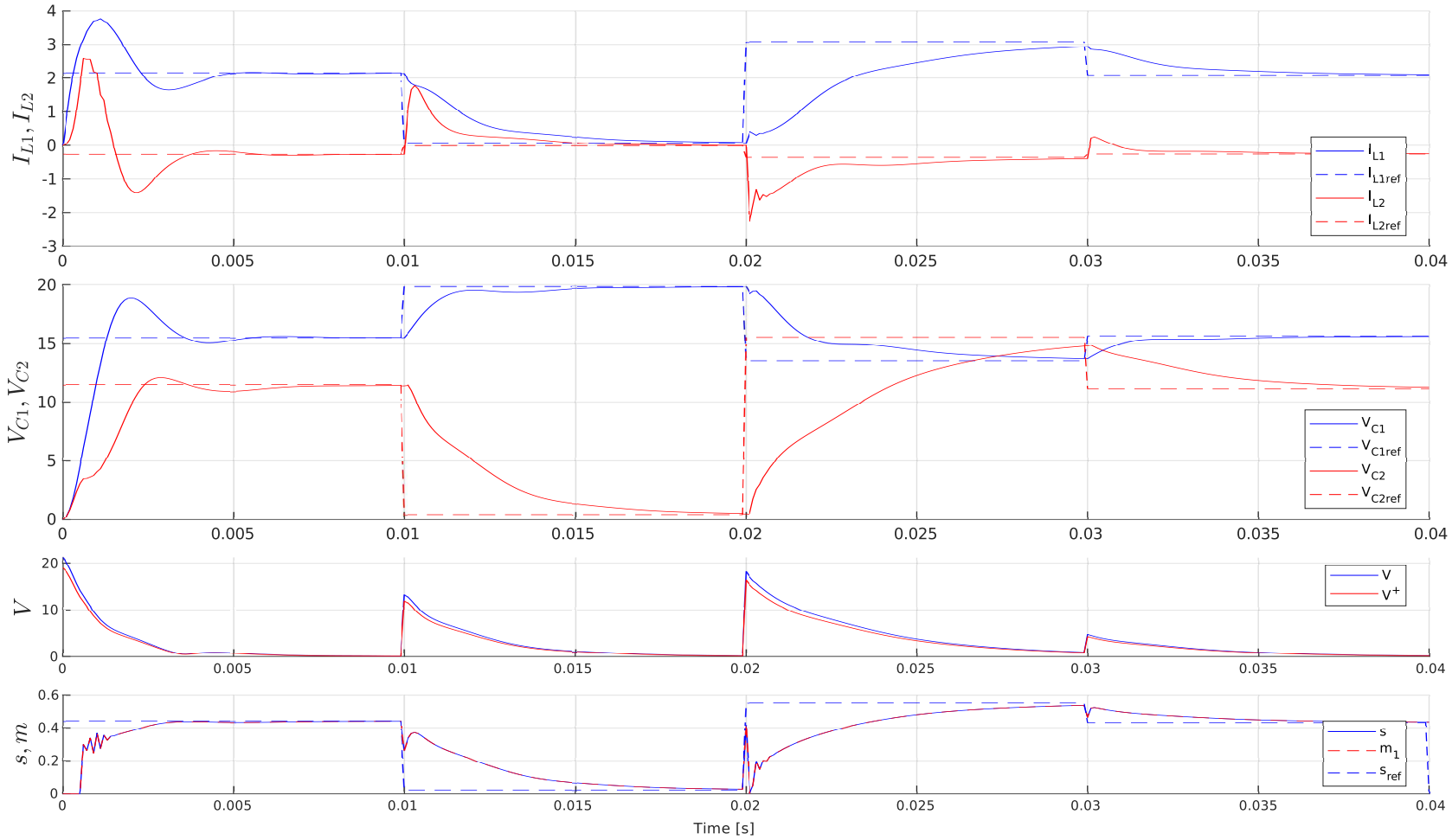

FIGURE 4.11 – SEPIC converter - simulation results: reference tracking for the polynomial model of the SEPIC converter. Currents and voltages (top), Lyapunov functions (center), control signal (bottom).

Cette thèse est accessible à l'adresse : http://theses.insa-lyon.fr/publication/2019LYSEI123/these.pdf
© [G. J. Becerra], [2019], INSA de Lyon, tous droits réservés

The simulation results are shown in Fig. 4.12, where the control tracks a random reference computed from the averaged equilibrium limit cycles of the switched system. In this case, the control also drives the system states towards the references, but there is a noticeable offset for V_{C2}. This offset appears because of the approximation error introduced when a discrete-time model is obtained from the original switched system, and can be decreased by increasing the switching frequency of the PWM generator.

Two-Cell Multicellular Converter

The two-cell multicellular converter presented in section 2.1.4 is used here for testing the tdCLF approach. This converter has two state variables and two independent switching inputs, yielding a system with 4 possible configurations. The discrete-time model is obtained as

$$x_{k+1} = A_{\sigma_k} x_k + B_{\sigma_k} u_k \tag{4.36}$$

by applying a discretization method to each subsystem. We use Tustin's method to obtain the following matrices:

$$\begin{aligned}
A_{\bar{s}_1} &= \begin{bmatrix} 1 & 0 \\ 0 & 0.9361 \end{bmatrix}, \quad B_{\bar{s}_1} = \begin{bmatrix} 0 \\ -0.001 \end{bmatrix}, \\
A_{\bar{s}_2} &= \begin{bmatrix} 0.9971 & -2.9292 \\ 0.0019 & 0.9333 \end{bmatrix}, \quad B_{\bar{s}_2} = \begin{bmatrix} 0.0015 \\ -0.001 \end{bmatrix}, \\
A_{\bar{s}_3} &= \begin{bmatrix} 0.9971 & 2.9292 \\ -0.0019 & 0.9333 \end{bmatrix}, \quad B_{\bar{s}_3} = \begin{bmatrix} 0.0015 \\ 0.001 \end{bmatrix}, \\
A_{\bar{s}_4} &= \begin{bmatrix} 1 & 0 \\ 0 & 0.9361 \end{bmatrix}, \quad B_{\bar{s}_4} = \begin{bmatrix} 0 \\ 0.001 \end{bmatrix}.
\end{aligned}$$

The sample time used in the discretization method is 0.2 ms. It was determined by running simulations and comparing the responses of the continuous and discrete time systems. The sample time was chosen as the highest time such that the discrete-time system yields a good approximation of the continuous-time system. The choice of the subsystem labels $\bar{s}_i$ is important in the context of the moment relaxation. For example, if the labels are chosen as integers $\bar{s}_1 = 0, \bar{s}_2 = 1, \bar{s}_3 = 2, \bar{s}_4 = 3$, the numerical solution of SDP (4.26) will be incorrect because the support points computed will have small values that will not allow the system to operate in modes $\bar{s}_3$ and $\bar{s}_4$. However, if the labels are chosen uniformly in the interval $[0, 1]$, the numerical solution will be correct, and the control will have access to operate the system in all available configurations. This may happen because the recovered measure has the form of a probability density function, but this fact needs to be further investigated. The labels chosen for each mode are $\bar{s}_1 = 0, \bar{s}_2 = 1/3, \bar{s}_3 = 2/3, \bar{s}_4 = 1$ The set of Lagrange polynomials for these

Cette thèse est accessible à l'adresse : http://theses.insa-lyon.fr/publication/2019LYSEI123/these.pdf
© [G. J. Becerra], [2019], INSA de Lyon, tous droits réservés

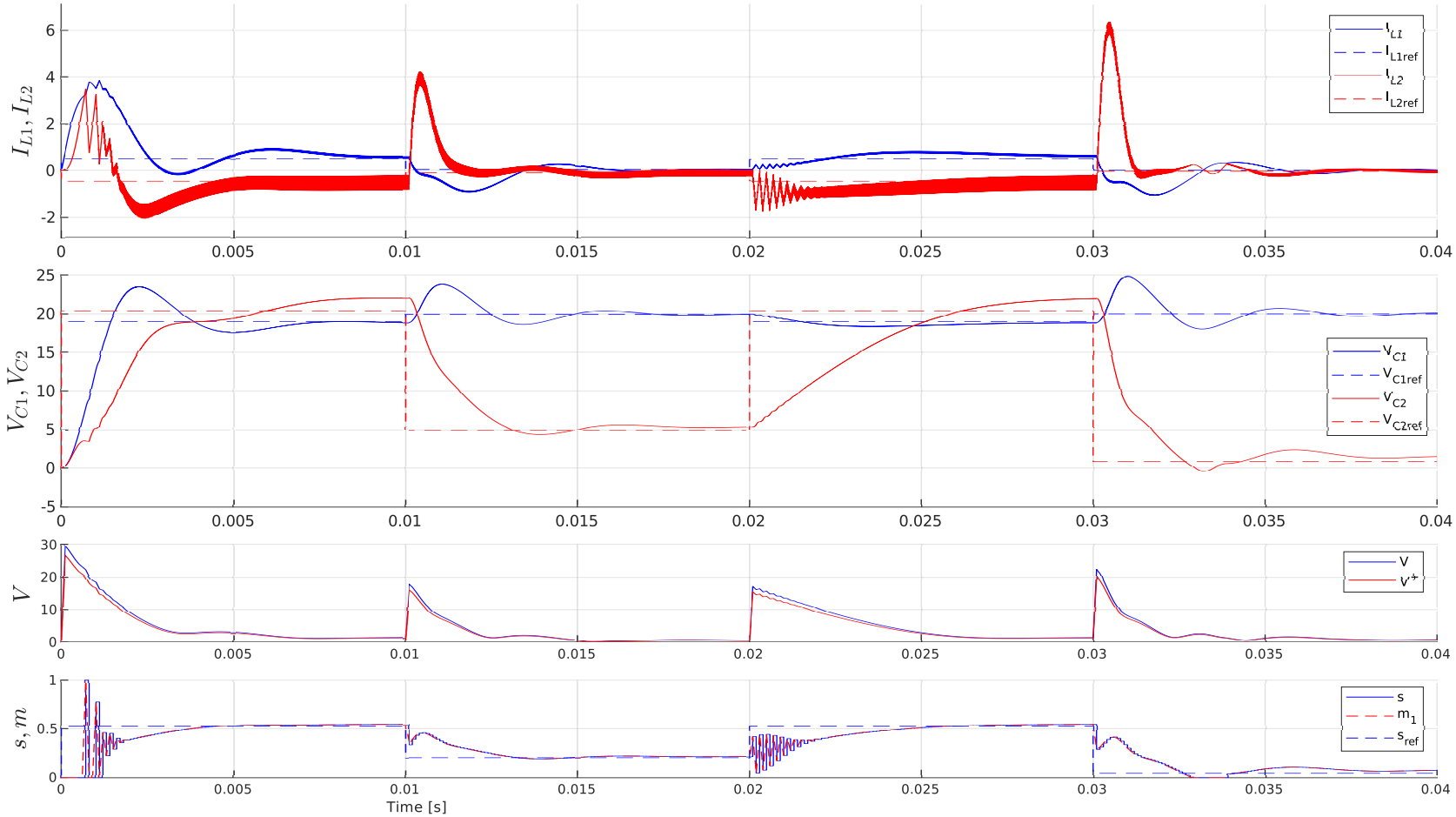

FIGURE 4.12 – SEPIC converter - simulation results: reference tracking for the switched model of the SEPIC converter. Currents and voltages (top), Lypunov functions (center), control signal (bottom).

Cette thèse est accessible à l'adresse : http://theses.insa-lyon.fr/publication/2019LYSEI123/these.pdf
© [G. J. Becerra], [2019], INSA de Lyon, tous droits réservés

labels is:

$$
\begin{aligned}
l_{\bar{s}_1}(s_k) &= -4.5s^3 + 9.0s^2 - 5.5s + 1.0 \\
l_{\bar{s}_2}(s_k) &= 13.5s^3 - 22.5s^2 + 9.0s \\
l_{\bar{s}_3}(s_k) &= -13.5s^3 + 18.0s^2 - 4.5s \\
l_{\bar{s}_4}(s_k) &= 4.5s^3 - 4.5s^2 + s
\end{aligned}
$$

The polynomial system obtained is

$$
x_{k+1} = \sum_{i=1}^{4} l_{\bar{s}_i}(s_k)\left(A_{\bar{s}_i}x_k + B_{\bar{s}_i}u_k\right) = \sum_{j=0}^{3} \alpha_j(x_k, u_k)s_k^j \tag{4.37}
$$

$$
0 = \sum_{i=1}^{4}(s_k - \bar{s}_i) = s^4 - 2s^3 + 1.2222s^2 - 0.22222s \tag{4.38}
$$

with the polynomial coefficients

$$
\begin{aligned}
\alpha_0(x_k, u_k) &= \begin{bmatrix} x_{1,k} \\ 0.93611x_{2,k} - 0.00096805u_k \end{bmatrix}, \\
\alpha_1(x_k, u_k) &= \begin{bmatrix} -0.013181x_{1,k} - 39.544x_{2,k} + 0.0065907u_k \\ 0.026099x_{1,k} - 0.01276x_{2,k} - 0.0067572u_k \end{bmatrix}, \\
\alpha_2(x_k, u_k) &= \begin{bmatrix} 0.013181x_{1,k} + 118.63x_{2,k} - 0.0065907u_k \\ -0.078298x_{1,k} + 0.01276x_{2,k} + 0.02608u_k \end{bmatrix}, \\
\alpha_3(x_k, u_k) &= \begin{bmatrix} -79.088x_{2,k} \\ 0.052198x_{1,k} - 0.017387u_k \end{bmatrix}.
\end{aligned}
$$

The tdCLF algorithm is executed at a rate of 5 kHz. The SDP parameter values used are $\gamma = 0.01$, $\Gamma = 100$ and $\rho = 0.9$. Fig. 4.13 shows the simulation results for the tracking of a random constant piecewise reference for the relaxed model (4.25). The control presents good tracking performance for both state variables. Fig. 4.14 shows the moment sequences obtained at each time k, and the recovered measure supports and weights. Notice that for different time intervals, the measure may be supported at one, two or three points. The approach described in section 4.4.4 is used to obtain a control signal for the switched system from the obtained measure. The obtained results are shown in Fig. 4.15, where the state variables have a good tracking performance, with a maximum settling time of approximately 5 ms.

Three-Cell Multicellular Converter

The approach introduced here is implemented for the three-cell flying capacitor converter used in the previous section. This converter has 3 binary control signals, yielding 8 different circuit configurations. The port-Hamiltonian model in Eq. (4.12) can be rewritten as:

$$
\dot{x}(t) = \mathcal{A}_{\sigma(t)}x(t) + \mathcal{B}_{\sigma(t)}u(t) \tag{4.39}
$$

Cette thèse est accessible à l'adresse : http://theses.insa-lyon.fr/publication/2019LYSEI123/these.pdf
© [G. J. Becerra], [2019], INSA de Lyon, tous droits réservés

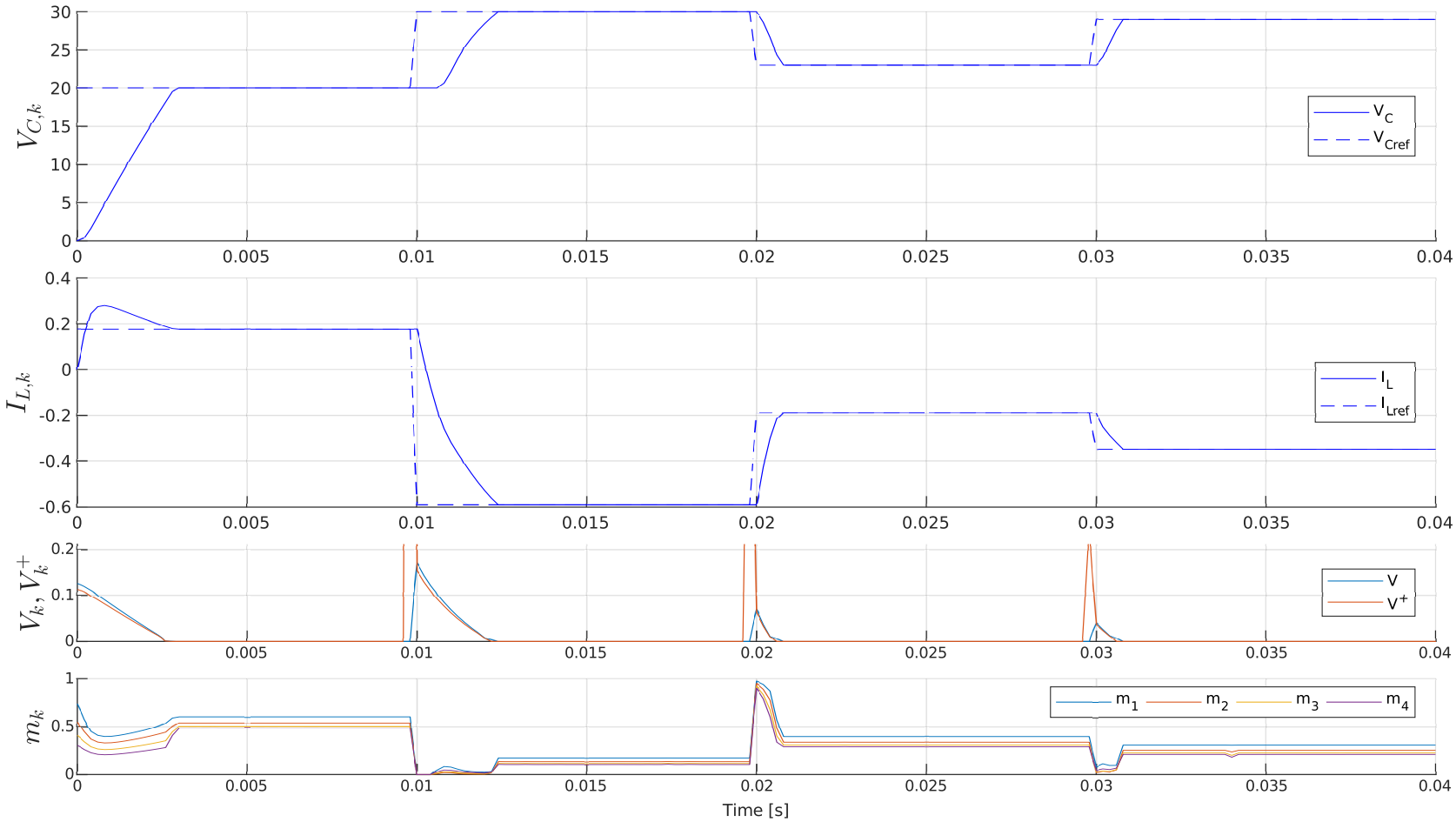

FIGURE 4.13 – Two-Cell converter - simulation results: reference tracking for the relaxed model in Eq. (4.25). Voltage and current tracking (top), Lyapunov functions (center) and moment sequences (bottom).

Cette thèse est accessible à l'adresse : http://theses.insa-lyon.fr/publication/2019LYSEI123/these.pdf
© [G. J. Becerra], [2019], INSA de Lyon, tous droits réservés

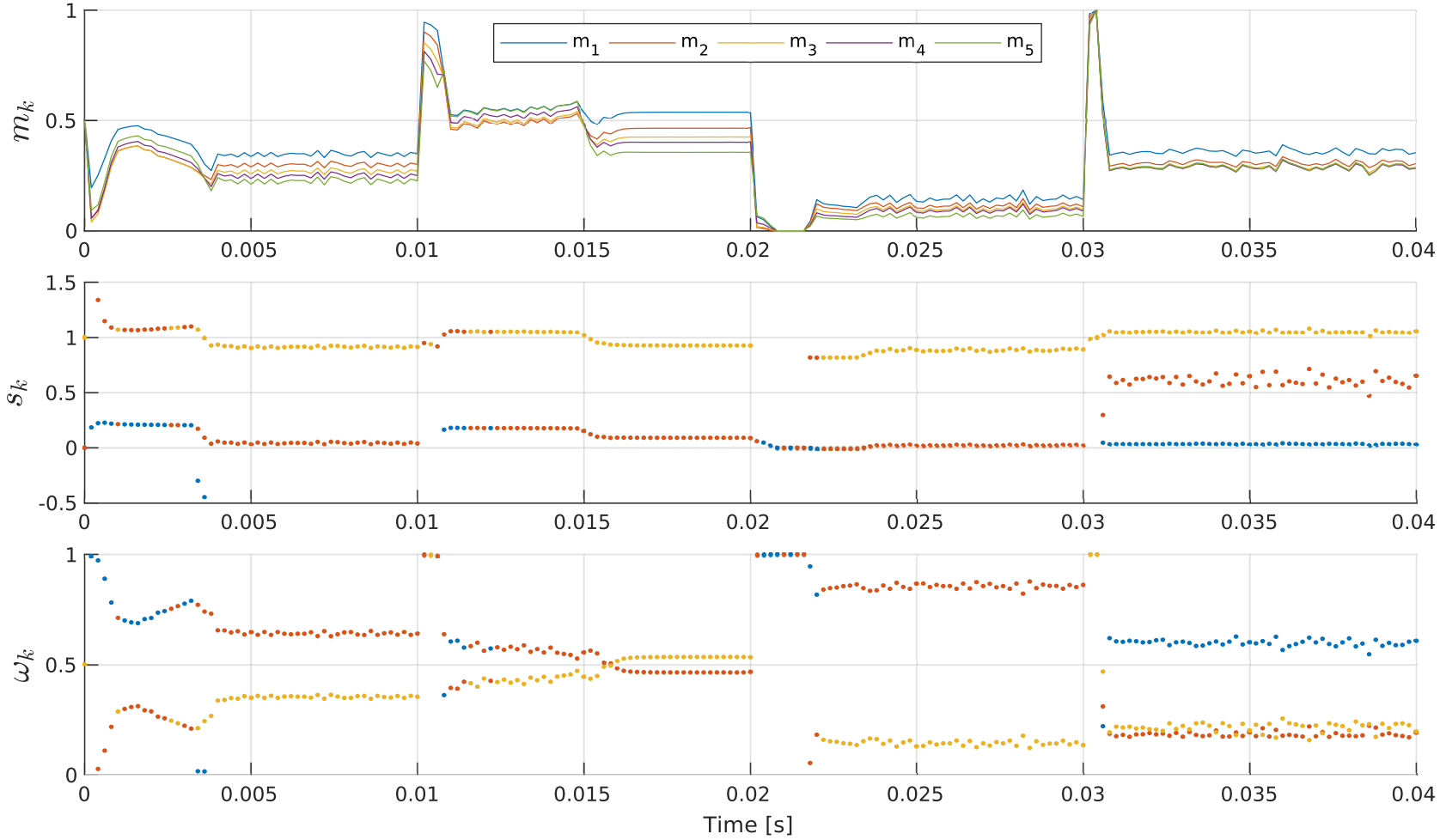

FIGURE 4.14 – Two-Cell converter - simulation results: Moment sequences (top), recovered measure support (center) and weights (bottom) for the switched system.

Cette thèse est accessible à l'adresse : http://theses.insa-lyon.fr/publication/2019LYSEI123/these.pdf
© [G. J. Becerra], [2019], INSA de Lyon, tous droits réservés

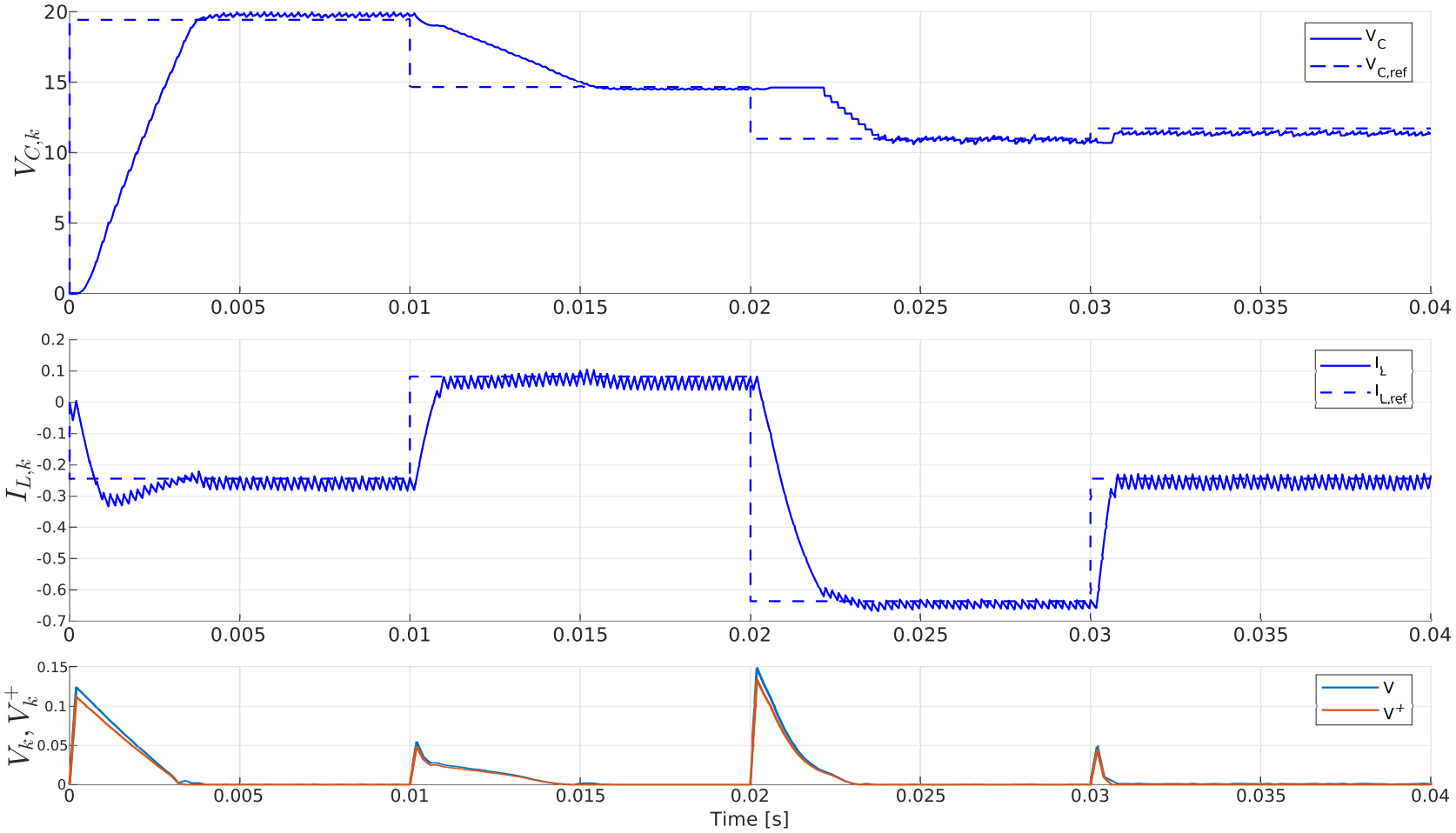

FIGURE 4.15 – Two-Cell converter - simulation results: reference tracking for the switched system. Voltage and current tracking (top, center) and Lyapunov functions (bottom).

Cette thèse est accessible à l'adresse : http://theses.insa-lyon.fr/publication/2019LYSEI123/these.pdf
© [G. J. Becerra], [2019], INSA de Lyon, tous droits réservés

where $\sigma(t) : \mathbb{R}_{>=0} \to \mathcal{S} = \{\bar{s}_1, \bar{s}_2, \ldots, \bar{s}_8\}$. The discrete-time model in Eq. (4.36) is obtained using Tustin's method for each of the 8 subsystems, using a sample time $T_s = 0.2$ ms. This sample time was chosen also by running simulations of the discrete and continuous time systems and choosing the highest value such that the discrete-time system yields a good approximation of the continuous-time system. The resulting system matrices are:

$$A_{\bar{s}_1} = \begin{bmatrix} 1 & 0 & 0 \\ 0 & 1 & 0 \\ 0 & 0 & 0.8763 \end{bmatrix}, \quad B_{\bar{s}_1} = \begin{bmatrix} 0 \\ 0 \\ -0.0019 \end{bmatrix},$$

$$A_{\bar{s}_2} = \begin{bmatrix} 0.9884 & 0 & -5.6547 \\ 0 & 1 & 0 \\ 0.0037 & 0 & 0.8653 \end{bmatrix}, \quad B_{\bar{s}_2} = \begin{bmatrix} 0.0058 \\ 0 \\ -0.0019 \end{bmatrix},$$

$$A_{\bar{s}_3} = \begin{bmatrix} 0.9884 & 0.0116 & 5.6319 \\ 0.0116 & 0.9884 & -5.6319 \\ -0.0037 & 0.0037 & 0.8542 \end{bmatrix}, \quad B_{\bar{s}_3} = \begin{bmatrix} -0.0058 \\ 0.0058 \\ -0.0019 \end{bmatrix},$$

$$A_{\bar{s}_4} = \begin{bmatrix} 1 & 0 & 0 \\ 0 & 0.9884 & -5.6547 \\ 0 & 0.0037 & 0.8653 \end{bmatrix}, \quad B_{\bar{s}_4} = \begin{bmatrix} 0 \\ 0.0058 \\ -0.0019 \end{bmatrix},$$

$$A_{\bar{s}_5} = \begin{bmatrix} 1 & 0 & 0 \\ 0 & 0.9884 & 5.6547 \\ 0 & -0.0037 & 0.8653 \end{bmatrix}, \quad B_{\bar{s}_5} = \begin{bmatrix} 0 \\ 0.0058 \\ 0.0019 \end{bmatrix},$$

$$A_{\bar{s}_6} = \begin{bmatrix} 0.9884 & 0.0116 & -5.6319 \\ 0.0116 & 0.9884 & 5.6319 \\ 0.0037 & -0.0037 & 0.8542 \end{bmatrix}, \quad B_{\bar{s}_6} = \begin{bmatrix} -0.0058 \\ 0.0058 \\ 0.0019 \end{bmatrix},$$

$$A_{\bar{s}_7} = \begin{bmatrix} 0.9884 & 0 & 5.6547 \\ 0 & 1 & 0 \\ -0.0037 & 0 & 0.8653 \end{bmatrix}, \quad B_{\bar{s}_7} = \begin{bmatrix} 0.0058 \\ 0 \\ 0.0019 \end{bmatrix},$$

$$A_{\bar{s}_8} = \begin{bmatrix} 1 & 0 & 0 \\ 0 & 1 & 0 \\ 0 & 0 & 0.8763 \end{bmatrix}, \quad B_{\bar{s}_8} = \begin{bmatrix} 0 \\ 0 \\ 0.0019 \end{bmatrix}.$$

The control objective is tracking a piecewise constant reference x_{ref}. The polynomial equations (4.22a) are written using a basis of Lagrange polynomials using the mode labels $\{\bar{s}_1 = 0,\ \bar{s}_2 = 1/7,\ \bar{s}_3 = 2/7,\ \ldots,\ \bar{s}_8 = 1\}$. The obtained polynomial is of the form

$$x_{k+1} = \sum_{j=0}^{7} \alpha_j(x_k, u_k) s_k^j \tag{4.40}$$

Cette thèse est accessible à l'adresse : http://theses.insa-lyon.fr/publication/2019LYSEI123/these.pdf
© [G. J. Becerra], [2019], INSA de Lyon, tous droits réservés

with coefficients $\alpha_j(x_k, u_k)$ expressed as follows:

$$\alpha_0(x_k,u_k) = \begin{bmatrix} x_{1,k} \\ x_{2,k} \\ 0.87634x_{3,k} - 0.0018736u_k \end{bmatrix}$$

$$\alpha_1(x_k,u_k) = \begin{bmatrix} 0.036812x_{1,k} - 0.50974x_{2,k} - 902.78x_{3,k} + 0.49133u_k \\ -0.50974x_{1,k} + 0.27327x_{2,k} - 228.63x_{3,k} - 0.13664u_k \\ 0.59584x_{1,k} + 0.1509x_{2,k} + 0.29669x_{3,k} - 0.14625u_k \end{bmatrix}$$

$$\alpha_2(x_k,u_k) = \begin{bmatrix} -2.0326x_{1,k} + 6.754x_{2,k} + 12711.0x_{3,k} - 5.7377u_k \\ 6.754x_{1,k} - 3.4278x_{2,k} + 4146.7x_{3,k} + 1.7139u_k \\ -8.3896x_{1,k} - 2.7368x_{2,k} - 5.2247x_{3,k} + 2.3754u_k \end{bmatrix}$$

$$\alpha_3(x_k,u_k) = \begin{bmatrix} 11.527x_{1,k} - 29.487x_{2,k} - 67611.0x_{3,k} + 23.723u_k \\ -29.487x_{1,k} + 13.845x_{2,k} - 27315.0x_{3,k} - 6.9224u_k \\ 44.623x_{1,k} + 18.028x_{2,k} + 24.277x_{3,k} - 14.125u_k \end{bmatrix}$$

$$\alpha_4(x_k,u_k) = \begin{bmatrix} -24.603x_{1,k} + 57.239x_{2,k} + 178988.0x_{3,k} - 44.937u_k \\ 57.239x_{1,k} - 25.762x_{2,k} + 82375.0x_{3,k} + 12.881u_k \\ -118.13x_{1,k} - 54.368x_{2,k} - 48.192x_{3,k} + 40.242u_k \end{bmatrix}$$

$$\alpha_5(x_k,u_k) = \begin{bmatrix} 22.608x_{1,k} - 50.995x_{2,k} - 252155.0x_{3,k} + 39.691u_k \\ -50.995x_{1,k} + 22.608x_{2,k} - 124055.0x_{3,k} - 11.304u_k \\ 166.42x_{1,k} + 81.873x_{2,k} + 43.264x_{3,k} - 58.958u_k \end{bmatrix}$$

$$\alpha_6(x_k,u_k) = \begin{bmatrix} -7.5358x_{1,k} + 16.998x_{2,k} + 180555.0x_{3,k} - 13.23u_k \\ 16.998x_{1,k} - 7.5358x_{2,k} + 91100.0x_{3,k} + 3.7679u_k \\ -119.17x_{1,k} - 60.126x_{2,k} - 14.421x_{3,k} + 42.861u_k \end{bmatrix}$$

$$\alpha_7(x_k,u_k) = \begin{bmatrix} -51587.0x_{3,k} \\ -26029.0x_{3,k} \\ 34.047x_{1,k} + 17.179x_{2,k} - 12.246u_k \end{bmatrix}$$

Notice that these functions can be numerically evaluated at each sample time k given the known state x_k and exogenous input u_k. Constraint (4.21b) becomes

$$0 = \sum_{j=1}^{8} (s_k - \bar{s}_j)$$

$$0 = s^8 - 4.0s^7 + 6.5714s^6 - 5.7143s^5 + 2.8192s^4 - 0.78134s^3 + 0.11108s^2 - 0.0061199s$$

The moment relaxation is obtained by substituting $\{s, s^2, \ldots, s^8\}$ in the polynomial model with the associated moments $\{m_1, m_2, \ldots, m_8\}$, and considering the following Hankel moment matrix:

$$H(m_k) = \begin{bmatrix} 1 & m_{1,k} & m_{2,k} & m_{3,k} & m_{4,k} \\ m_{1,k} & m_{2,k} & m_{3,k} & m_{4,k} & m_{5,k} \\ m_{2,k} & m_{3,k} & m_{4,k} & m_{5,k} & m_{6,k} \\ m_{3,k} & m_{4,k} & m_{5,k} & m_{6,k} & m_{7,k} \\ m_{4,k} & m_{5,k} & m_{6,k} & m_{7,k} & m_{8,k} \end{bmatrix} \succeq 0. \tag{4.42}$$

Cette thèse est accessible à l'adresse : http://theses.insa-lyon.fr/publication/2019LYSEI123/these.pdf
© [G. J. Becerra], [2019], INSA de Lyon, tous droits réservés

Solving the SDP (4.26) at each time k yields a moment sequence m_k which is used as the control signal for the relaxed model of the multicellular converter. The tdCLF algorithm is executed at a rate of 5 kHz. The SDP parameter values used are $\gamma = 0.01$, $\Gamma = 100$ and $\rho = 0.9$. Fig. 4.16 shows the simulation results for this case, where the state variables are tracking random piecewise-constant references. It can be observed that the control achieves the tracking objective with good performance for all the state variables. The first and second subplots (top to bottom) show the converter voltages and current with their respective references. The third subplot shows the Lyapunov functions $V(x_k, Q(x_k))$, $V(x_k^+, Q(x_k^+))$. The fourth subplot shows the computed moment sequences m_k.

The procedure described in section 4.4.3 is used to recover the measure μ_s. Fig. 4.17 shows (top to bottom) the moment sequences m_k and the computed supports s_k and weights ω_k for the measure μ_k. Notice that the measure may be supported in one point (e.g. $t = [0.04, 0.044]$), two points (e.g. $t = [0, 0.01]$), three points (e.g. $t = [0.03, 0.04]$), and four points (e.g. $t = [0.062, 0.063]$).

Using the approach proposed in section 4.4.4 we synthesize the control signal for the original switched system (4.36). Fig. 4.18 shows the detail of the control signal σ_k obtained for one switching interval $dT = T_s = 0.2$ ms. The first and second subplots (top to bottom) show that, at $t = 0.0108$ s, the measure is supported on two points: $\mu_k = 0.1035\delta(s_k - 0.6813) + 0.8965\delta(s_k - 0.9980)$. The third subplot shows that the switching interval dT corresponds to 10 times the switching interval dt. The support points are used to evaluate the Lagrange polynomials $l_{\bar{s}_i}$ as shown in the fourth subplot. The last subplot shows the obtained control signal σ_k that selects the active subsystem during a period of time proportional to the associated *weight* given by the Lagrange polynomials for each subsystem. Fig. 4.19 shows the simulation results for the synthesized control signal σ_k. Both capacitor voltages and the inductor current track random references, showing good performance with a maximum settling time of approximately 13 ms. Notice that the Lyapunov functions $V(x_k, Q(x_k)), V(x_k^+, Q(x_k^+))$ during the transient at $t = 0.02$ s increase their value for a brief period while the state is settling towards the references. This is a characteristic of this approach, where the monotone decreasing property of CLFs is relaxed to achieve improvements in performance.

4.5 Computational Aspects of the tdCLF Method

The main computational difficulty to obtain the control signal for a switched system using the tdCLF approach is the solution of the SDP in Eq. (4.26). It is known that SDPs are a subset of convex optimization problems that can be efficiently solved in polynomial time using interior point methods [51], [52]. Also, it has been recognized that many problems in control systems can be solved efficiently, sometimes in real time, using interior point methods [53]. In our case the SDP was modeled using YALMIP [54] version R20190425.

Cette thèse est accessible à l'adresse : http://theses.insa-lyon.fr/publication/2019LYSEI123/these.pdf
© [G. J. Becerra], [2019], INSA de Lyon, tous droits réservés

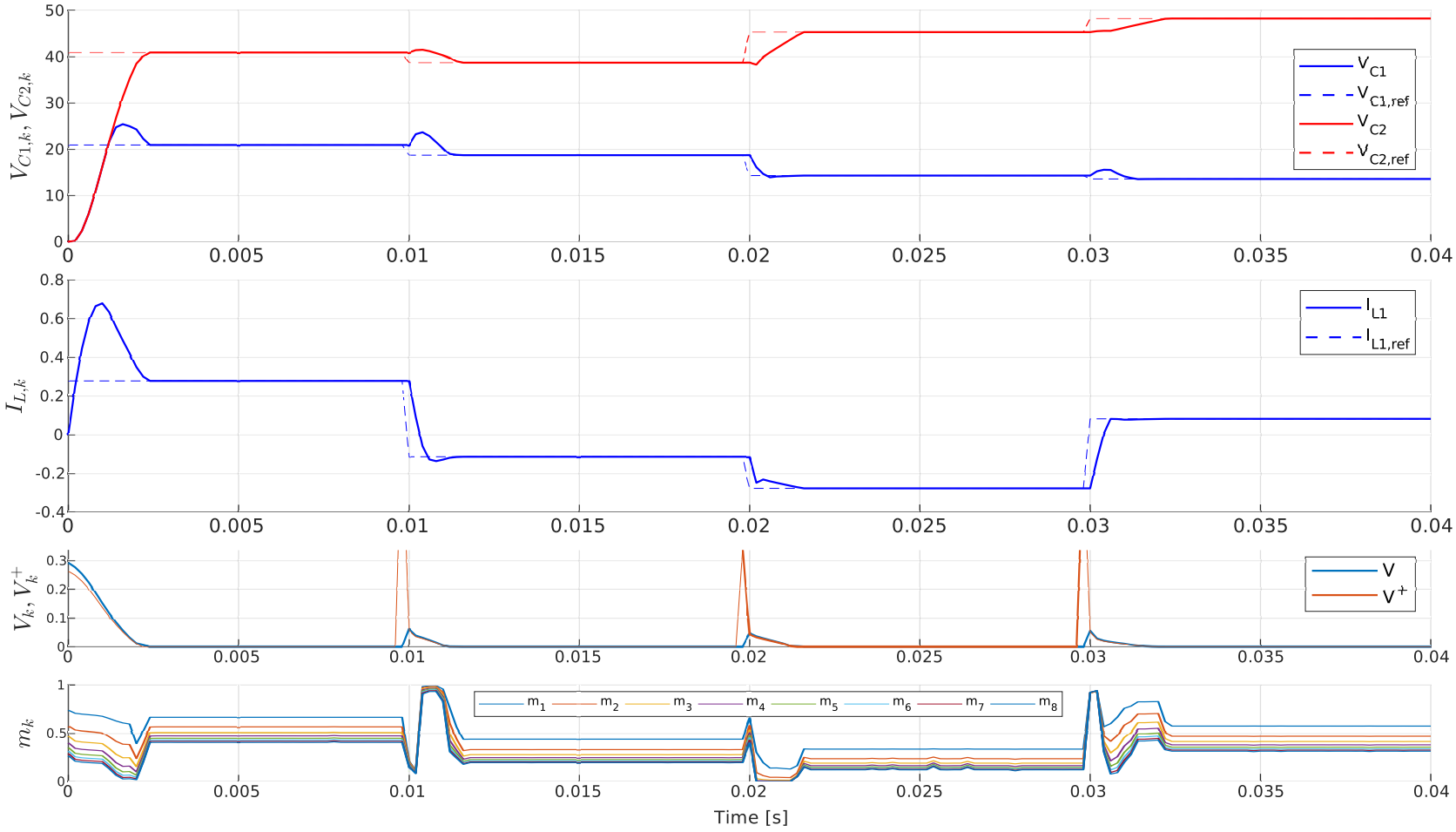

FIGURE 4.16 – Three-cell converter - simulation results: reference tracking for the relaxed model in Eq. (4.25). Voltages and current tracking (top), Lyapunov functions (center) and moment sequences (bottom).

Cette thèse est accessible à l'adresse : http://theses.insa-lyon.fr/publication/2019LYSEI123/these.pdf
© [G. J. Becerra], [2019], INSA de Lyon, tous droits réservés

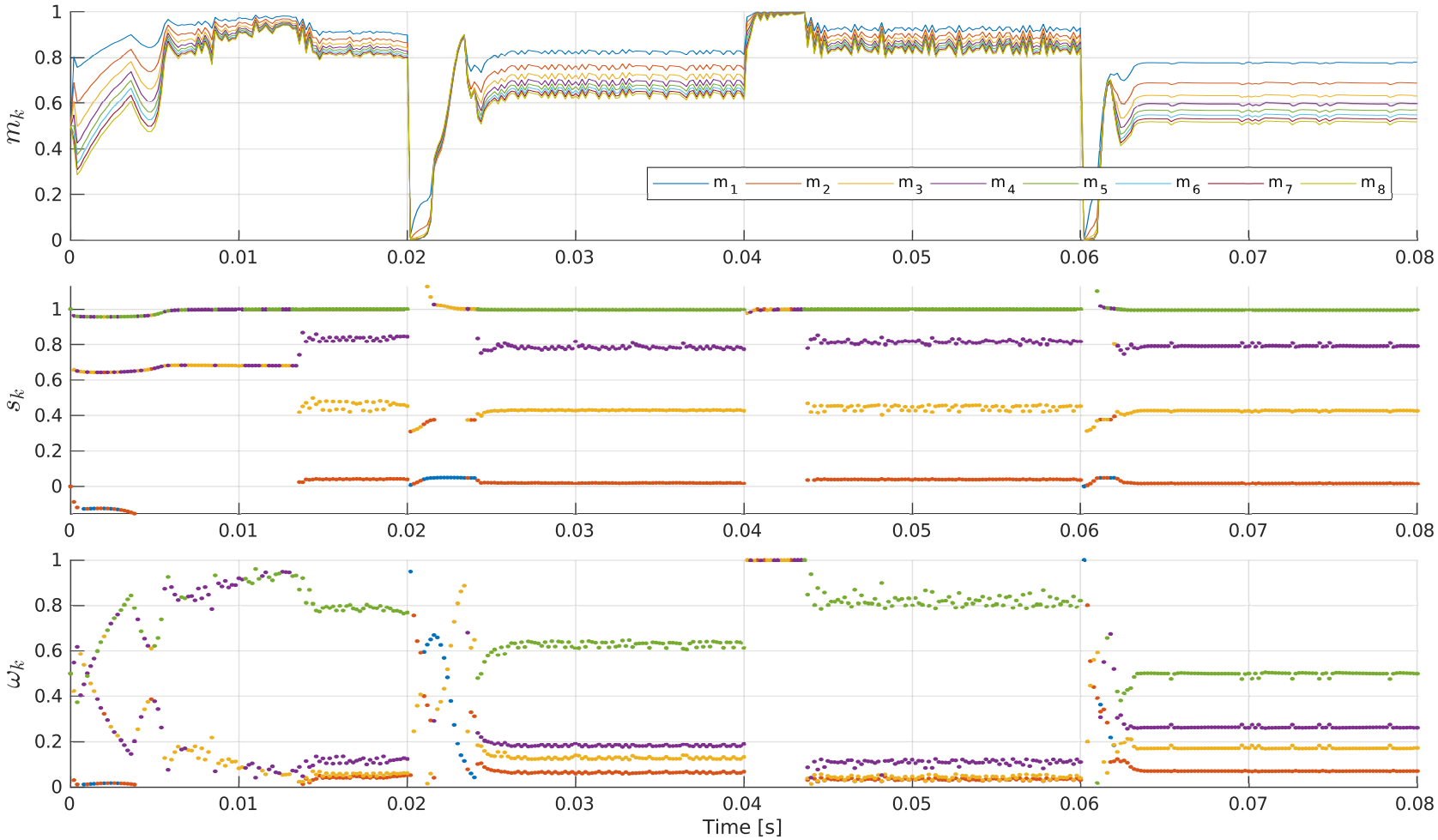

FIGURE 4.17 – Three-cell converter - simulation results: moment sequences (top), recovered measure support (center) and weights (bottom) for the switched model (4.36).

Cette thèse est accessible à l'adresse : http://theses.insa-lyon.fr/publication/2019LYSEI123/these.pdf
© [G. J. Becerra], [2019], INSA de Lyon, tous droits réservés

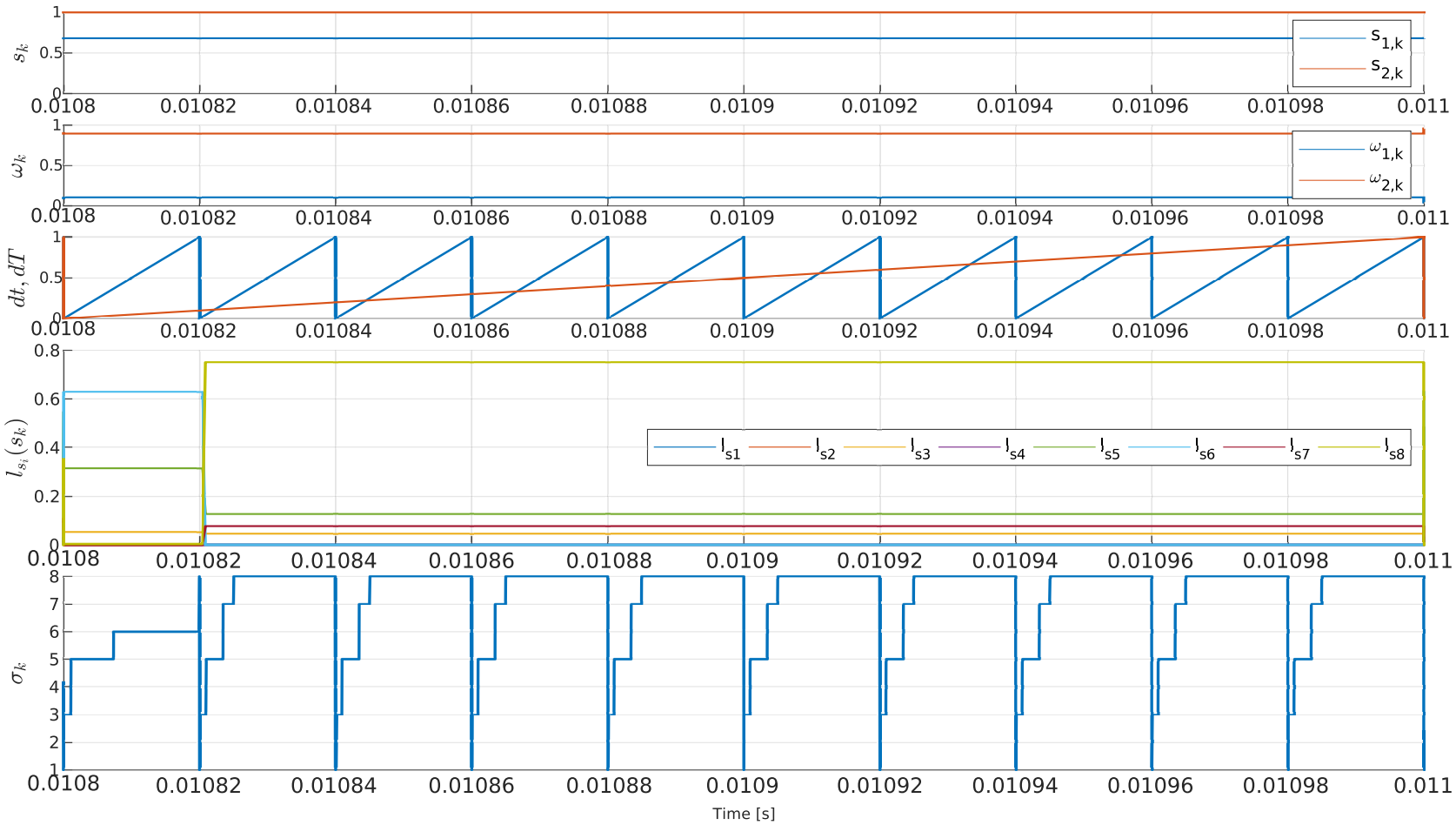

FIGURE 4.18 – Three-cell converter: detail of the synthesized control signal σ_k for the switched model.

Cette thèse est accessible à l'adresse : http://theses.insa-lyon.fr/publication/2019LYSEI123/these.pdf
© [G. J. Becerra], [2019], INSA de Lyon, tous droits réservés

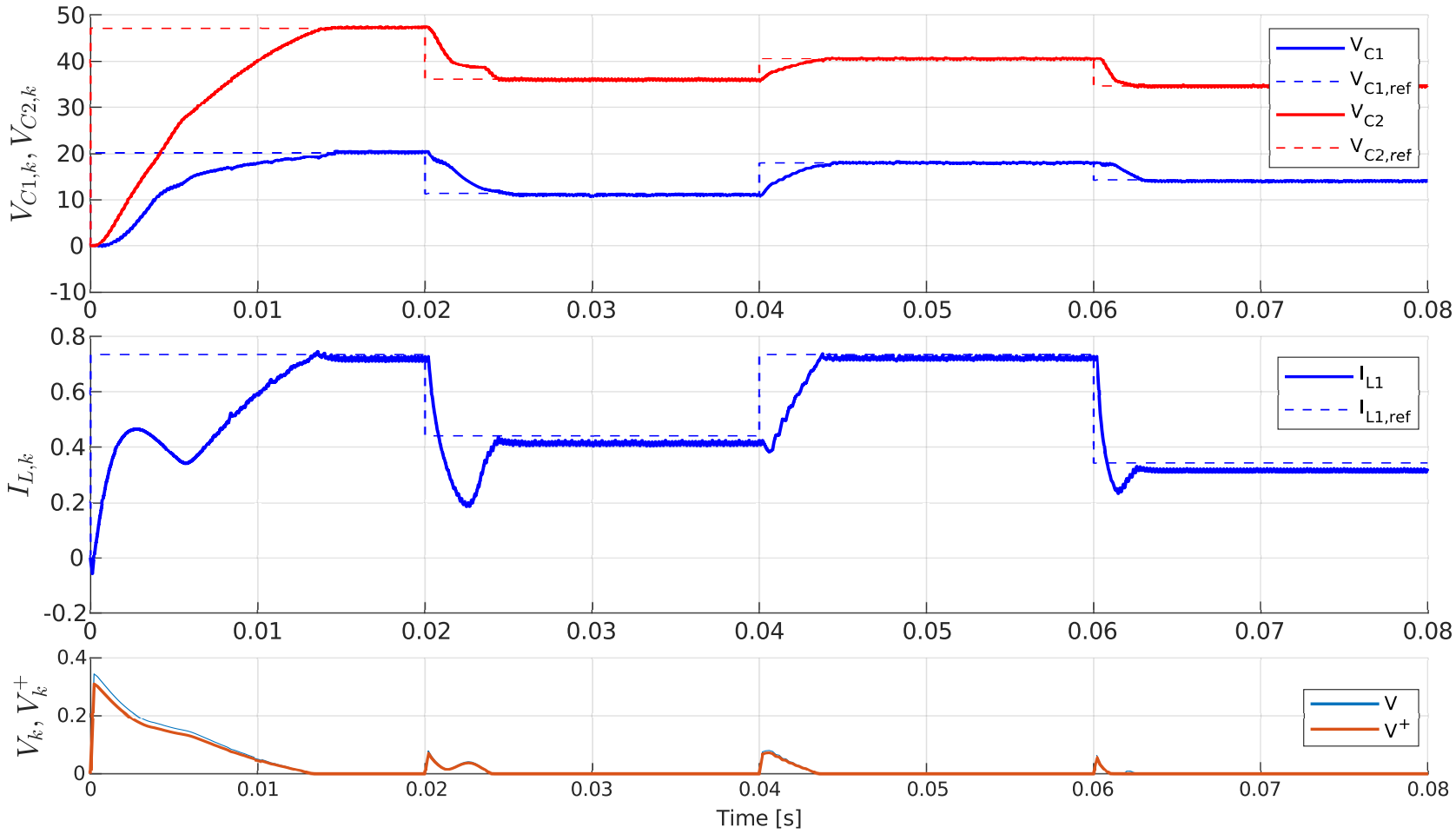

FIGURE 4.19 – Three-cell converter: reference tracking for the switched model.

Cette thèse est accessible à l'adresse : http://theses.insa-lyon.fr/publication/2019LYSEI123/these.pdf
© [G. J. Becerra], [2019], INSA de Lyon, tous droits réservés

Converter	Problem size			Execution time (ms)		
	Constraints	Scalar Vars	Matrix Vars	Mean	Std dev	N
SEPIC	23	5	5	5.141	0.410	400
2-cell multicellular	11	8	5	2.621	0.230	200
3-cell multicellular	21	11	5	4.843	0.748	200

TABLE 4.2 – MOSEK solver performance for each example: size of the numerical problem and execution time for a test run of 0.04 s.

This is a Matlab toolbox that is useful for easily constructing the semidefinite constraints. YALMIP translates the problem into a matrix structure suitable for computation using numerical solvers. We used MOSEK [55] version 9.0.86 to solve the resulting numerical problem. This solver implements a homogeneous interior point algorithm characterized by a robust performance.

Table 4.2 shows, for each of the examples presented in this chapter, the size of the numerical problem and the time taken by the solver to compute the solution. The numbers shown in the *problem size* column are reported by the interior-point optimizer log, and the execution times are reported by YALMIP's `solvertime` property. The results were obtained by running a simulation for each example, all with a test duration of 0.04 s. The solver time is recorded for each of the N iterations of the algorithm, and at the end the mean and standard deviation are computed. It can be observed from these tests that the main contributing factor to the performance is the number of constraints. These results show that the execution time is not small enough to achieve real-time performance. This time has to be reduced at least one order of magnitude to make an experimental implementation feasible. This is the main reason why the results presented in this chapter are only for simulation. The tests described in this section were carried out in a Linux/64-X86 machine with an Intel Core i7-4700MQ CPU running at 2.4 GHz and with 16 GB of RAM.

More tests are still needed to determine possible ways to improve the performance. A starting point would be a detailed comparison with other solvers like SEDUMI or SDPT3. Also, some implementations of interior-point methods using graphical processing units (GPU) have shown important performance improvements. The main computational task in these algorithms is the solution of a linear system to compute the Newton direction in each iteration. This step uses a method like the Cholesky factorization, which has been shown to be suitable for efficient implementation in a GPU. For instance in [56] this approach was tested for solving a model predictive control (MPC) problem represented as a linear programming problem. Finally, the optimality criterion in problem (4.26) could be dropped and only solve the feasibility problem. This should decrease the time required to find a solution. However, the obtained tdCLF could have a faster decay rate than the one set by the ρ parameter. In this case, it would be necessary to check the impact of these solutions on the control performance.

Cette thèse est accessible à l'adresse : http://theses.insa-lyon.fr/publication/2019LYSEI123/these.pdf
© [G. J. Becerra], [2019], INSA de Lyon, tous droits réservés

4.6 Conclusion

Lyapunov's stability theory is used to synthesize stabilizing control laws for switched systems. The general approach relies on the formulation of a parameterized Lyapunov function, considering two cases: fixed and varying parameters.

In the first part it is shown that a proper choice for the fixed parameters can improve the tracking performance with respect to other similar methods. The shape of the decision surfaces that emerge from the parameterization define the trajectories followed by the system. Simulation and experimental results are presented for the case of a three-cell converter, although this approach can be applied to a multicellular converter with an arbitrary number of cells, as well as other converter topologies. It can be observed that the proposed control law ensures good closed loop performance in terms of reference tracking, presenting improvements during transient conditions with a proper choice in the control Lyapunov parameterization. The main advantages are that the control law is simple to implement and is computationally cheap.

However, this approach has several drawbacks that limit its performance and applicability. This is the main reason for developing an alternative approach based on trajectory-dependent CLFs. The Lyapunov functions considered in this case depend on parameters that are computed on-line. This method allows to improve upon the fixed parameter case, because adding varying parameters to the Lyapunov function makes them less conservative, improving performance while guaranteeing the closed-loop stability.

The main contribution in this chapter is in the extension of the tdCLF approach originally developed for nonlinear control affine systems to the case of switched systems. To the best of our knowledge, it is the first time that tdCLFs are used in the context of switched systems and power converters. This is achieved by using the method of moments to obtain equivalent linear models that can be plugged into a semidefinite problem suitable to be solved efficiently using numerical methods. The control signal for the switched system is synthesized from the solution of the numerical problem, yielding good tracking performance of the closed-loop system. Several examples are presented for different converter topologies, and the performance of the approach is explored in simulation.

There are still issues that need to be addressed in the proposed tdCLF approach. A practical implementation able to execute at a fast enough rate to run in real-time requires improvements in the solution of the SDP. Tests including a comparison with other solvers or a GPU implementation are possible ways to solve this problem. Also, it would be interesting to compare the Lagrange polynomial basis to other alternatives such as *splines* or the *sinc* function. These bases could reduce the error introduced by the approximation done when the polynomial basis is evaluated in the control signal synthesis procedure.

Cette thèse est accessible à l'adresse : http://theses.insa-lyon.fr/publication/2019LYSEI123/these.pdf
© [G. J. Becerra], [2019], INSA de Lyon, tous droits réservés

Cette thèse est accessible à l'adresse : http://theses.insa-lyon.fr/publication/2019LYSEI123/these.pdf
© [G. J. Becerra], [2019], INSA de Lyon, tous droits réservés

Chapter 5

Direct Filtering for State Estimation in Power Converters

5.1 Introduction

In the well known pulse width modulated (PWM) converter topologies (buck, boost, buck-boost, Ćuk, SEPIC) a pair of switching devices (usually a transistor and a diode) are used. The normal operation consists in the complementary activation and deactivation of these devices, in what is known as the continuous conduction mode (CCM). However, under particular circumstances it may occur that both devices are conducting or blocking at the same time, yielding what is known as discontinuous conduction modes (DCM). This condition is a consequence of the unidirectionality properties of the semiconductor devices [1], which may cause an autonomous switching event before the end of the PWM periodic cycle. Under DCM operation, properties like the power converter's dynamic behavior and conversion ratio change drastically with respect to the CCM operation.

Power converters operating in DCM have properties that make them ideal for different applications, like soft switching on the boundary between CCM and DCM [57],[58], higher efficiency on low voltage/battery powered systems under light load conditions [59],[60] and avoidance of inductor core saturation [61],[62]. Also, these converters are typically used for power factor correction (PFC) [63],[58],[64] and power factor preregulation (PFP) [65],[63].

Discontinuous conduction modes have been studied extensively, beginning with classical results [22],[66],[67], where the discontinuous inductor current mode is presented and averaging methods are used to obtain small signal linear models for the buck, boost and buck-boost topologies. In [23], the different discontinuous modes present in basic PWM converter topologies are discussed: discontinuous inductor current mode (DICM), discontinuous capacitor voltage mode (DCVM) and discontinuous quasi-resonant mode (DQRM). It also introduces averaged small signal models for each of these modes. In [68],[69],[63] averaged models for SEPIC, Ćuk and flyback topologies in DCM are presented.

Transitions between CCM and DCM happen when a parameter (inductance, capacitance) or operating condition (output load, duty cycle) exceed a critical value. These transitions may be imposed by the designer or can happen when an external condition is present. An example of the former

Cette thèse est accessible à l'adresse : http://theses.insa-lyon.fr/publication/2019LYSEI123/these.pdf
© [G. J. Becerra], [2019], INSA de Lyon, tous droits réservés

case is [70], where the energy efficiency of a battery-powered application is improved by adaptively driving the converter into DCM operation when the system is operating in light load conditions on stand-by mode. Under these conditions, the current ripple is decreased, minimizing the switching and conduction losses.

Classic approaches to modeling and control of power converters consider only one operation mode (either CCM or DCM), and can not provide performance and stability guarantees when transitions to another operation mode happen. However, alternatives have been proposed recently, based on average and hybrid models which are valid in both CCM and DCM. For instance, in [71] average models are formulated by including numerical correction terms, obtained from simulations of the detailed switching model, in order to account for the fast dynamics present in the discontinuous mode. In [72] the converter operating in CCM and DCM is represented as a hybrid system using the mixed logical dynamical (MLD) framework. This allows to formulate the predictive control problem by including the system and state constraints and minimizing a cost dependent on the tracking error. However, this approach requires the use of mixed-integer quadratic programming (MIQP) solvers, and is limited to short prediction horizons to achieve a practical implementation. In [73] an alternative approach to hybrid modeling of a boost converter operating in CCM and DCM is presented.

Recent approaches to control of power converters operating in CCM and DCM include [74], where a control law for a Ćuk converter is signed based on a common quadratic Lyapunov function, with guaranteed stability when it enters DCM. In this work DCVM and DICM are considered. Also, in [75] a switched and adaptive control method with global asymptotic stability is proposed for power converter operating in both CCM and DCM. An observer for estimating the state and the unknown parameters is designed, making this approach robust with respect to changes in the load resistance and input voltage.

There are not many works in the literature regarding the problem of observation in power converters operating in CCM and DCM. The existing works rely on the existence of a model for the power converter and require the use of an estimator to obtain the operation mode at each time instant. For example, [76] presents the design of a current observer for the PFC boost converter, based on an average model that represents CCM and DCM. In [77] an observer-based control for a buck converter operating in CCM and DCM is considered. The observer is based on the discrete time LC-filter model in CCM, and an integral compensation loop is included to correct the estimates when the system enters DCM. In [78] Luenberger-type switched observers are considered, and the observer gains for the different operation modes are obtained by solving LMIs.

In the present work we consider the problem of current estimation in PWM converters operating in CCM and DCM. We propose an approach based on the set membership framework [36] for identification of nonlinear systems. This method allows to formulate a discrete-time data-based state estimator without knowledge of the system model equations, but assuming

Cette thèse est accessible à l'adresse : http://theses.insa-lyon.fr/publication/2019LYSEI123/these.pdf
© [G. J. Becerra], [2019], INSA de Lyon, tous droits réservés

the existence of bounds to the model functions gradients and the availability of a sufficiently informative dataset. The structure of the obtained estimator is a causal nonlinear finite impulse response (NFIR) filter, where the output depends on the history of past measured inputs and outputs of the observed system. The resulting estimate includes not only the estimate but also the tightest error bounds, giving a measure of uncertainty in the estimation process. This approach has several advantages with respect to other estimation methods:

1. It does not require to formulate an explicit model for the power converter.
2. It does not require to implement an estimator for the operation mode.
3. It represents the system dynamics in the complete operating range, including CCM and DCM.
4. It gives a measure of uncertainty of the estimate at each sample time.
5. The estimator is BIBO stable, because of the filter structure.
6. The resulting algorithm is inherently parallelizable.

The SEPIC converter is used as an application example to illustrate the results obtained with the proposed approach.

5.2 Contribution

The main original contributions in this chapter are:

1. Definition of the direct filter design procedure for power converters operating in CCM and DCM (Section 5.4).
2. Parallel implementation of the direct filter estimator procedure using the CUDA framework (Section 5.5).
3. Use of the principal component analysis (PCA) dimensionality reduction technique for compressing the regressor datasets in the direct filter implementation (Section 5.6).
4. Extension of the direct filter approach to full-state estimation (Section 5.7.2).

5.3 Current Estimation for Power Converters in CCM and DCM

In switched power converter applications, having accurate measurements of currents and voltages is an important requirement for achieving high performance in control and monitoring tasks. In particular, current measurement

Cette thèse est accessible à l'adresse : http://theses.insa-lyon.fr/publication/2019LYSEI123/these.pdf
© [G. J. Becerra], [2019], INSA de Lyon, tous droits réservés

is critical in several feedback control strategies, where the outer voltage loop produces a current reference for the inner current loop. However, accurate current measurements require special sensing circuits [79] which in some applications may increase complexity and be cost prohibitive. Furthermore, these measurements are contaminated by switching noise. An alternative is not to measure the currents directly, but to estimate them using observers. The usual approach relies on the availability of other measurable signals (inputs and outputs), and on knowledge of a mathematical model for the system. With this information, the observer is able to make predictions on the system behavior, providing estimates of the unmeasurable signals.

The classic observer structure consists of a prediction term using a simulation of the system model subject to the measured inputs, and a correction term depending on the measured outputs. Then, the observer design problem corresponds to the assignment of the correction term gains, in order to guarantee asymptotic stability in the estimation error [80]. In the context of power converters this approach can be used under CCM operation in the form of switched observers [81], where the main assumption is that the system mode is known. However when the system enters DCM the underlying dynamics become hybrid, requiring the design of a hybrid observer [82] that simultaneously estimates the continuous system state and the discrete operation mode, even under the occurrence of uncontrolled-unmeasured switching events.

Consider the switched model for power converters presented in Eq. (5.1). where $x(t) \in \mathbb{R}^{n_x}$ corresponds to the state vector, $\tilde{u}(t) \in \mathbb{R}^{n_u}$ the inputs and $\tilde{y}(t) \in \mathbb{R}^{n_y}$ the measurable outputs.The terms $B_x w(t)$ and $B_y w(t)$ correspond to process and measurement noise, respectively.

$$\mathcal{P}_{\sigma(t)}\dot{x}(t) = \mathcal{A}_{\sigma(t)}x(t) + \mathcal{B}_{\sigma(t)}\tilde{u}(t) + B_x w(t) \tag{5.1a}$$

$$\tilde{y}(t) = \mathcal{C}_{y,\sigma(t)}x(t) + \mathcal{D}_{y,\sigma(t)}\tilde{u}(t) + B_y w(t) \tag{5.1b}$$

Notice that in the present approach we assume no knowledge on the system matrices of system (5.1), but assume that a set of input and output measurements is available. Let us define $v(t) \in \mathbb{R}$ as one of the variables in the state vector $x(t)$. We proceed now to formulate the estimation problem.

Problem 5.3.1. *Consider system* (5.1)*, and assume no knowledge of system matrices is available. Based on measurements of* $\tilde{u}(t)$*,* $\tilde{y}(t)$ *and* $s(t)$*, obtain estimates* $\hat{v}(t)$ *of the unmeasured state* $v(t)$*.*

Notice that in the context of power converters, the unmeasured state to be estimated is a current, while measures of the input and output voltages, and the state of the controlled switching devices are usually known.

In the present work, we propose an alternative approach to this problem. An algorithm is developed for directly providing discrete-time estimates of the average inductor current without requiring an estimator for the operating mode, and without formulating a mathematical model for the system. The estimates are computed from the history of recent input and output measurements, and from a dataset of measurements prepared from experiments

Cette thèse est accessible à l'adresse : http://theses.insa-lyon.fr/publication/2019LYSEI123/these.pdf
© [G. J. Becerra], [2019], INSA de Lyon, tous droits réservés

carried out on the system under different operating conditions. The design of these experiments require special considerations for obtaining an informative enough dataset, which are considered in the system identification literature [83]. This algorithm computes optimal error bounds on the estimated variable, yielding information on the estimation accuracy under different operating conditions. The resulting approach can be extended to full state observation by implementing separate estimators for each state variable.

5.4 Direct Filter Design for Power Converters Operating in CCM and DCM

In section 2.5 we introduced the design of estimators for unknown systems from data in the context of the set membership (SM) framework for system identification. We propose to use this approach for designing discrete-time current estimators for the average currents and voltages in power converters operating in CCM and DCM. This approach does not require to have knowledge of the operation mode because the changes in dynamic behavior when mode transitions happen are encoded in the dataset.

Let us assume that the power converter operating in CCM and DCM is represented by the discrete-time unknown model in Eq. (2.25), where x^t is the state (inductor currents and capacitor voltages), $\tilde{d}^t$ the duty cycle of the PWM signal controlling the switching device, $\tilde{u}^t$ the uncontrolled measured input voltage, $\tilde{y}^t$ the measured output voltage and v^t an unmeasured unknown state variable. Also, let us assume that the nonlinearities associated to CCM - DCM mode transitions are represented by the nonlinear functions F, G and H in (2.25). Algorithm 2 specifies the proposed steps for designing direct filters for power converters.

Algorithme 2 : Direct filter design for power converters (offline)

Result : $\mathcal{D}$, γ, ε

1. Design test signals $\tilde{d}(t)$, $\tilde{u}(t)$ for driving the power converter to operate under varied conditions (CCM and DCM).
2. Measure $\tilde{y}(t)$, $\tilde{v}(t)$ resulting from the test signals. The sampling time should be sufficiently high to obtain detailed waveforms of the switching behavior.
3. Compute $\bar{y}(t) = \texttt{average}(\tilde{y}(t))$, $\bar{v}(t) = \texttt{average}(\tilde{v}(t))$, with $\texttt{average}(\cdot)$ a non-causal filter.
4. Obtain $\tilde{y}^t = \texttt{resample}(\bar{y}(t), T_s)$, $\tilde{v}^t = \texttt{resample}(\bar{v}(t), T_s)$, $\tilde{d}^t = \texttt{resample}(\tilde{d}(t), T_s)$, $\tilde{u}^t = \texttt{resample}(\tilde{u}(t), T_s)$, with T_s a sample time small enough to capture the low frequency behavior.
5. Prepare dataset $\mathcal{D}$ using $\tilde{d}^t$, $\tilde{y}^t$, $\tilde{u}^t$, $\tilde{v}^t$.
6. Take $\varepsilon = \|\tilde{v}(t) - \bar{v}(t)\|_\infty$.
7. Take $\gamma^* = \min \gamma$, subject to $\overline{f}_c(\tilde{\boldsymbol{\varphi}}^k) > \tilde{v}^k - \varepsilon$, $k = 1, \ldots, N$ (sufficient condition in Theorem 2.5.1), with $\tilde{\boldsymbol{\varphi}}^k = [\tilde{\mathbf{d}}^{k,m}; \tilde{\mathbf{y}}^{k,m}; \tilde{\mathbf{u}}^{k,m}]$.

Cette thèse est accessible à l'adresse : http://theses.insa-lyon.fr/publication/2019LYSEI123/these.pdf
© [G. J. Becerra], [2019], INSA de Lyon, tous droits réservés

Notice that this algorithm is performed offline, as part of the design process. Once a dataset $\mathcal{D}$ is available and the parameters γ and ε have been obtained, the filter estimates are computed online using algorithm 3.

Algorithme 3 : Direct filtering estimation for power converters (online)

Data : $\mathcal{D}$, γ, ε
Result : Estimate $\hat{v}^t$
while *true* **do**
1. Measure $\tilde{d}^t$, $\tilde{y}^t$, $\tilde{u}^t$.
2. Construct the regressor $\tilde{\boldsymbol{\varphi}}^t$ in Eq. (2.27).
3. Compute the optimal tightest bounds $\overline{f}(\tilde{\boldsymbol{\varphi}}^t)$, $\underline{f}(\tilde{\boldsymbol{\varphi}}^t)$ using Eqs. (2.32), (2.33), with $\tilde{\boldsymbol{\varphi}}^k$, $\tilde{v}^k$ available in dataset $\mathcal{D}$.
4. Compute the direct filter estimate $\hat{v}^t$ using Eq. (2.34).

end

5.5 Direct Filter Parallel Implementation using CUDA

In practice, obtaining the tightest upper and lower bounds of DF in Eqs. (2.32),(2.33) requires computing the distance between the measured regressor $\tilde{\boldsymbol{\varphi}}^t$ at each sample time t with respect to all the N regressors $\tilde{\boldsymbol{\varphi}}^k$ in the dataset. This computation can be very expensive when the datasets have thousands of regressors. To address this problem, [84] proposes an approximation of the optimal filter f_c by computing the DF estimates on a grid defined over the regressor space. The estimates are stored in a look-up table, reducing the computation speed at the cost of a decrease in estimation performance. The problem with this approach is that some applications may require to increase the regressor length to achieve the required estimation performance, growing exponentially the amount of memory required to store the resulting look-up table.

However, the DF algorithm is inherently parallelizable, and this structure is exploited here to obtain a real time implementation using a graphical processing unit (GPU). Also, we propose a novel approach to reduce the lengths of the regressors in the datasets for speeding up the direct filter computation without significantly affecting the estimation performance. The implementation details of this approach are given next.

The most compute-intensive task in the online part of the direct filter algorithm 3 is step 3: obtaining the optimal tightest bounds $\overline{f}(\tilde{\boldsymbol{\varphi}}^t)$, $\underline{f}(\tilde{\boldsymbol{\varphi}}^t)$. It involves computing the distance, at each sample time, between the measured regressor $\tilde{\boldsymbol{\varphi}}^t$ and all the regressors $\tilde{\boldsymbol{\varphi}}^k$ in the dataset. Then, computing the worst-case bounds around the output value $\tilde{v}^k$ associated with each k^{th}-regressor in the dataset. The final result is obtained by computing the minimum upper and maximum lower bounds. Each of these steps can be broken up into specific operations to be executed independently over large

Cette thèse est accessible à l'adresse : http://theses.insa-lyon.fr/publication/2019LYSEI123/these.pdf
© [G. J. Becerra], [2019], INSA de Lyon, tous droits réservés

amounts of data, allowing a parallel implementation. The parallel structure of the direct filter algorithm can be exploited to obtain real time execution, even for datasets with thousands of regressors.

For the parallel implementation of the direct filter we used CUDA, a framework developed by Nvidia for GPU programming. In this framework the parallel tasks are called *kernels*, which are executed simultaneously over thousands of concurrent threads. The basic sequence in a parallel program consists on a data transfer from CPU to GPU memory, a *kernel* call that executes parallel code on the GPU over the data stored on its memory, and a data transfer of the computed results from the GPU memory back to the CPU. These data transfers can be quite expensive, but recent hardware allows simultaneous *kernel* execution and data transfers for maximum throughput. Three *kernels* were implemented for each iteration of the DF algorithm at time t:

Kernel 1 : $\psi_i^k = (\tilde{\boldsymbol{\varphi}}_i^t - \tilde{\boldsymbol{\varphi}}_i^k)^2,\ i = 1, \ldots, 3m,\ k = 1, \ldots, N_D.$

Kernel 2 : $\Delta^k = \sqrt{\sum_{i=1}^{3m} \psi_i^k},\ \overline{f}_c^k = \tilde{v}^k + \varepsilon + \gamma\Delta^k,\ \underline{f}_c^k = \tilde{v}^k - \varepsilon - \gamma\Delta^k.$

Kernel 3 : $\overline{f}_c = \min_{k=1,\ldots,N}(\overline{f}_c^k),\ \underline{f}_c = \max_{k=1,\ldots,N}(\underline{f}_c^k).$

These *kernels* compute the 2-norm of the distance between regressors, but other norms can be similarly implemented. Notice that *kernels* 1, 2 and 3 require the execution of $3mN_D$, N_D and N_D concurrent threads, respectively.

5.6 PCA Dimensionality Reduction in Regressor Datasets

Principal Component Analysis (PCA) [85] is a technique used in many image processing and machine learning applications. It is used in the present context to reduce the regressor lengths in the DF datasets. The method considers the regressors as $3m$-dimensional vectors and finds a change of basis that maps them into a new space where the components are ranked according to the amount of information they contain. This is achieved by constructing the covariance matrix of the regressor dataset and computing its eigenvalues and eigenvectors. The eigenvectors correspond to the independent directions where the variability of the data is maximized. The associated eigenvalues provide a measure of the information contents for each of these directions, and provide a way to rank them. The dimensionality reduction is achieved by taking a subset of the eigenvectors associated with most of the information content, and use it to map the original regressors into a lower dimensional space.

Consider the dataset $\mathcal{D}$ formed by $3m$-dimensional column vectors $\tilde{\boldsymbol{\varphi}}^k$. Organize the N_D vectors into a matrix $\Phi \in \mathbb{R}^{3m \times N_D}$. The goal is to find a linear transformation $\Omega = Z^\intercal \Phi$ with $Z \in \mathbb{R}^{3m \times l}$, such that the reduced-dimension regressors in $\Omega \in \mathbb{R}^{l \times N_D}$ describe the data with less variables:

Cette thèse est accessible à l'adresse : http://theses.insa-lyon.fr/publication/2019LYSEI123/these.pdf
© [G. J. Becerra], [2019], INSA de Lyon, tous droits réservés

$l < 3m$. Algorithm 4 presents the general approach to obtain the reduced-size dataset Ω and the transformation matrix Z using the covariance method. Notice that the parameter ζ makes reference to the relative information content of the principal components with respect to the complete dataset. A rule of thumb to choose this value is $\zeta = 0.9$. The columns in matrix Ω represent reduced-size vectors of the columns in Φ.

Algorithme 4 : Principal Component Analysis Dataset Preparation

Data : $\mathcal{D}$
Result : Z, $\mathcal{O}$
1. Organize the regressors $\tilde{\boldsymbol{\varphi}}^k$ in dataset $\mathcal{D}$ into matrix $\Phi \in \mathbb{R}^{3m \times N_D}$.
2. Compute the empirical mean $u \in \mathbb{R}^{3m \times 1}$ with $u_i = \frac{1}{N_D} \sum_{j=1}^{N_D} \Phi_{ij}$.
3. Substract the deviations form the mean: $B = \Phi - uh$, where $h \in \mathbb{R}^{1 \times N_D} = [1, 1, \ldots, 1]$.
4. Compute the covariance matrix $C = \frac{1}{N_D - 1} BB^\intercal$.
5. Compute eigenvectors $V \in \mathbb{R}^{3m \times 3m}$ and eigenvalues $D \in \mathbb{R}^{3m \times 1}$ of covariance matrix C.
6. Sort the eigenvectors V in decreasing order of associated eigenvalues and save them in matrix V_s.
7. Compute the cumulative eigenvalues $g_i = \sum_{k=1}^{i} D_k$ for $i = 1, \ldots, 3m$.
8. Choose l as the smallest integer such that $g_l / g_{3m} >= \zeta$.
9. Select the first l columns of V_s and save them as matrix Z.
10. Compute the reduced-size regressors as $\Omega = Z^\intercal \Phi$.
11. Save the columns of matrix $\Omega = [\boldsymbol{\omega}^1, \boldsymbol{\omega}^2, \ldots, \boldsymbol{\omega}^{N_D}]$ in the new dataset $\mathcal{O} = \{(\boldsymbol{\omega}^k, \tilde{v}^k), k = 1, 2, \ldots, N_D\}$.

5.7 Application Examples

5.7.1 Current Estimation for SEPIC Converter

Consider the single-ended primary inductor converter (SEPIC) DC-DC power converter described in section 2.1.4. The approach introduced in the previous section is used to design direct filters for estimating the input current $\hat{v}^t = I_{L_1}(t)$ from sampled noisy measurements of the input voltage $\tilde{u}^t = E(t)$, the output voltage $\tilde{y}^t = V_{C_2}(t)$ and from knowledge of the controlled PWM duty cycle $\tilde{d}^t$. A dataset $\mathcal{D}$ is obtained by applying an amplitude modulated pseudo random binary signal (APRBS) [86, Sect. 17.1] to the duty cycle input of the SEPIC converter in open loop and measuring the output voltage while maintaining a constant input voltage. The APRB signal maintains a random constant value for the duration of a given dwell time T_d. The signals are randomly generated by defining minimum and maximum dwell times $T_{d,min}$, $T_{d,max}$ for both the training and test datasets. Assuming a constant load resistance R_o, the duty cycle boundary value $\bar{d}$ separating the CCM and DCM

Cette thèse est accessible à l'adresse : http://theses.insa-lyon.fr/publication/2019LYSEI123/these.pdf
© [G. J. Becerra], [2019], INSA de Lyon, tous droits réservés

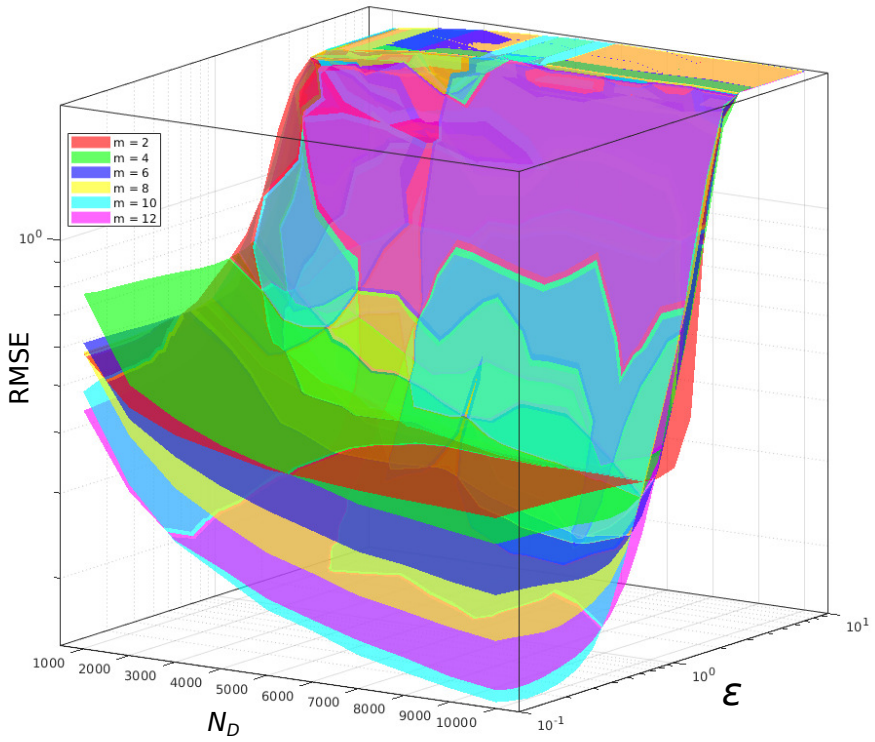

FIGURE 5.1 – Direct filter estimation error (RMSE) for different regressor lengths m, dataset sizes N_D and ε values.

operating regions can be computed by static analysis [87], using Eq. (5.2).

$$\bar{d} = 1 - \frac{2 f_{pwm} L_1 L_2}{R_o (L_1 + L_2)} = 0.2756 \tag{5.2}$$

The minimum and maximum levels of the duty cycle signal applied to the converter are selected in a wide operation range to force operation in both CCM and DCM regions. The results presented in the following subsections are based on the acquisition of detailed waveforms of the SEPIC converter response to APRB signals. These are then averaged and resampled at a sufficiently high rate f_s to capture the low frequency behavior of the converter. A scaling scheme is applied to the regressor dataset as described in [36] to improve the estimation performance in both simulation and experiment.

Simulation Results

A detailed noiseless simulation of the SEPIC converter is run and all the variables are sampled at $f_s = 1$ MSa/s, and then averaged and resampled at $f_{rs} = 5$ kSa/s. Multiple filters are designed and tested for different regressor lengths m, dataset sizes N_D and noise bounds ε. Fig.5.1 shows the performance of the direct filters measured as the root mean squared error (RMSE) of the estimate current $\hat{v}^t = \hat{\bar{I}}_{L1}$ with respect to the true average current $\bar{v}^t = \bar{I}_{L1}$, where each surface is associated to a given regressor length

Cette thèse est accessible à l'adresse : http://theses.insa-lyon.fr/publication/2019LYSEI123/these.pdf
© [G. J. Becerra], [2019], INSA de Lyon, tous droits réservés

m. The RMSE was obtained by running the estimation algorithm for each combination of (ε, N_D, m) over the intervals shown in Fig. 5.1 for 15 different random APRBS test signals, and then averaging the results.

The shapes of the surfaces suggest that increasing N_D can improve the estimation performance up to a certain point. After that, the surfaces flatten out in the selected interval, as observed for $m = \{2, 4, 6, 8\}$. Notice that the RMSE shows a heavy dependence on the value of parameter ε. Step 6 in algorithm 2 gives a criterion for obtaining a preliminary estimation of this parameter from the available data. Running the DF estimation for different ε values can help refine this parameter's choice. In the interval (ε, N_D) shown, the best performance is achieved when $m = 10$, $\varepsilon = 0.1$ and $N_D = 10000$.

The performance of the direct filter (DF) is compared with respect to other estimation approaches: extended Kalman filter (EKF) [88], particle filter (PF) [89] and neural networks (NN) [90]. For the model-based approaches (EKF, PF) the nonlinear average model of the SEPIC converter is used. The PF computes the evolution of 50 particles using Euler's method for 10 subintervals on each sample step. For the data-based approaches (DF, NN) a dataset with $N_D = 10000$ regressors and total regressor length $3m = 60$ was obtained from simulation. This dataset was used for estimating the parameters (ε, γ) for the DF, and for training a feed-forward neural network with $3m$ inputs, $3m$ neurons in the hidden layer, and 1 output. Also, an alternative implementation of the direct filter is implemented using a dimensionality reduction technique known as principal component analysis (PCA). This allows to decrease the size of the regressor datasets, improving the computation speed of the algorithm. Further details for the DF PCA implementation are given in section 5.6.

Four different datasets (DS1, DS2, DS3, DS4) are prepared for comparison, using different minimum and maximum constant duty cycle periods $(T_{d,min}, T_{d,max})$ for the APRB signal, specified in Table 5.1. 20 different test runs are prepared for each dataset. Fig. 5.2 shows the performance of the estimators for these datasets, using as error measures the relative absolute error (RAE), root relative square error (RRSE) and relative worst-case error (RWCE) defined as:

$$\begin{aligned} RAE &= 100 \left\| v - \hat{v} \right\|_1 / \left\| v - \bar{v} \right\|_1 \\ RRSE &= 100 \left\| v - \hat{v} \right\|_2 / \left\| v - \bar{v} \right\|_2 \\ RWCE &= 100 \left\| v - \hat{v} \right\|_\infty / \left\| v - \bar{v} \right\|_\infty \end{aligned} \tag{5.3}$$

where v corresponds to the measured signal, $\bar{v}$ its average and $\hat{v}$ the estimate. These error measures quantify different properties of the estimate with respect to the real signal: RAE indicates the mean deviation, RRSE penalizes outliers and RWCE indicates the maximum deviation.

For all datasets the model-based estimators have worse performance than the data-based ones. This is caused by their dependence on the nonlinear average model, which doesn't provide a good approximation of the switched linear system, particularly during transients and DCM operation. Regarding the data-based estimators, NN has better performance than DF for all

Cette thèse est accessible à l'adresse : http://theses.insa-lyon.fr/publication/2019LYSEI123/these.pdf
© [G. J. Becerra], [2019], INSA de Lyon, tous droits réservés

	Training		Test	
Dataset	$T_{d,min}$	$T_{d,max}$	$T_{d,min}$	$T_{d,max}$
DS1	5 ms	5 ms	10 ms	10 ms
DS2	10 ms	10 ms	20 ms	20 ms
DS3	5 ms	10 ms	10 ms	20 ms
DS4	5 ms	10 ms	10 ms	30 ms

TABLE 5.1 – Constant duty cycle periods in the training and test APRB signals for different datasets.

datasets. This is expected, because the parameter γ in the DF represents global worst-case bounds on the partial derivatives of the approximated function, while the NN approximates the partial derivatives locally.

Fig.5.3 shows a small section of a particular test run, comparing the estimates for all the implemented methods with respect to the switching input current I_{L1} and its average, shown in light and dark gray, respectively. Notice that the model-based approaches (EKF, PF) exhibit noticeable oscillations during high to low duty cycle transitions. These oscillations are the main cause for the high 2-norm and ∞-norm errors for these estimators. EKF and PF estimates also have an offset during steady state operation. Fig.5.3(a) shows the upper and lower bounds $(\overline{f}_c, \underline{f}_c)$ for the DF and DFPCA estimates, using dashed lines. Notice that the distance between these bounds grows during transients, which indicates an increase on estimation uncertainty under these conditions. Fig.5.3(b) shows the detail of a CCM to DCM transition, where the switched current I_{L1} exhibits the typical discontinuous waveform. The DF and DFPCA estimates track correctly the change in the average current during the transition from the symmetric to the asymmetric waveform.

Experimental Results

The experimental SEPIC converter test bench shown in Fig. 5.4 is used for testing the proposed estimation approach. Multiple experimental runs are executed by applying an APRB duty cycle signal in open loop to the SEPIC test bench, and measuring all the variables with an oscilloscope at $f_s = 2$ MSa/s. Then the acquired signals are resampled at $f_{rs} = 4$ KSa/s. Algorithm 2 is followed to prepare four different regressor datasets, each with $T_{d,min}$ and $T_{d,max}$ specified in Table 5.1. For each dataset, $N_D = 10000$ training regressors with total length $3m = 60$ are prepared using 5 captures of 500 ms, and each of the 20 test signals are prepared taking 3 captures of 500 ms.

Fig.5.5 shows the performance comparison for all the implemented estimators. It can be observed that in this case the data-based estimators also have better performance than the model-based ones. However, the NN performance is noticeably worse than the DF and DFPCA. In particular, the RWCE measure grows considerably faster than the others, indicating the presence of high amplitude outliers. This can be observed in Fig.5.6 where the NN estimate presents large amounts of noise, especially in the time intervals $t = [1.034, 1.052]$ and $t = [1.07, 1.083]$ where the measured input u and

Cette thèse est accessible à l'adresse : http://theses.insa-lyon.fr/publication/2019LYSEI123/these.pdf
© [G. J. Becerra], [2019], INSA de Lyon, tous droits réservés

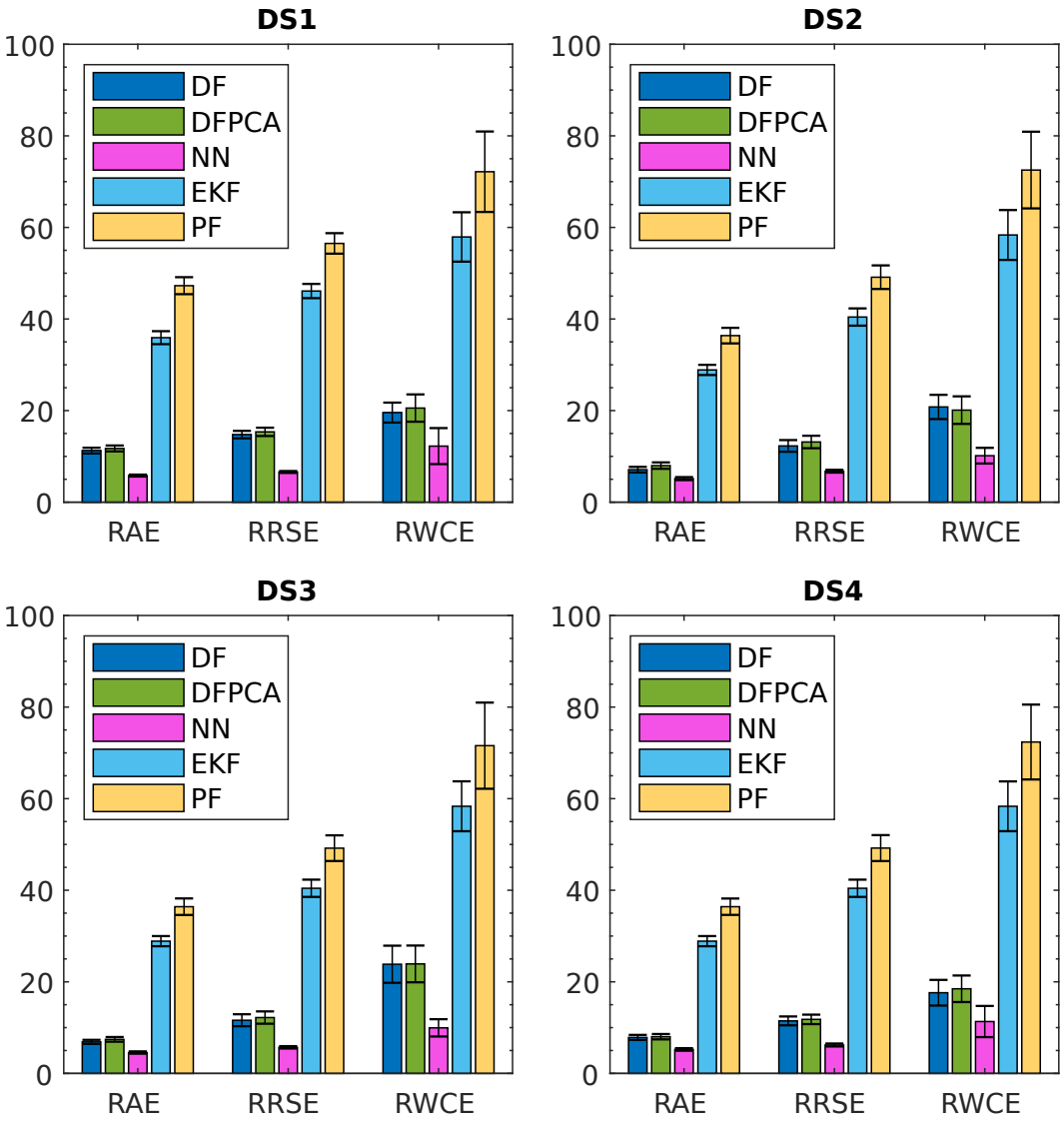

FIGURE 5.2 – Estimation error measures (mean±stdev, 20 test runs of 1.5 s each) for direct filter (DF), direct filter with PCA dataset (DFPCA), neural networks (NN), extended Kalman filter (EKF) and particle filter (PF) with 4 different simulation datasets ($m = 20$, $N_D = 10000$, $\varepsilon = 0.1292$).

Cette thèse est accessible à l'adresse : http://theses.insa-lyon.fr/publication/2019LYSEI123/these.pdf
© [G. J. Becerra], [2019], INSA de Lyon, tous droits réservés

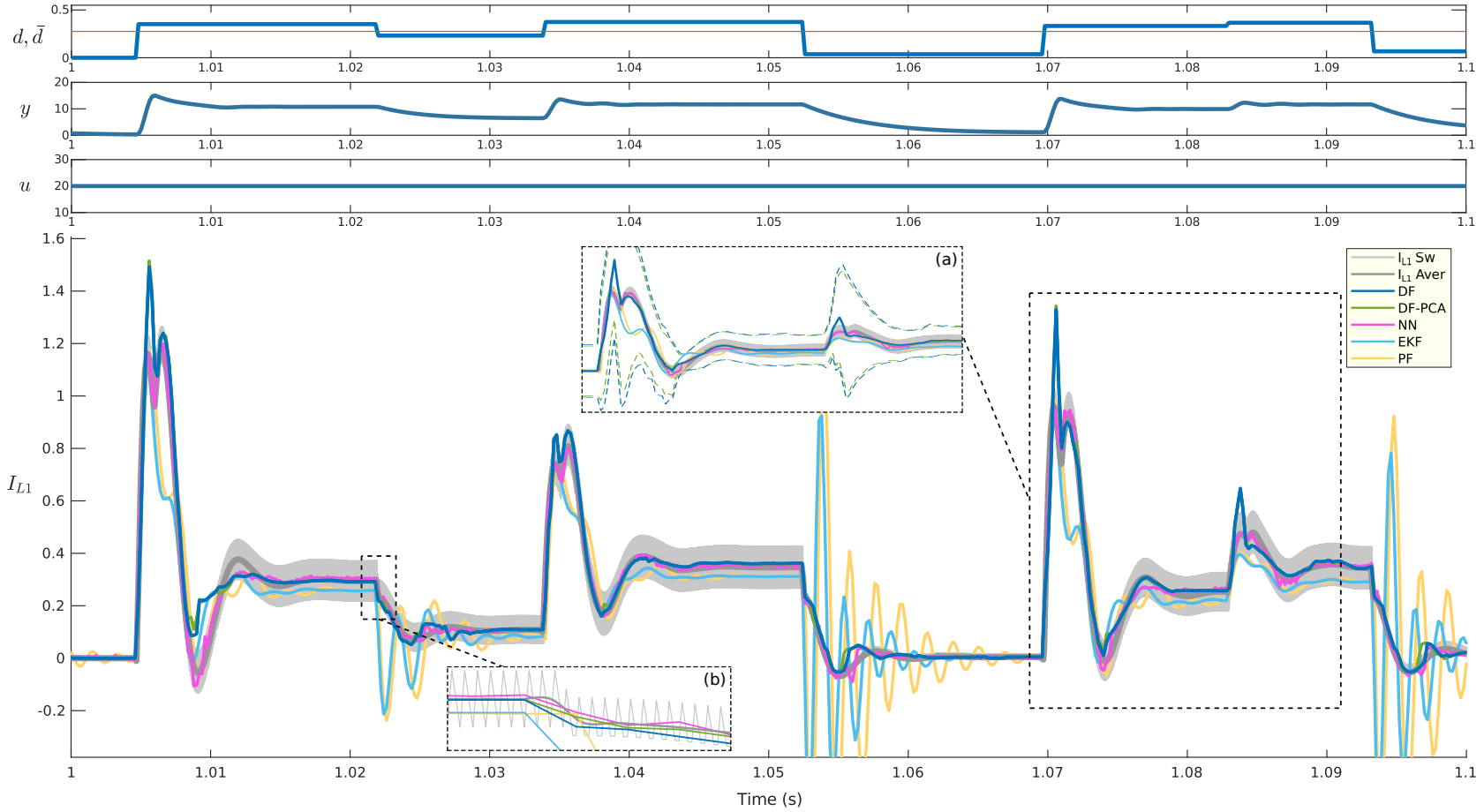

FIGURE 5.3 – Simulation results (top to bottom): Duty cycle d and DCM boundary $\bar{d}$. Output voltage $y = V_{C2}$. Input voltage $u = E$. Input current I_{L1} estimation using direct filter (DF), direct filter with PCA dataset (DFPCA), neural networks (NN), extended Kalman Filter (EKF) and particle filter (PF).

Cette thèse est accessible à l'adresse : http://theses.insa-lyon.fr/publication/2019LYSEI123/these.pdf
© [G. J. Becerra], [2019], INSA de Lyon, tous droits réservés

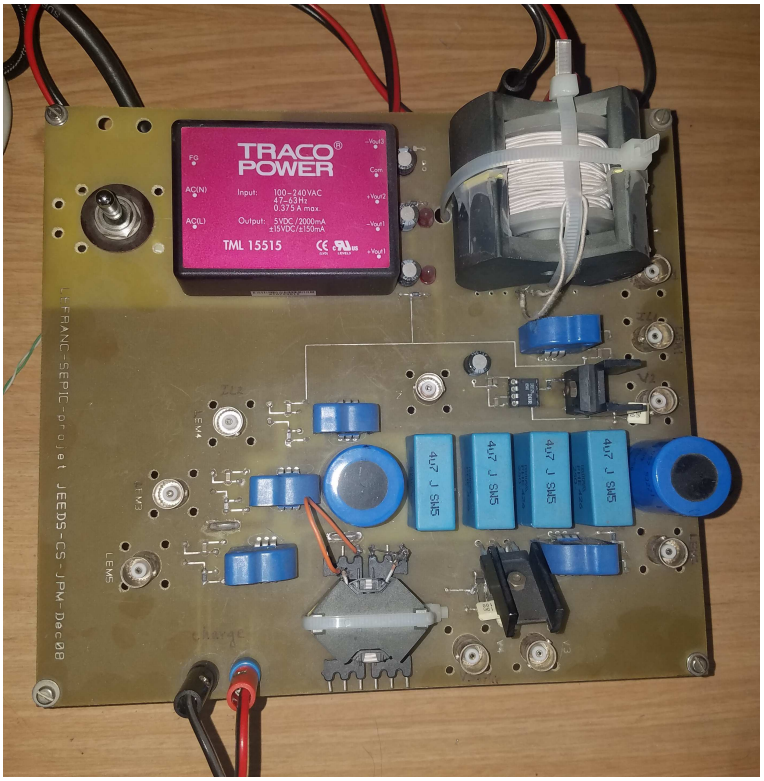

FIGURE 5.4 – SEPIC converter test bench.

output y show the most variability. The DF and DFPCA estimators show better noise rejection than all the other estimators.

Fig.5.6(a) shows the detail of the upper and lower bounds $(\overline{f}_c, \underline{f}_c)$ for DF and DFPCA. Notice here that the estimation uncertainty is increased by the presence of noise, but DF and DFPCA still give good estimates of the average current. Fig.5.6(b) shows the average current for all estimators during CCM to DCM transitions, where DF and DFPCA show the best behavior.

One important remark is that DF in this example takes as the only uncontrolled input $u^t = E$, the input voltage. However, we could define the load resistance as another uncontrolled input $u^t = [E, R_0]$. This would allow the DF to give estimates under input and load disturbances. This would require to include in the dataset $\mathcal{D}$ the typical load disturbance scenarios that the system could be subject to.

Performance Results for the Parallel Implementation

The reduced datasets are used for running the DFPCA estimator. Its performance results are shown in Figs. 5.3, 5.6, and a particular test run for this estimator is included in Figs. 5.2, 5.5. Notice that the performance of the DFPCA estimator is slightly worse than that of the DF estimator, but still provides good estimates compared to the other approaches.

Table 5.2 shows a comparison between these estimators using the four experimental datasets available. The mean performance loss of the DFPCA with respect to the DF is shown for the three error measures: RAE, RRSE and

Cette thèse est accessible à l'adresse : http://theses.insa-lyon.fr/publication/2019LYSEI123/these.pdf
© [G. J. Becerra], [2019], INSA de Lyon, tous droits réservés

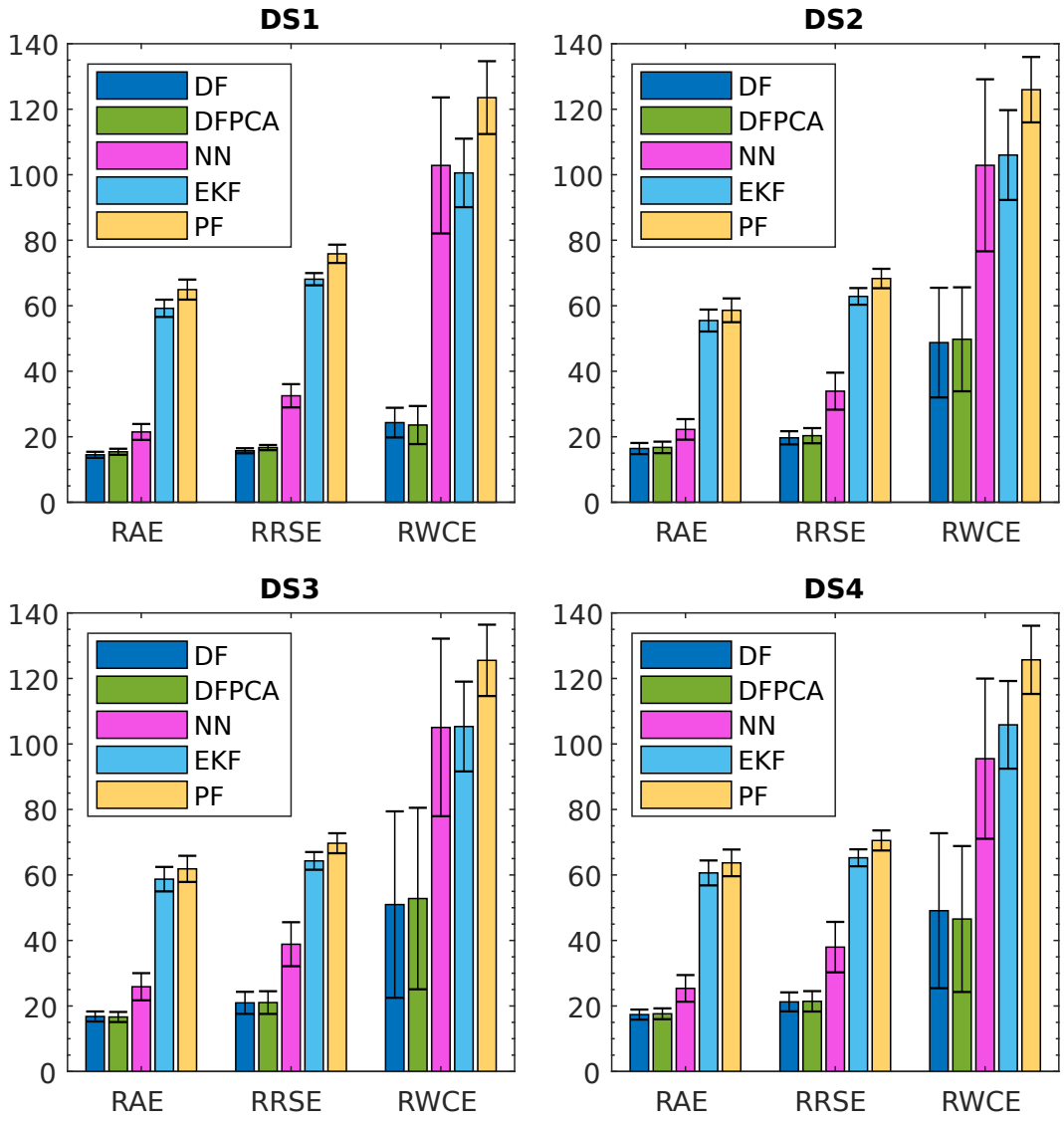

FIGURE 5.5 – Estimation performance (mean±stdev, 20 test runs of 1.5 s each) for direct filter (DF), direct filter with PCA dataset (DFPCA), neural networks (NN), extended Kalman filter (EKF) and particle filter (PF) with 4 different experimental datasets ($m = 20$, $N_D = 10000$, $\varepsilon = 0.1292$).

Cette thèse est accessible à l'adresse : http://theses.insa-lyon.fr/publication/2019LYSEI123/these.pdf
© [G. J. Becerra], [2019], INSA de Lyon, tous droits réservés

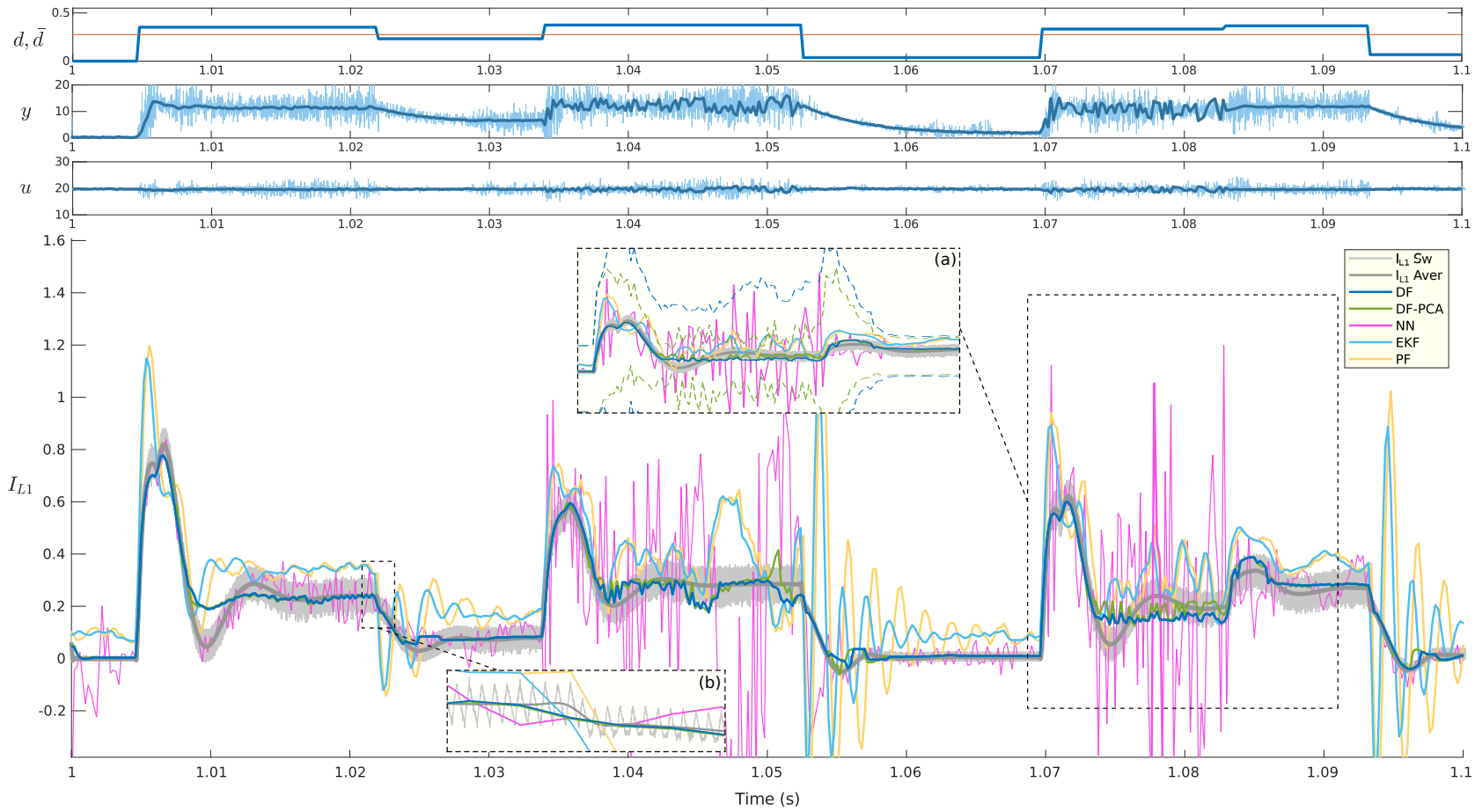

FIGURE 5.6 – Experimental results (top to bottom): Duty cycle d and DCM boundary $\bar{d}$. Output voltage $y = V_{C2}$. Input voltage $u = E$. Input current I_{L1} estimate with direct filter (DF), direct filter with PCA dataset (DFPCA), neural networks (NN), extended Kalman Filter (EKF) and particle filter (PF).

Cette thèse est accessible à l'adresse : http://theses.insa-lyon.fr/publication/2019LYSEI123/these.pdf
© [G. J. Becerra], [2019], INSA de Lyon, tous droits réservés

Dataset	Mean performance loss (%)			Execution time (ms) / speedup w.r.t CPU		
	RAE	RRSE	RWCE	CPU	GPU	GPU+PCA
DS1	1.5446	1.6832	3.0170	1.6410	1.0141 / 1.6183X	0.2419 / 6.7847X
DS2	0.2641	0.8726	4.0489	1.6445	1.0157 / 1.6191X	0.2434 / 6.7577X
DS3	0.6703	0.1592	6.4868	1.6491	1.0172 / 1.6212X	0.2437 / 6.7660X
DS4	0.4993	0.7582	1.9521	1.6428	1.0176 / 1.6144X	0.2443 / 6.7235X

TABLE 5.2 – Performance comparison between DF implementations in CPU and GPU using PCA reduced dataset. $N_D = 10000$, regressor length in original dataset $3m = 60$, regressor length in PCA reduced dataset $= 13$.

RWCE. The average execution time of one iteration of algorithm 3 is shown for three different implementations: CPU running the algorithm sequentially, GPU running the parallel implementation, and GPU running the parallel implementation and using the PCA reduced dataset. Also, the speedup of the GPU implementations with respect to the base CPU case are also shown. Notice that the estimation performance is decreased when using the reduced dataset by less than 2% for the absolute error. On the other hand, the computation speed is increased 1.6 times for the GPU case, and more than 6 times for the GPU+PCA case. This last implementation allows to obtain estimates at a rate of 4 kHz, corresponding to the sample time of the experimental dataset. These results show that the use of the reduced dimension datasets provide a computation speed gain that heavily outweighs the estimation loss and also make feasible the implementation of the DF algorithm for real time applications.

The hardware used for these tests is the Nvidia Jetson TX2, using one of the four available ARM Cortex-A57 CPU cores running at 2.0 GHz, and the Pascal GPU running at 1.12 GHz.

5.7.2 Observer-based Control for SEPIC Converter

This example presents the case of a SEPIC power converter, dealing with the control and observation problems. The tdCLF control method introduced in the previous chapter was used, and a brief explanation of the implementation details is provided. The results presented here are only for the case of simulation.

Fig. 5.7 shows a diagram illustrating the different elements in the implementation. The SEPIC converter described introduced in section 2.1.4 is used. The model for this converter takes as inputs the supply voltage $u(t) = E$ assumed constant in this case, and the switching signal $\sigma(t)$ that selects the active subsystem at each time instant. The converter output is the voltage in the second capacitor $y(t) = V_{C2}(t)$. The control signal $\sigma(t)$ is generated using a PWM module that takes as input a signal $s(t) \in [0, 1]$, representing the duty cycle value.

The control is implemented using the trajectory-dependent control Lyapunov function (tdCLF) approach, designed using a moment relaxation of the converter's switched model. The control also takes the desired reference

Cette thèse est accessible à l'adresse : http://theses.insa-lyon.fr/publication/2019LYSEI123/these.pdf
© [G. J. Becerra], [2019], INSA de Lyon, tous droits réservés

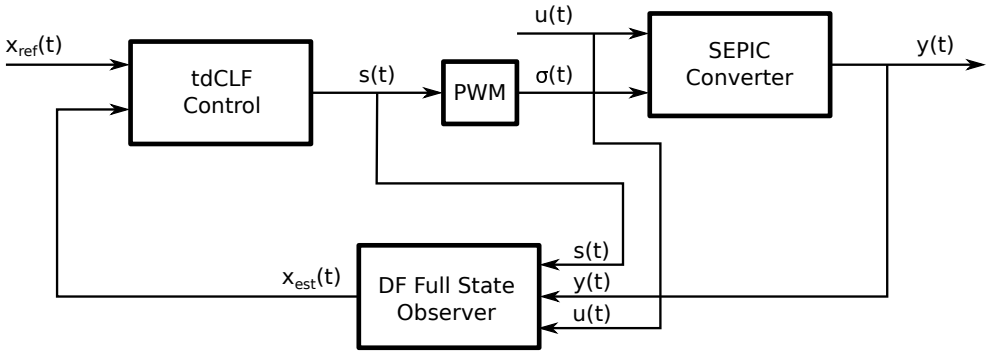

FIGURE 5.7 – Block diagram for the observer-based control of the SEPIC converter.

for the state variables $x_{ref}(t)$, which is a piece-wise constant signal obtained generated from the equilibrium points of the converter's switched model. The last part in the diagram is the observer. This is implemented using the approach described in chapter 5, where a direct filter (DF) was designed for estimating the input current I_{L1}. The observer takes as inputs the duty cycle signal $s(t)$, the converter output voltage $y(t)$ and the converter supply voltage $u(t)$. This DF implementation was extended to give estimates of the full state vector $x_{est}(t)$.

5.7.3 Implementation Details

The continuous-time switched model presented in section 2.1.4 was used for the SEPIC converter. The converter has an input voltage $u(t) = E$ assumed constant, a switching input $\sigma(t)$ that selects the active subsystem, and 4 state variables: $x(t) = [I_{L1}, V_{C1}, I_{L2}, V_{C2}]^\intercal$. The output voltage is $y(t) = V_{C2}$. The parameter values used are specified in Table 2.1.

Pulse Width Modulator

The pulse width modulator (PWM) is used to generate the control signal $\sigma(t)$ from the duty cycle signal $s(t)$ supplied by the tdCLF controller. The PWM is configured with a switching frequency $f_{pwm} = 50$ kHz.

Direct Filter Full State Observer

The direct filter (DF) approach introduced in chapter 5 was used. There, a DF was designed and implemented for estimating the control input I_{L1} in a SEPIC converter operating in CCM and DCM, controlled by a signal $s(t)$ in open loop. However, the following case study was implemented assuming that the converter operates only in CCM. The reason for this is because the tdCLF approach is still yet to be extended to deal with the case of DCM.

The DF implementation shown here has been extended to the case of full state estimation. To achieve this, the design procedure 2 and estimation algorithm 3 in chapter 5 were modified to provide estimates for all the unmeasured state variables at the same time. Also, the signals used for constructing

Cette thèse est accessible à l'adresse : http://theses.insa-lyon.fr/publication/2019LYSEI123/these.pdf
© [G. J. Becerra], [2019], INSA de Lyon, tous droits réservés

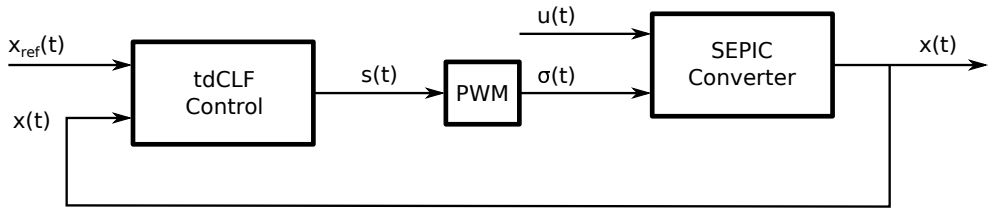

FIGURE 5.8 – Block diagram for the control of the SEPIC converter, used for obtaining the DF dataset.

the dataset $\mathcal{D}$ were captured in a closed loop configuration. Algorithm 5 is shown next with the required changes to achieve the functionality described.

Algorithme 5 : Full-state direct filter design for power converters (offline)

Result : $\mathcal{D} = \{\tilde{\varphi}_k, \tilde{x}_k\}, \gamma_j, \varepsilon_j, j \in \mathcal{J}$

1. Design the reference test signal $x_{ref}(t)$ for driving the closed loop system in Fig. 5.8 to run under different operating conditions.
2. Measure the inputs $u(t)$, $s(t)$, the state variables $\tilde{x}(t)$ and the output $\tilde{y}(t)$. The sampling time should be sufficiently high to obtain detailed waveforms of the switching behavior.
3. Compute $\bar{y}(t) = \texttt{average}(\tilde{y}(t))$, $\bar{x}(t) = \texttt{average}(\tilde{x}(t))$, with $\texttt{average}(\cdot)$ a non-causal filter.
4. Obtain $\tilde{y}^t = \texttt{resample}(\bar{y}(t), T_s)$, $\tilde{x}^t = \texttt{resample}(\bar{x}(t), T_s)$, $\tilde{s}^t = \texttt{resample}(\tilde{s}(t), T_s)$, $\tilde{u}^t = \texttt{resample}(\tilde{u}(t), T_s)$, with T_s a sample time small enough to capture the low frequency behavior.
5. Prepare dataset $\mathcal{D}$ using $\tilde{\varphi}_k = [\tilde{s}^t; \tilde{y}^t; \tilde{u}^t], \tilde{x}^t$.
6. Take $\varepsilon_j = \left\| \tilde{x}_j(t) - \bar{x}_j(t) \right\|_\infty, j \in \mathcal{J}$.
7. Take $\gamma_j^* = \min \gamma_j$, subject to $\overline{f}_c(\tilde{\boldsymbol{\varphi}}^k) > \tilde{x}_j^k - \varepsilon_j, k = 1, \ldots, N$ (sufficient condition in Theorem 2.5.1), with $\tilde{\boldsymbol{\varphi}}^k = [\tilde{\mathbf{s}}^{k,m}; \tilde{\mathbf{y}}^{k,m}; \tilde{\mathbf{u}}^{k,m}]$.

The main difference between this design procedure and the one described in chapter 5 is that all the state variables need to be measured in order to prepare the dataset. However in the case of the SEPIC converter the measured output $y(t)$ is directly the 4^{th} state variable $x_4(t) = V_{C2}(t)$, and only the other state variables $\{x_1(t), x_2(t), x_3(t)\}$ need to be estimated. Therefore $\mathcal{J} = \{1, 2, 3\}$ is the set of indexes for the unmeasured state variables. The noise bounds ε_j and the maximum variation γ_j of each state variable x_i with respect to the regressors φ_k are computed independently. The reason for this is that each state variable may have different noise bounds, and the map $f_j : \varphi \to x_j$ may have different maximum partial derivatives for each state variable.

The first step in the design procedure requires the use of state references $x_{ref}(t)$ as test signals. We assume that piece-wise constant references will always be used. The test signals should be randomly generated to have the system operating in a wide operation range. However, these references $x_{ref}(t)$

Cette thèse est accessible à l'adresse : http://theses.insa-lyon.fr/publication/2019LYSEI123/these.pdf
© [G. J. Becerra], [2019], INSA de Lyon, tous droits réservés

can not be assigned arbitrarily, because there is only 1 degree of freedom (the control signal $s(t)$) to manipulate the 4 state variables in the SEPIC converter. Therefore, the approach used requires to compute the equilibrium points of the switched system in open loop for different values of the duty cycle $s(t) \in [0, 1]$. This is achieved by running simulations of the system for a sufficiently long time until the states have stabilized in a steady limit cycle, and computing the average of this cycle. These equilibrium points are used as the references for the closed loop system.

The closed loop system is simulated for the random test references, and the variables are measured, filtered and resampled at $T_s = 0.1$ ms. Then, the regressors $\mathcal{D}$ are constructed, and used to obtain the parameters ε_j, γ_j for each state variable x_i. The procedure for obtaining these parameters is the same used in the original DF implementation, but is done independently for each state variable. The size used for the dataset regressor was $N_{tr} = 10000$ with a regressor length $m = 20$.

Algorithme 6 : Full-state direct filter estimation for power converters (online)

Data : $\mathcal{D} = \{\tilde{\varphi}_k, \tilde{x}_k\}$, γ_j, ε_j, $j \in \mathcal{J}$
Result : Estimate $\hat{x}^t$
while *true* **do**
  1. Measure $\tilde{s}^t$, $\tilde{y}^t$, $\tilde{u}^t$.
  2. Construct the regressor $\tilde{\boldsymbol{\varphi}}^t$ in Eq. (2.27).
  3. Compute $\Delta^t = \left\|\tilde{\boldsymbol{\varphi}}^t - \tilde{\boldsymbol{\varphi}}^k\right\|$, with $\tilde{\boldsymbol{\varphi}}^k$ available in dataset $\mathcal{D}$.
  foreach $j \in \mathcal{J}$ **do**
    4. Compute the optimal tightest bounds $\overline{f}_{c,j}(\Delta^t)$, $\underline{f}_{c,j}(\Delta^t)$ using Eqs. (5.4a), with $\tilde{x}_j^k$ available in dataset $\mathcal{D}$.
    5. Compute the direct filter estimate $\hat{x}_j^t$ using Eq. (2.34).
  end
end

The estimates are computed in the on-line algorithm 6. The only difference between this algorithm and the one described in chapter 5 is that the tightest bounds are computed independently for each state variable x_i, using Eqs. 5.4a. It is important to remark that the term $\Delta^t = \left\|\tilde{\boldsymbol{\varphi}}^t - \tilde{\boldsymbol{\varphi}}^k\right\|$ is the same for all state variables. Recall from section 5.5 that the first two CUDA *kernels* are the ones that compute this term. This is the most expensive part in the computation of the tightest bounds. In the full state estimation implementation this term only has to be computed once for all state variables, so the computational cost of extending the DF approach from single to full state should not be significant. The on-line algorithm is executed with the same sample time used for resampling the signals during the filter design

Cette thèse est accessible à l'adresse : http://theses.insa-lyon.fr/publication/2019LYSEI123/these.pdf
© [G. J. Becerra], [2019], INSA de Lyon, tous droits réservés

procedure: $T_s = 0.1$ ms.

$$\overline{f}_{c,j}(\Delta^t) = \min_{k=1,\dots,N} \left(\tilde{x}_i^k + \varepsilon_i + \gamma_i \Delta^t \right) \tag{5.4a}$$

$$\underline{f}_{c,j}(\Delta^t) = \max_{k=1,\dots,N} \left(\tilde{x}_i^k - \varepsilon_i - \gamma_i \Delta^t \right) \tag{5.4b}$$

Trajectory-dependent Control Lyapunov Function Controller

The approach described in section 4.4 was used to implement a tdCLF control approach using the moment relaxation for the switched model of the power converter. The control implementation is the same that was used in the SEPIC example from section 4.4.6. The only difference is that the state feedback is supplied by the DF full state observer, instead of being directly measured from the plant. The sample time used for obtaining the discrete-time models is also $T_s = 0.1$ ms.

Simulation Results

Fig. 5.9 shows the closed-loop response of the system for random piece-wise references x_{ref}. The control exhibits good tracking response in all variables, with a maximum settling time of approximately 0.02 s for the slowest one, which is the output voltage. There is an offset present in some cases, in particular for the output voltage, as was observed in the results from section 4.4.6. The DF full state observer provides good estimates for the unmeasured variables $I_{L1}(t)$, $V_{C1}(t)$ and $I_{L2}(t)$.

These results illustrate the performance of the combined observer-based control of power converters using the proposed methods for the SEPIC converter topology. The closed loop has shown good tracking performance for randomly selected piece-wise constant references. The direct filter approach is extended to the case of full-state estimation, as required by the tdCLF control. This extension was made possible by computing the optimal bounds independently for each estimated state variable. Obtaining the regressor distances is the most expensive part of the computation, but in the proposed approach this term is common for all estimators, simplifying the implementation without generating much overhead with respect to the single-state estimator presented in chapter 5.

5.8 Conclusion

A method for direct design of estimators without exact knowledge of the system model has been presented. This approach is shown to be useful for estimation in power converters working in both CCM and DCM. Because of drastic dynamic changes in the system behavior when traversing the boundary between CCM and DCM, the average model does not provide a good approximation. The proposed data-based approach is based on assumptions

Cette thèse est accessible à l'adresse : http://theses.insa-lyon.fr/publication/2019LYSEI123/these.pdf
© [G. J. Becerra], [2019], INSA de Lyon, tous droits réservés

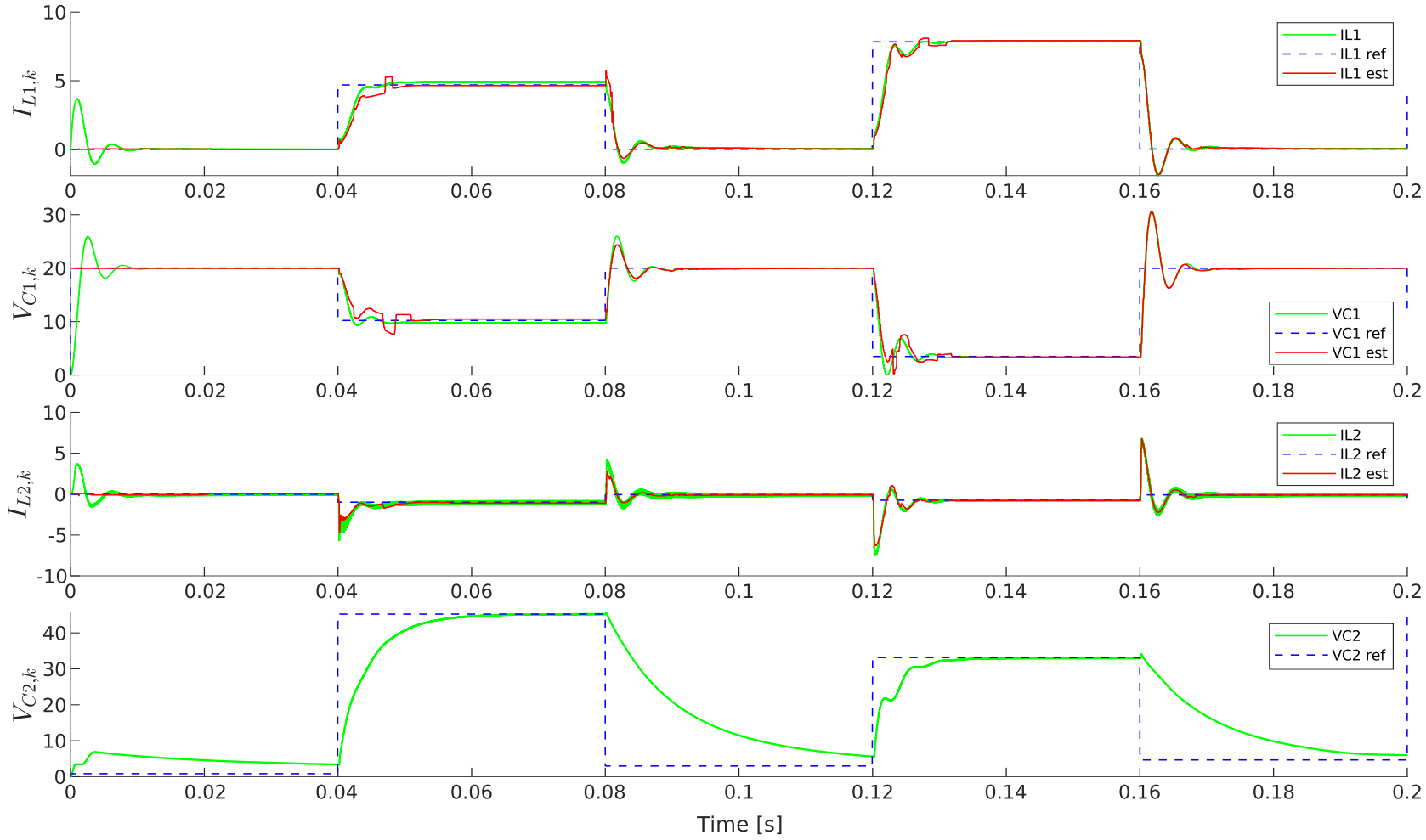

FIGURE 5.9 – Simulation results: SEPIC control using the tdCLF approach for the relaxed model and the full-state DF observer.

Cette thèse est accessible à l'adresse : http://theses.insa-lyon.fr/publication/2019LYSEI123/these.pdf
© [G. J. Becerra], [2019], INSA de Lyon, tous droits réservés

on the regularity of the approximated functions that are made for computing worst case bounds on the estimate. This method can be applied to PWM power converters, and is demonstrated for the case of the SEPIC DC-DC converter. Simulation and experimental results have been obtained, showing that the direct filter approach provides good estimation results with respect to other model-based and data-based estimation methods.

The main contribution in this chapter is the development of a practical design procedure for obtaining direct filters in the context of power converters operating in CCM and DCM. Also, we show that a real-time implementation of the direct filter algorithm is possible using parallel programming running on a GPU. To the best of our knowledge, this is the first time that the parallel structure of the direct filter algorithm has been identified and exploited in a practical setting. Furthermore, the use of PCA as a tool for dimensionality reduction in the regressor datasets has shown improvements in the computation performance. This application of PCA is also novel in the context of direct filtering.

There are still many directions which can be followed to improve this estimation method. For instance, it would be interesting to study the dependence of the estimation performance on the parameter space (m, N_D, ε) for other converter topologies where discontinuous conduction modes are present. Also, it would be interesting to investigate the relationship between the information loss when the original dataset regressors are mapped to a lower dimensional space, and the performance loss in the estimation using the reduced dataset.

Cette thèse est accessible à l'adresse : http://theses.insa-lyon.fr/publication/2019LYSEI123/these.pdf
© [G. J. Becerra], [2019], INSA de Lyon, tous droits réservés

Cette thèse est accessible à l'adresse : http://theses.insa-lyon.fr/publication/2019LYSEI123/these.pdf
© [G. J. Becerra], [2019], INSA de Lyon, tous droits réservés

Chapter 6

Conclusion and Perspectives

6.1 General Conclusion

This work proposes new approaches to control and observation of switched systems, in the context of power converters. Ideas from different subjects like Lyapunov stability, the method of moments, algebraic geometry and direct filtering have been used in novel ways to obtain the proposed solutions.

It was shown in chapter 3 that switched systems and the moment relaxations obtained from these have a common geometric structure in the equilibria regions. In particular, the equilibria regions for these models are embedded in the same affine variety. The importance of this is that a map between the space of the switched system control variable σ and the space of moments m can be established. This transformation allows to derive an equivalent linear model that can be used in the computation of a control law. Existing works like [40], [41], [42] have presented the use of moment relaxations for nonlinear and switched systems, but none offered an analysis on the geometric and algebraic structure of the equilibria regions.

The model relaxation technique is used in chapter 4 to solve the control problem of switched systems using trajectory dependent control Lyapunov functions. This method has the advantage of allowing non-conservative solutions to the control problem while guaranteeing the stability conditions given by Lyapunov's theory. This is achieved by expressing the control problem as an optimization problem, where the parameters of the Lyapunov function are computed iteratively along the system trajectory. To the best of our knowledge this control method has not been used before in the context of switched systems and power converters. The procedure developed for recovering the control signal for the switched system is also a novel contribution, because existing works like [40] and [41] present results for optimal control of switched systems with only two operation modes. Our approach can be used for switched systems with an arbitrary number of operation modes, as illustrated in the 2-cell and 3-cell multicellular converter examples.

Regarding the observation problem, a practical implementation of the direct filter approach was proposed in chapter 5 for state estimation in switched systems. The importance of this approach is that it does not require knowledge of the mathematical model of the system. This allows us to apply this

Cette thèse est accessible à l'adresse : http://theses.insa-lyon.fr/publication/2019LYSEI123/these.pdf
© [G. J. Becerra], [2019], INSA de Lyon, tous droits réservés

method in the case of power converters operating in continuous and discontinuous modes. It was found that the performance of the developed estimators is superior in practice to other model-based and data-based estimation approaches. The main contribution in this chapter is the proposal of a practical implementation in the context of power converters. To achieve real-time operation we proposed the use of two combined techniques: a parallel implementation of the direct filter algorithm using a GPU and a dimensionality-reduction method for the datasets. It was shown that the achieved performance increase surpasses the degradation in estimation accuracy due to the information loss incurred when applying the dimensionality reduction technique to the filter datasets. None of the existing works regarding direct filtering in the literature have proposed the use of parallel programming or dimensionality reduction to improve the computation speed of the direct filter. Also, the direct filter method has been reported in the literature for mechanical [38] or chemical systems [91]. Power converters exhibit a dynamical behavior that is several orders of magnitude faster than mechanical or chemical systems, making the requirements for a real-time implementation harder to achieve in our context. We also developed an extension for a full-state estimator in the case of an observer-based control. It was shown that the structure of the direct filter algorithm allows to naturally extend it from single to full state estimation without incurring in significant additional computational costs.

Another advantage of the proposed control and observation methods is that these have been developed from the general perspective of switched systems, allowing their application to various kinds of switched systems, in particular to power converters with different topologies. The performance of the proposed methods has been evaluated under different conditions, in simulation as well as in the available experimental test benches.

6.2 Perspectives

The methods proposed in this work leave open new lines that can be followed to obtain improvements and allow the practical implementation in a setting beyond the prototype stage.

Regarding the moment relaxations of switched systems, the study of the operation regions for different converter topologies is still yet to be investigated. This analysis could provide better insights into the behavior of the system under different operating conditions and the structure of the equilibria. Also, the use of alternative polynomial basis like *splines* or piecewise *sinc* functions could be explored to reduce the size of the mathematical problem and the approximation error in the control signal synthesis step.

The application of trajectory-dependent control Lyapunov functions to switched systems have yielded interesting results for different converter topologies. However, the solution of the mathematical problem is still not feasible to be achieved at the speed required for a real-time implementation. Possible ways to reduce the computational complexity of this optimization problem need to be explored. For instance, solving the feasibility problem instead of

Cette thèse est accessible à l'adresse : http://theses.insa-lyon.fr/publication/2019LYSEI123/these.pdf
© [G. J. Becerra], [2019], INSA de Lyon, tous droits réservés

the optimality problem could improve performance while maintaining stability guarantees. Another possibility could be using a parallel implementation of the semidefinite solver for reducing the computation time.

It was observed that the length of the moment sequences has a relation with the controllability of the system. Investigating this relation could provide some criterion for determining the minimum length required to guarantee system controllability. A detailed comparison between the fixed parameter and trajectory dependent parameter cases would be interesting to quantify the performance improvements obtained when using less conservative Lyapunov functions. Also, more tests are required to characterize the performance of this control method with respect to disturbance rejection. Finally, it would be interesting to investigate possible ways to extend the control method to the case of power converters with CCM/DCM operation.

The proposed estimation approach using direct filters has proven to give good performance with respect to other methods. However, the application to converter topologies with multiple control signals, like the case of the multicellular converter, may increase the difficulty during the design stage when the identification experiments must be carried out. It would be interesting to review the system identification theory and identify strategies for the design of experiments for systems with multiple inputs. This would allow to test the direct filter approach in the case of the multicellular converter.

It was shown that the estimation performance depends on parameters like regressor length and the dataset size. However, this relation has been found to be specific for different converter topologies. A detailed analysis of this dependence is required for having a more refined criterion in the selection of the optimal values for these parameters.

The use of a dimensionality reduction approach like PCA has shown to improve the computational performance of the direct filter. It would be interesting to test other dimensionality reduction techniques like Kernel PCA, discriminant analysis, generalized discriminant analysis or auto-encoders to compare performance.

Finally, the proposed observer-based approach should be compared to other methods in the context of power converters and with different converter topologies, to have a better understanding of the achieved performance.

Cette thèse est accessible à l'adresse : http://theses.insa-lyon.fr/publication/2019LYSEI123/these.pdf
© [G. J. Becerra], [2019], INSA de Lyon, tous droits réservés

Cette thèse est accessible à l'adresse : http://theses.insa-lyon.fr/publication/2019LYSEI123/these.pdf
© [G. J. Becerra], [2019], INSA de Lyon, tous droits réservés

Bibliography

[1] R. Erickson and D. Maksimovic, *Fundamentals of Power Electronics*, ser. Power electronics. Springer US, 2001, ISBN: 9780792372707. [Online]. Available: https://books.google.com.co/books?id=S91G_Nz_KjEC.

[2] R. Middlebrook and S. Cuk, "A general unified approach to modelling switching-converter power stages", in *Power Electronics Specialists Conference, 1976 IEEE*, Jun. 1976, pp. 18–34. DOI: 10.1109/PESC.1976.7072895.

[3] M. Kazmierkowski, R. Krishnan, F. Blaabjerg, and J. Irwin, *Control in Power Electronics: Selected Problems*, ser. Academic Press Series in Engineering. Elsevier Science, 2002, ISBN: 9780124027725. [Online]. Available: https://books.google.com.co/books?id=cHuYj49Ivt4C.

[4] N. Mohan and T. Undeland, *Power electronics: converters, applications, and design*. Wiley India, 2007, ISBN: 9788126510900. [Online]. Available: https://books.google.com.co/books?id=oxR8vB2XjgIC.

[5] V. I. Utkin, "Sliding mode control design principles and applications to electric drives", *IEEE Transactions on Industrial Electronics*, vol. 40, no. 1, pp. 23–36, Feb. 1993, ISSN: 0278-0046. DOI: 10.1109/41.184818.

[6] S. Tan, Y. M. Lai, and C. K. Tse, "General design issues of sliding-mode controllers in dcdc converters", *IEEE Transactions on Industrial Electronics*, vol. 55, no. 3, pp. 1160–1174, Mar. 2008, ISSN: 0278-0046. DOI: 10.1109/TIE.2007.909058.

[7] S. Gomariz, E. Alarcon, J. A. Martinez, A. Poveda, J. Madrenas, and F. Guinjoan, "Minimum time control of a buck converter by means of fuzzy logic approximation", in *IECON '98. Proceedings of the 24th Annual Conference of the IEEE Industrial Electronics Society (Cat. No.98CH36200)*, vol. 2, Aug. 1998, 1060–1065 vol.2. DOI: 10.1109/IECON.1998.724242.

[8] S. Durgadevi and M. G. Umamaheswari, "Adaptive neuro fuzzy logic controller based current mode control for single phase power factor correction using dc-dc sepic converter", in *2017 International Conference on Power and Embedded Drive Control (ICPEDC)*, Mar. 2017, pp. 490–495. DOI: 10.1109/ICPEDC.2017.8081139.

[9] P. Cortes, M. P. Kazmierkowski, R. M. Kennel, D. E. Quevedo, and J. Rodriguez, "Predictive control in power electronics and drives", *IEEE Transactions on Industrial Electronics*, vol. 55, no. 12, pp. 4312–4324, Dec. 2008, ISSN: 0278-0046. DOI: 10.1109/TIE.2008.2007480.

Cette thèse est accessible à l'adresse : http://theses.insa-lyon.fr/publication/2019LYSEI123/these.pdf
© [G. J. Becerra], [2019], INSA de Lyon, tous droits réservés

[10] S. Kouro, P. Cortes, R. Vargas, U. Ammann, and J. Rodriguez, "Model predictive controla simple and powerful method to control power converters", *IEEE Transactions on Industrial Electronics*, vol. 56, no. 6, pp. 1826–1838, Jun. 2009, ISSN: 0278-0046. DOI: 10.1109/TIE.2008.2008349.

[11] D. Patino, P. Riedinger, and C. Iung, "Practical optimal state feedback control law for continuous-time switched affine systems with cyclic steady state.", *International Journal of Control*, vol. 82, no. 7, pp. 1357–1376, 2009, ISSN: 00207179. [Online]. Available: http://search.ebscohost.com/login.aspx?direct=true&db=cph&AN=39567010&lang=es&site=ehost-live.

[12] A.-R. Meghnous, D. Patino, M. T. Pham, and X. Lin-Shi, "Hybrid optimal control with singular arcs for dc-dc power converters", in *52nd IEEE Conference on Decision and Control*, IEEE, 2013, pp. 103–108.

[13] D. J. Bates, A. G. Beccuti, I. A. Fotiou, and M. Morari, "An optimal control application in power electronics using numerical algebraic geometry", in *2008 American Control Conference*, Jun. 2008, pp. 2221–2226. DOI: 10.1109/ACC.2008.4586822.

[14] H. Bevrani, M. Abrishamchian, and N. Safari-Shad, "Nonlinear and linear robust control of switching power converters", in *Control Applications, 1999. Proceedings of the 1999 IEEE International Conference on*, vol. 1, 1999, 808–813 vol. 1. DOI: 10.1109/CCA.1999.807765.

[15] I. Cervantes, A. Mendoza-Torres, A. Emadi, and I. A. Diaz-Diaz, "Robust switched current control of converters", *IET Control Theory Applications*, vol. 7, no. 10, pp. 1398–1407, Jul. 2013, ISSN: 1751-8644. DOI: 10.1049/iet-cta.2013.0015.

[16] H. Sira-Ramirez and R. Ortega, "Passivity-based controllers for the stabilization of dc-to-dc power converters", in *Decision and Control, 1995., Proceedings of the 34th IEEE Conference on*, vol. 4, Dec. 1995, 3471–3476 vol.4. DOI: 10.1109/CDC.1995.479122.

[17] G. Escobar, R. Ortega, H. Sira-Ramfrez, and H. Ludvigsen, "A hybrid passivity based controller design for a three phase voltage source reversible boost type rectifier", in *Decision and Control, 1998. Proceedings of the 37th IEEE Conference on*, vol. 2, Dec. 1998, 2035–2040 vol.2. DOI: 10.1109/CDC.1998.758630.

[18] M. Lazar and A. Jokic, "Synthesis of trajectory-dependent control lyapunov functions by a single linear program", in *Hybrid Systems: Computation and Control*, R. Majumdar and P. Tabuada, Eds., Berlin, Heidelberg: Springer Berlin Heidelberg, 2009, pp. 237–251, ISBN: 978-3-642-00602-9.

[19] M. Lazar and R. Gielen, "On parameterized lyapunov and control lyapunov functions for discrete-time systems", in *49th IEEE Conference on Decision and Control (CDC)*, Dec. 2010, pp. 3264–3270. DOI: 10.1109/CDC.2010.5716952.

Cette thèse est accessible à l'adresse : http://theses.insa-lyon.fr/publication/2019LYSEI123/these.pdf
© [G. J. Becerra], [2019], INSA de Lyon, tous droits réservés

[20] D. Henrion and M. Korda, "Convex computation of the region of attraction of polynomial control systems", *IEEE Transactions on Automatic Control*, vol. 59, no. 2, pp. 297–312, Feb. 2014, ISSN: 0018-9286. DOI: 10.1109/TAC.2013.2283095.

[21] A. Alawieh, R. Ortega, H. Pillai, A. Astolfi, and E. Berthelot, "Adaptive control of the boost converter in discontinuous conduction mode", *IFAC Proceedings Volumes*, vol. 44, no. 1, pp. 3310 –3315, 2011, 18th IFAC World Congress, ISSN: 1474-6670. DOI: http://dx.doi.org/10.3182/20110828-6-IT-1002.03558. [Online]. Available: http://www.sciencedirect.com/science/article/pii/S1474667016441224.

[22] R. D. Middlebrook and S. Cuk, "A general unified approach to modelling switching-converter power stages", in *1976 IEEE Power Electronics Specialists Conference*, Jun. 1976, pp. 18–34. DOI: 10.1109/PESC.1976.7072895.

[23] D. Maksimovic and S. Cuk, "A unified analysis of pwm converters in discontinuous modes", *IEEE Transactions on Power Electronics*, vol. 6, no. 3, pp. 476–490, Jul. 1991, ISSN: 0885-8993. DOI: 10.1109/63.85890.

[24] R. Goebel, R. G. Sanfelice, and A. R. Teel, "Hybrid dynamical systems", *IEEE Control Systems Magazine*, vol. 29, no. 2, pp. 28–93, Apr. 2009, ISSN: 1066-033X. DOI: 10.1109/MCS.2008.931718.

[25] A. Alawieh, R. Ortega, H. Pillai, A. Astolfi, and E. Berthelot, "Voltage regulation of a boost converter in discontinuous conduction mode: A simple robust adaptive feedback controller", *IEEE Control Systems Magazine*, vol. 33, no. 3, pp. 55–65, Jun. 2013, ISSN: 1066-033X. DOI: 10.1109/MCS.2013.2249431.

[26] A. Lopez, D. Patino, R. Diez, and G. Perilla, "An equivalent continuous model for switched systems", *Systems and Control Letters*, vol. 62, no. 2, pp. 124 –131, 2013, ISSN: 0167-6911. DOI: http://dx.doi.org/10.1016/j.sysconle.2012.11.012. [Online]. Available: http://www.sciencedirect.com/science/article/pii/S0167691112002368.

[27] J. Rodriguez, J.-S. L., and F. Z. P., "Multilevel inverters: A survey of topologies, controls, and applications", *Industrial Electronics, IEEE Transactions on*, vol. 49, no. 4, pp. 724–738, Aug. 2002, ISSN: 0278-0046. DOI: 10.1109/TIE.2002.801052.

[28] A. van der Schaft and J. D., "Port-hamiltonian systems theory: An introductory overview", *Foundations and Trendső in Systems and Control*, vol. 1, no. 2-3, pp. 173–378, 2014, ISSN: 2325-6818. DOI: 10.1561/2600000002. [Online]. Available: http://dx.doi.org/10.1561/2600000002.

[29] R. Shorten, K. S. Narendra, and O. Mason, "A result on common quadratic lyapunov functions", *IEEE Transactions on Automatic Control*, vol. 48, no. 1, pp. 110–113, Jan. 2003, ISSN: 0018-9286. DOI: 10.1109/TAC.2002.806661.

Cette thèse est accessible à l'adresse : http://theses.insa-lyon.fr/publication/2019LYSEI123/these.pdf
© [G. J. Becerra], [2019], INSA de Lyon, tous droits réservés

[30] D. Liberzon, J. P. Hespanha, and A. Morse, "Stability of switched systems: A lie-algebraic condition", *Systems & Control Letters*, vol. 37, no. 3, pp. 117 –122, 1999, ISSN: 0167-6911. DOI: http://dx.doi.org/10.1016/S0167-6911(99)00012-2. [Online]. Available: http://www.sciencedirect.com/science/article/pii/S0167691199000122.

[31] H. Lin and P. J. Antsaklis, "Persistent disturbance attenuation properties for networked control systems", in *Decision and Control, 2004. CDC. 43rd IEEE Conference on*, vol. 1, Dec. 2004, 953–958 Vol.1. DOI: 10.1109/CDC.2004.1428808.

[32] A. Tanwani, H. Shim, and D. Liberzon, "Observability for switched linear systems: Characterization and observer design", *Automatic Control, IEEE Transactions on*, vol. 58, no. 4, pp. 891–904, Apr. 2013, ISSN: 0018-9286. DOI: 10.1109/TAC.2012.2224257.

[33] R. A. Decarlo, M. S. Branicky, S. Pettersson, and B. Lennartson, "Perspectives and results on the stability and stabilizability of hybrid systems", *Proceedings of the IEEE*, vol. 88, no. 7, pp. 1069–1082, Jul. 2000, ISSN: 0018-9219. DOI: 10.1109/5.871309.

[34] J. Lasserre, "Global optimization with polynomials and the problem of moments", *SIAM Journal on Optimization*, vol. 11, no. 3, pp. 796–817, 2001.

[35] D. Cox, J. Little, and D. O'Shea, *Ideals, Varieties, and Algorithms: An Introduction to Computational Algebraic Geometry and Commutative Algebra*, ser. Undergraduate Texts in Mathematics. Springer, 1997, ISBN: 9780387946801. [Online]. Available: http://books.google.com.co/books?id=E3sKOHH3990C.

[36] M. Milanese and C. Novara, "Set membership identification of nonlinear systems", *Automatica*, vol. 40, no. 6, pp. 957 –975, 2004, ISSN: 0005-1098. DOI: http://dx.doi.org/10.1016/j.automatica.2004.02.002. [Online]. Available: http://www.sciencedirect.com/science/article/pii/S0005109804000470.

[37] C. Novara, F. Ruiz, and M. Milanese, "Direct filtering: A new approach to optimal filter design for nonlinear systems", *IEEE Transactions on Automatic Control*, vol. 58, no. 1, pp. 86–99, Jan. 2013, ISSN: 0018-9286. DOI: 10.1109/TAC.2012.2204160.

[38] F. Ruiz, C. Novara, and M. Milanese, "Direct design from data of optimal filters for lpv systems", *Systems and Control Letters*, vol. 59, no. 1, pp. 1 –8, 2010, ISSN: 0167-6911. DOI: http://dx.doi.org/10.1016/j.sysconle.2009.10.008. [Online]. Available: //www.sciencedirect.com/science/article/pii/S0167691109001339.

[39] B. Ingalls, E. Sontag, Y. Wang, *et al.*, "An infinite-time relaxation theorem for differential inclusions", *Proceedings of the American Mathematical Society*, vol. 131, no. 2, pp. 487–500, 2003.

Cette thèse est accessible à l'adresse : http://theses.insa-lyon.fr/publication/2019LYSEI123/these.pdf
© [G. J. Becerra], [2019], INSA de Lyon, tous droits réservés

[40] E. Mojica-Nava, R. Meziat, N. Quijano, A. Gauthier, and N. Rakoto-Ravalontsalama, "Optimal control of switched systems: A polynomial approach", in *Proceedings of the 17th IFAC World Congress*, 2008, pp. 7808–7813.

[41] E. Mojica-Nava, N. Quijano, and N. Rakoto-Ravalontsalama, "A polynomial approach for optimal control of switched nonlinear systems", *International Journal of Robust and Nonlinear Control*, vol. 24, no. 12, pp. 1797–1808, 2014, ISSN: 1099-1239. DOI: 10.1002/rnc.2964. [Online]. Available: http://dx.doi.org/10.1002/rnc.2964.

[42] R. Meziat, D. Patino, and P. Pedregal, "An alternative approach for non-linear optimal control problems based on the method of moments", *Computational Optimization and Applications*, vol. 38, pp. 147–171, 1 2007, 10.1007/s10589-007-9032-1, ISSN: 0926-6003. [Online]. Available: http://dx.doi.org/10.1007/s10589-007-9032-1.

[43] G. Becerra, D. Patino, P. Minh Tu, and X. Lin-Shi, "Algebraic and geometric properties of equilibria in cyclic switched dynamic systems", *International Journal of Robust and Nonlinear Control*, vol. 27, no. 13, pp. 2218–2233, DOI: 10.1002/rnc.3679. eprint: https://onlinelibrary.wiley.com/doi/pdf/10.1002/rnc.3679. [Online]. Available: https://onlinelibrary.wiley.com/doi/abs/10.1002/rnc.3679.

[44] J. Daafouz and J. Bernussou, "Parameter dependent lyapunov functions for discrete time systems with time varying parametric uncertainties", *Systems & Control Letters*, vol. 43, no. 5, pp. 355 –359, 2001, ISSN: 0167-6911. DOI: https://doi.org/10.1016/S0167-6911(01)00118-9. [Online]. Available: http://www.sciencedirect.com/science/article/pii/S0167691101001189.

[45] P. Seiler, U. Topcu, A. Packard, and G. Balas, "Parameter-dependent lyapunov functions for linear systems with constant uncertainties", *IEEE Transactions on Automatic Control*, vol. 54, no. 10, pp. 2410–2416, Oct. 2009, ISSN: 0018-9286. DOI: 10.1109/TAC.2009.2029294.

[46] M. Johansson, "Lyapunov stability", in *Piecewise Linear Control Systems: A Computational Approach*. Berlin, Heidelberg: Springer Berlin Heidelberg, 2003, pp. 41–84, ISBN: 978-3-540-36801-4. DOI: 10.1007/3-540-36801-9_4. [Online]. Available: https://doi.org/10.1007/3-540-36801-9_4.

[47] G. Becerra, A. R. Meghnous, M. T. Pham, X. Lin-Shi, and D. Patino, "A unified hybrid control for dc/dc power converters using port-hamiltonian formulation", in *IECON 2017 - 43rd Annual Conference of the IEEE Industrial Electronics Society*, Oct. 2017, pp. 4851–4856. DOI: 10.1109/IECON.2017.8216837.

[48] M. Defoort, J. Van Gorp, and M. Djemai, "Multicellular converter: A benchmark for control and observation for hybrid dynamical systems", English, in *Hybrid Dynamical Systems*, ser. Lecture Notes in Control and Information Sciences, M. Djemai and M. Defoort, Eds., vol. 457,

Cette thèse est accessible à l'adresse : http://theses.insa-lyon.fr/publication/2019LYSEI123/these.pdf
© [G. J. Becerra], [2019], INSA de Lyon, tous droits réservés

Springer International Publishing, 2015, pp. 293–313, ISBN: 978-3-319-10794-3. DOI: 10.1007/978-3-319-10795-0_12. [Online]. Available: http://dx.doi.org/10.1007/978-3-319-10795-0_12.

[49] J. Buisson, P.-Y. Richard, and H. Cormerais, "On the stabilisation of switching electrical power converters", in *Hybrid Systems: Computation and Control: 8th International Workshop, HSCC 2005, Zurich, Switzerland, March 9-11, 2005. Proceedings*, M. Morari and L. Thiele, Eds. Berlin, Heidelberg: Springer Berlin Heidelberg, 2005, pp. 184–197, ISBN: 978-3-540-31954-2. DOI: 10.1007/978-3-540-31954-2_12. [Online]. Available: https://doi.org/10.1007/978-3-540-31954-2_12.

[50] R. Meziat and D. Patiño, "Exact relaxations of non-convex variational problems", *Optimization Letters*, vol. 2, no. 4, pp. 505–519, 2008.

[51] Y. Nesterov and A. Nemirovskii, *Interior-point Polynomial Algorithms in Convex Programming*, ser. Studies in Applied Mathematics. Society for Industrial and Applied Mathematics (SIAM, 3600 Market Street, Floor 6, Philadelphia, PA 19104), 1994, ISBN: 9781611970791. [Online]. Available: https://books.google.com.co/books?id=MgWY_clJXusC.

[52] N. Karmarkar, "A new polynomial-time algorithm for linear programming", *Combinatorica*, vol. 4, no. 4, pp. 373–395, Dec. 1984, ISSN: 1439-6912. DOI: 10.1007/BF02579150. [Online]. Available: https://doi.org/10.1007/BF02579150.

[53] S. Boyd and L. Vandenberghe, *Convex optimization*. Cambridge University Press, 2004, ISBN: 9780521833783. [Online]. Available: http://books.google.com.co/books?id=mYm0bLd3fcoC.

[54] J. Lofberg, "Yalmip : A toolbox for modeling and optimization in matlab", in *2004 IEEE International Conference on Robotics and Automation (IEEE Cat. No.04CH37508)*, Sep. 2004, pp. 284–289. DOI: 10.1109/CACSD.2004.1393890.

[55] E. D. Andersen and K. D. Andersen, "The mosek interior point optimizer for linear programming: An implementation of the homogeneous algorithm", in *High Performance Optimization*, H. Frenk, K. Roos, T. Terlaky, and S. Zhang, Eds. Boston, MA: Springer US, 2000, pp. 197–232, ISBN: 978-1-4757-3216-0. DOI: 10.1007/978-1-4757-3216-0_8. [Online]. Available: https://doi.org/10.1007/978-1-4757-3216-0_8.

[56] N. F. Gade-Nielsen, B. Dammann, and J. B. Jørgensen, "Interior point methods on gpu with application to model predictive control", 2014.

[57] A. Khaligh and A. Emadi, "Modified pulse adjustment technique with variable states to control dc-dc converters operating in discontinuous conduction mode and driving constant power loads", in *2006 1ST IEEE Conference on Industrial Electronics and Applications*, May 2006, pp. 1–6. DOI: 10.1109/ICIEA.2006.257140.

Cette thèse est accessible à l'adresse : http://theses.insa-lyon.fr/publication/2019LYSEI123/these.pdf
© [G. J. Becerra], [2019], INSA de Lyon, tous droits réservés

[58] T.-L. Chern, L.-H. Liu, C.-N. Huang, Y.-L. Chern, and J.-H. Kuang, "High power factor flyback converter for led driver with boundary conduction mode control", in *2010 5th IEEE Conference on Industrial Electronics and Applications*, Jun. 2010, pp. 2088–2093. DOI: 10.1109/ICIEA.2010.5516684.

[59] B. Sahu and G. A. Rincon-Mora, "An accurate, low-voltage, cmos switching power supply with adaptive on-time pulse-frequency modulation (pfm) control", *IEEE Transactions on Circuits and Systems I: Regular Papers*, vol. 54, no. 2, pp. 312–321, Feb. 2007, ISSN: 1549-8328. DOI: 10.1109/TCSI.2006.887472.

[60] W. Fu, S. T. Tan, and A. Fayed, "Switching and conduction loss analysis of buck converters operating in dcm-only scenarios", in *2013 IEEE International Symposium on Circuits and Systems (ISCAS2013)*, May 2013, pp. 921–924. DOI: 10.1109/ISCAS.2013.6571998.

[61] S. C. Chung, S. R. Huang, and C. I. Ln, "Applications of describing functions to estimate the continuous and discontinuous conduction mode for a dc-to-dc buck converter", *IEE Proceedings - Electric Power Applications*, vol. 147, no. 6, pp. 513–519, Nov. 2000, ISSN: 1350-2352. DOI: 10.1049/ip-epa:20000589.

[62] M. Salimi, J. Soltani, A. Zakipour, and V. Hajbani, "Two-loop adaptive and nonlinear control of the dc-dc boost converter in discontinuous conduction mode", in *4th Annual International Power Electronics, Drive Systems and Technologies Conference*, Feb. 2013, pp. 164–169. DOI: 10.1109/PEDSTC.2013.6506696.

[63] D. S. L. Simonetti, J. Sebastian, and J. Uceda, "A small-signal model for sepic, cuk and flyback converters as power factor preregulators in discontinuous conduction mode", in *Proceedings of IEEE Power Electronics Specialist Conference - PESC '93*, Jun. 1993, pp. 735–741. DOI: 10.1109/PESC.1993.472006.

[64] M. Ferdowsi and A. Emadi, "Estimative current mode control technique for dc-dc converters operating in discontinuous conduction mode", *IEEE Power Electronics Letters*, vol. 2, no. 1, pp. 20–23, Mar. 2004, ISSN: 1540-7985. DOI: 10.1109/LPEL.2004.830245.

[65] D. S. L. Simonetti, J. Sebastian, and J. Uceda, "The discontinuous conduction mode sepic and cuk power factor preregulators: Analysis and design", *IEEE Transactions on Industrial Electronics*, vol. 44, no. 5, pp. 630–637, Oct. 1997, ISSN: 0278-0046. DOI: 10.1109/41.633459.

[66] S. Cuk and R. D. Middlebrook, "A general unified approach to modelling switching dc-to-dc converters in discontinuous conduction mode", in *1977 IEEE Power Electronics Specialists Conference*, Jun. 1977, pp. 36–57. DOI: 10.1109/PESC.1977.7070802.

[67] S. Cuk, "Discontinuous inductor current in the optimum topology switching converter", in *1978 IEEE Power Electronics Specialists Conference*, Jun. 1978, pp. 105–123. DOI: 10.1109/PESC.1978.7072344.

Cette thèse est accessible à l'adresse : http://theses.insa-lyon.fr/publication/2019LYSEI123/these.pdf
© [G. J. Becerra], [2019], INSA de Lyon, tous droits réservés

[68] J. Kunze, "Computer-aided analysis of regulated switched power supplies with unified baseband models for continuous and discontinuous conduction mode", in *INTELEC '85 - Seventh International Telecommunications Energy Conference*, Oct. 1985, pp. 331–338.

[69] L. G. D. Vicuna, F. Guinjoan, J. Majo, and L. Martinez, "Discontinuous conduction mode in the sepic converter", in *Proceedings. Electrotechnical Conference Integrating Research, Industry and Education in Energy and Communication Engineering',*, Apr. 1989, pp. 38–42. DOI: 10.1109/MELCON.1989.49976.

[70] S. Zhou and G. A. Rincon-Mora, "A high efficiency, soft switching dc-dc converter with adaptive current-ripple control for portable applications", *IEEE Transactions on Circuits and Systems II: Express Briefs*, vol. 53, no. 4, pp. 319–323, Apr. 2006, ISSN: 1549-7747. DOI: 10.1109/TCSII.2005.859572.

[71] A. Davoudi, J. Jatskevich, and T. D. Rybel, "Numerical state-space average-value modeling of pwm dc-dc converters operating in dcm and ccm", *IEEE Transactions on Power Electronics*, vol. 21, no. 4, pp. 1003–1012, Jul. 2006, ISSN: 0885-8993. DOI: 10.1109/TPEL.2006.876848.

[72] M. Hejri and H. Mokhtari, "Hybrid predictive control of a dcdc boost converter in both continuous and discontinuous current modes of operation", *Optimal Control Applications and Methods*, vol. 32, no. 3, pp. 270–284, 2011, ISSN: 1099-1514. DOI: 10.1002/oca.933. [Online]. Available: http://dx.doi.org/10.1002/oca.933.

[73] J. Han, B. Zhang, and D. Qiu, "Unified model of boost converter in continuous and discontinuous conduction modes", *IET Power Electronics*, vol. 9, no. 10, pp. 2036–2043, 2016, ISSN: 1755-4535. DOI: 10.1049/iet-pel.2015.0754.

[74] A. Leki and D. M. Stipanovi, "Hysteresis switching control of the uk converter operating in discontinuous conduction modes", *IEEE Transactions on Circuits and Systems II: Express Briefs*, vol. 64, no. 9, pp. 1077–1081, Sep. 2017, ISSN: 1549-7747. DOI: 10.1109/TCSII.2016.2631510.

[75] G. Beneux, P. Riedinger, J. Daafouz, and L. Grimaud, "Stabilisation of power converters with uncertain equilibrium: An adaptive switched approach with guarantee of stability in continuous and discontinuous conduction modes", *IFAC-PapersOnLine*, vol. 50, no. 1, pp. 10401–10 406, 2017, 20th IFAC World Congress, ISSN: 2405-8963. DOI: https://doi.org/10.1016/j.ifacol.2017.08.1715. [Online]. Available: http://www.sciencedirect.com/science/article/pii/S2405896317323224.

[76] G. Cimini, G. Ippoliti, G. Orlando, and M. Pirro, "Current sensorless solution for pfc boost converter operating both in dcm and ccm", in *21st Mediterranean Conference on Control and Automation*, Jun. 2013, pp. 137–142. DOI: 10.1109/MED.2013.6608711.

Cette thèse est accessible à l'adresse : http://theses.insa-lyon.fr/publication/2019LYSEI123/these.pdf
© [G. J. Becerra], [2019], INSA de Lyon, tous droits réservés

[77] C. H. van der Broeck, R. W. D. Doncker, S. A. Richter, and J. v. Bloh, "Unified control of a buck converter for wide-load-range applications", *IEEE Transactions on Industry Applications*, vol. 51, no. 5, pp. 4061–4071, Sep. 2015, ISSN: 0093-9994. DOI: 10.1109/TIA.2015.2431994.

[78] V. Spinu, M. Dam, and M. Lazar, "Observer design for dc/dc power converters with bilinear averaged model", *IFAC Proceedings Volumes*, vol. 45, no. 9, pp. 204 –209, 2012, 4th IFAC Conference on Analysis and Design of Hybrid Systems, ISSN: 1474-6670. DOI: https://doi.org/10.3182/20120606-3-NL-3011.00091. [Online]. Available: http://www.sciencedirect.com/science/article/pii/S1474667015371974.

[79] M. Biglarbegian, S. J. Nibir, H. Jafarian, and B. Parkhideh, "Development of current measurement techniques for high frequency power converters", in *2016 IEEE International Telecommunications Energy Conference (INTELEC)*, Oct. 2016, pp. 1–7. DOI: 10.1109/INTLEC.2016.7749133.

[80] A. Alessandri and P. Coletta, "Switching observers for continuous-time and discrete-time linear systems", in *Proceedings of the 2001 American Control Conference. (Cat. No.01CH37148)*, vol. 3, Jun. 2001, 2516–2521 vol.3. DOI: 10.1109/ACC.2001.946132.

[81] A. R. Meghnous, M. T. Pham, and X. Lin-Shi, "A hybrid observer for a class of dc-dc power converters", in *2013 American Control Conference*, Jun. 2013, pp. 6225–6230. DOI: 10.1109/ACC.2013.6580814.

[82] M. Djemai, N. Manamanni, and J. P. Barbot, "Nonlinear observer for autonomous switching systems with jumps", in *Hybrid Dynamical Systems: Observation and Control*, M. Djemai and M. Defoort, Eds. Cham: Springer International Publishing, 2015, pp. 103–128, ISBN: 978-3-319-10795-0. DOI: 10.1007/978-3-319-10795-0_4. [Online]. Available: https://doi.org/10.1007/978-3-319-10795-0_4.

[83] L. Ljung, *System Identification: Theory for the User*, ser. Prentice Hall information and system sciences series. Prentice Hall PTR, 1999, ISBN: 9780136566953. [Online]. Available: https://books.google.com.co/books?id=nHFoQgAACAAJ.

[84] J. Castaño, F. Ruiz, and J. Régnier, "A fast approximation algorithm for set-membership system identification", *IFAC Proceedings Volumes*, vol. 44, no. 1, pp. 4410 –4415, 2011, 18th IFAC World Congress, ISSN: 1474-6670. DOI: https://doi.org/10.3182/20110828-6-IT-1002.03212. [Online]. Available: http://www.sciencedirect.com/science/article/pii/S1474667016443028.

[85] I. Jolliffe, *Principal Component Analysis*, ser. Springer Series in Statistics. Springer, 2002, ISBN: 9780387954424. [Online]. Available: https://books.google.com.co/books?id=_olByCrhjwIC.

[86] O. Nelles, "Nonlinear dynamic system identification", in *Nonlinear System Identification: From Classical Approaches to Neural Networks and Fuzzy Models*. Berlin, Heidelberg: Springer Berlin Heidelberg, 2001, pp. 547–577.

Cette thèse est accessible à l'adresse : http://theses.insa-lyon.fr/publication/2019LYSEI123/these.pdf
© [G. J. Becerra], [2019], INSA de Lyon, tous droits réservés

[87] N. Li, "Digital control strategies for DC/DC SEPIC converters towards integration", Theses, INSA de Lyon, May 2012. [Online]. Available: https://tel.archives-ouvertes.fr/tel-00760064.

[88] P. S. Maybeck, "The kalman filter: An introduction to concepts", in *Autonomous robot vehicles*, Springer, 1990, pp. 194–204.

[89] R. Y. Rubinstein, *Simulation and the Monte Carlo Method*, 1st. New York, NY, USA: John Wiley & Sons, Inc., 1981, ISBN: 0471089176.

[90] M. H. Hassoun *et al.*, *Fundamentals of artificial neural networks*. MIT press, 1995.

[91] F. Ruiz, F. Sanchez, H. Arevalo, J. Alméciga-Díaz, and A. Rodríguez-López, "A set membership approach to oxygen transport modeling with unmodeled dynamics", in *2015 IEEE 2nd Colombian Conference on Automatic Control (CCAC)*, Oct. 2015, pp. 1–6. DOI: 10.1109/CCAC.2015.7345189.

Cette thèse est accessible à l'adresse : http://theses.insa-lyon.fr/publication/2019LYSEI123/these.pdf
© [G. J. Becerra], [2019], INSA de Lyon, tous droits réservés

Notation

$\mathbb{R}$	Set of real numbers
$\mathbb{Z}$	Set of integer numbers
$\mathbb{Z}_+$	Set of positive integers
$\mathbb{R}_{\geq a}$	Set of real numbers greater than or equal to a
$\mathbb{R}_{[0,1)}$	Set of real numbers in the interval $[0, 1)$
$\emptyset$	Empty set
$co(\cdot)$	Convex cover of set
$int(\cdot)$	Interior of set
$\mathbb{R}^n$	n-dimensional real vector
$\mathbb{R}^{n\times m}$	n by m real matrix
$A^\intercal$	Transpose of matrix A
$\|x\|_p$	p-norm of vector x
$sign$	Sign function
$Z \succ 0$	Positive definite matrix P
$Z \succeq 0$	Positive semidefinite matrix P
$\hat{x}$	Estimate of vector x
$\tilde{x}$	Measured vector x
$\mathcal{K}$	Class of continuous, strictly increasing functions with value zero at zero
$\mathcal{K}_\infty$	Class of unbounded $\mathcal{K}$ functions
$[x; y]$	Vertical concatenation of vectors x and y.
$\delta(s)$	Dirac function

Cette thèse est accessible à l'adresse : http://theses.insa-lyon.fr/publication/2019LYSEI123/these.pdf
© [G. J. Becerra], [2019], INSA de Lyon, tous droits réservés

Cette thèse est accessible à l'adresse : http://theses.insa-lyon.fr/publication/2019LYSEI123/these.pdf
© [G. J. Becerra], [2019], INSA de Lyon, tous droits réservés

FOLIO ADMINISTRATIF

THESE DE L'UNIVERSITE DE LYON OPEREE AU SEIN DE L'INSA LYON

NOM : BECERRA

DATE de SOUTENANCE : 02/12/2019

Prénoms : Gerardo de Jesus

TITRE : CONTROL AND OBSERVATION OF SWITCHED SYSTEMS. APPLICATION TO POWER CONVERTERS

NATURE : Doctorat

Numéro d'ordre : 2019LYSEI123

Ecole doctorale : EEA DE LYON (ELECTRONIQUE, ELECTROTECHNIQUE, AUTOMATIQUE) – ED160

Spécialité : AUTOMATIQUE

RESUME :

En matière de production énergétique, les tendances actuelles indiquent que la part de marché mondiale des énergies renouvelables continuera d'augmenter du fait de l'amélioration continue de l'efficacité des équipements et de la réduction de leurs coûts. Les convertisseurs de puissance jouent un rôle fondamental dans le fonctionnement des réseaux électriques car ils permettent les transferts d'énergie entre les sources, les éléments de stockage et les charges. Ces dispositifs doivent répondre à des exigences particulières d'efficacité, de robustesse et de stabilité pour garantir un fonctionnement correct. Le travail présenté dans ce mémoire est centré sur deux problèmes particuliers liés au comportement des convertisseurs de puissance : la commande et l'observation. Ces problèmes sont difficiles à résoudre en raison des non-linéarités et des phénomènes physiques complexes présents dans ces composants. Le modèle mathématique utilisé pour représenter les convertisseurs de puissance est le modèle dit à commutation. Sur la base de ce modèle, nous exploitons des outils abordés dans des problématiques telles que la stabilité de Lyapunov, la méthode des moments, la géométrie algébrique et le filtrage direct. Nous proposons des approches novatrices pour commander et observer ces systèmes commutés. Nous introduisons notamment la notion de moments de relaxation pour les systèmes commutés. Ces représentations permettent d'obtenir des modèles permettant d'établir une cartographie de l'entrée de commutations dans l'espace des moments. Cette carte supprime la non-linéarité associée à l'entrée de commutation et fournit un modèle plus approprié pour effectuer les calculs numériques de la commande. C'est l'idée fondamentale de la méthode de commande à variation de paramètres proposée. Après avoir calculé un signal de commande pour le modèle relaxé, le signal d'entrée pour le système commuté peut alors être déduit. Cette approche a montré de bonnes performances en termes de suivi de référence et de stabilité. Une approche reposant sur les données pour l'observation des systèmes commutés est proposée. Cette méthode implique la synthèse d'un filtre direct qui calcule les limites du cas le plus défavorable sur l'erreur d'estimation. Cette méthode est appliquée au cas des convertisseurs de puissance fonctionnant en mode continu et discontinu. Une mise en oeuvre pratique est effectuée et ses performances sont comparées à d'autres méthodes d'estimation.

ABSTRACT:

Current trends in global energy production indicate that renewables will continue to increase their market share due to continuous efficiency improvements and cost reductions. Power converters constitute the interfaces that enable energy transfers in microgrids between sources, storage and loads, playing a fundamental role in their operation. These devices are required to meet particular efficiency, robustness and stability requirements to guarantee a proper operation. The present work is focused on two particular problems present in the operation of power converters: control and observation. These problems are hard to solve because of the nonlinearities and complex behaviors present in power converters. The mathematical model used to represent power converters is the switched system. Based on this model we take elements from subjects like Lyapunov stability, the method of moments, algebraic geometry and direct filtering, and propose novel approaches to control and observation of switched systems. We introduce moment relaxations of switched systems. These representations allow to obtain models where the switching input is mapped to a moment space. This map removes the nonlinearity associated to the switching input and yields a model which is more suitable for performing numerical computations. This is the fundamental idea in the proposed parameter-varying control method. After computing a control signal for the relaxed model, the control signal for the switched system can be recovered. This approach has shown good performance with respect to reference tracking and stability. A data-driven approach for the observation of switched systems is proposed. This method involves the design of a direct filter that computes worst-case bounds on the estimation error. This method is applied to the case of power converters operating in continuous and discontinuous modes. A practical implementation is described, and its performance is compared with other estimation approaches.

MOTS-CLÉS : commande, observation, systèmes commutés, convertisseurs de puissance, méthodes de Lyapunov, méthode des moments, estimation, filtrage

Laboratoire (s) de recherche : Laboratoire Ampère

Directrice de thèse : Xuefang LIN-SHI

Président de jury : Emmanuel GODOY

Composition du jury :

DJEMAI, Mohamed	Professeur des Universités	University of Valenciennes	Rapporteur
QUIJANO, Nicanor	Profesor Asociado	Universidad de los Andes	Rapporteur
GODOY, Emmanuel	Professeur des Universités	CentraleSupélec	Examinateur
COLORADO, Julian	Profesor Asociado	Pontificia Universidad Javeriana	Examinateur
LIN-SHI, Xuefang	Professeur des Universités	INSA Lyon	Directrice de thèse
PHAM, Minh Tu	Maître de Conférence HDR	INSA Lyon	Co-directeur de thèse
PATIÑO, Diego	Profesor Asociado	Pontificia Universidad Javeriana	Co-directeur de thèse, Invité
RUIZ, Fredy	Professore Associato	Politecnico di Milano	Invité

Cette thèse est accessible à l'adresse : http://theses.insa-lyon.fr/publication/2019LYSEI123/these.pdf
© [G. J. Becerra], [2019], INSA de Lyon, tous droits réservés

Cette thèse est accessible à l'adresse : http://theses.insa-lyon.fr/publication/2019LYSEI123/these.pdf
© [G. J. Becerra], [2019], INSA de Lyon, tous droits réservés